The Economic Geography of Global Warming

José Luis Cruz and Esteban Rossi-Hansberg
OCTOBER 2021

Becker Friedman Institute

International Economics
and Economic
Geography Initiative

The Economic Geography of Global Warming[*]

José-Luis Cruz

Princeton University

Esteban Rossi-Hansberg

University of Chicago

October 30, 2021

Abstract

Global warming is a worldwide and protracted phenomenon with heterogeneous local economic effects. In order to evaluate the aggregate and local economic consequences of higher temperatures, we propose a dynamic economic assessment model of the world economy with high spatial resolution. Our model features a number of mechanisms through which individuals can adapt to global warming, including costly trade and migration, and local technological innovations and natality rates. We quantify the model at a $1° \times 1°$ resolution and estimate damage functions that determine the impact of temperature changes on a region's fundamental productivity and amenities depending on local temperatures. Our baseline results show welfare losses from global warming as large as 20% in parts of Africa and Latin America but also high heterogeneity across locations, with northern regions in Siberia, Canada, and Alaska experiencing gains. We find that global warming will increase spatial inequality, since estimated welfare losses across locations are negatively correlated with current real income and welfare. There is large uncertainty about average welfare effects, but much less uncertainty about the spatial distribution of losses. Our quantification points to migration and, to a lesser extent, innovation as important adaptation mechanisms. We use the model to assess the impact of carbon taxes, abatement technologies, and clean energy subsidies. Carbon taxes delay consumption of fossil fuels and help *flatten the temperature curve* but are much more effective when an abatement technology is forthcoming.

1   Introduction

The world is getting warmer due to carbon emissions generated by the economic activity of humans. Global carbon emissions will affect temperatures everywhere over long periods of time and in geographically heterogeneous ways. What will be the impact of carbon emissions, and the implied changes in temperatures, on the world economy and on the economy of particular regions? How will individuals react to these changes and how are these reactions impacted by their ability to migrate, trade, or invest and develop alternative centers of economic activity? What are the best policies to combat global warming and what are their implications for different regions across the world? In this paper we propose and quantify a novel global spatial dynamic assessment model to address these questions.

The nature of the global warming phenomenon determines the elements of our assessment model. Global carbon emissions affect local temperatures around the world, so we want a model of the world economy. Because these effects are extremely heterogeneous across regions, even within countries, we want a model with local geographic detail where temperatures affect both productivity and the living amenities from residing in particular locations. Agents facing adverse temperature conditions that affect their welfare in a given location will react by moving, by trading with other locations, and by developing centers of economic activity in areas that are not so heavily affected or that benefit from warmer temperatures. Hence, we require a model with costly trade and migration, as well as private technological investments. We also need to introduce clean and carbon-based energy as inputs in production so that fossil fuels create carbon dioxide emissions, which in turn affect global and local temperatures through a global carbon cycle and a temperature down-scaling model. Because global warming is a protracted phenomenon developing over hundreds of years and happening in a growing economy, we need an assessment model that is dynamic and incorporates the implications of this growth on carbon emissions and adaptation over time. Such a model will also allow us to study and understand the dynamic implications of this phenomenon across locations. Once we incorporate dynamics over long periods of time, we also need to incorporate population changes by means of birth and mortality rates that vary across regions with different incomes and temperatures.

Our starting point is the spatial growth framework in Desmet et al., 2018. We model trade, migration, and innovation as in that paper. We add clean and carbon-based energy as inputs in production with imperfect substitutability, a carbon extraction technology that determines its cost as a function of the stock of carbon extracted, and the associated carbon cycle that determines global temperature and, through a local down-scaling factor, local temperatures. We model the effect of local temperature on fundamental productivities and amenities through two distinct damage functions that determine the impact of temperature changes on each local characteristic, as a function of the current temperature. The estimated functions indicate, as expected, that warm regions' productivities and amenities are impacted negatively by increases in temperatures, while the opposite is the case for the coldest regions. We also incorporate fertility into the model, so every period agents living at a particular location have a natality rate (birth minus death rate)

2

that depends on their income and the local temperature. This adds local and global population dynamics to our model.

We quantify the model devoting particular attention to identify the effect that changes in local climatic conditions have on local productivities and amenities. We start by using data from G-Econ, the Human Development Index, together with a number of parameters obtained from the literature, to invert the model and obtain the local productivities and amenities that rationalize populations and income every five year-period from 1990 to 2005 (the years for which G-Econ is available). This model inversion also yields the migration costs that rationalize population movements across regions given the natality function we estimate using United Nations net natality rates. We then use the fundamental productivities and amenities to estimate how they are affected by changes in local temperatures. Because these fundamental productivities and amenities come from a model with costly trade, migration, innovation, and fertility, these adaptation mechanism are already taken explicitly into account. This is clearly preferable to estimating damage functions from endogenous outcomes like output or population. We estimate the effect of climate on these fundamentals allowing for the semi-elasticity to depend on local temperatures and include location as well as time fixed effects. The estimated damage functions yield significant effects of changes in temperature for wide ranges of initial current temperatures, but they also yield relatively large confidence intervals that we use to assess the uncertainty underlying our results.

The final step in the quantification is to parameterize the effect of carbon use for future carbon extraction costs and the carbon cycle. We model energy as a constant elasticity of substitution composite between fossil fuels and clean energy. The cost of these two sources of energy evolves with the world's endogenous technology, but the cost of fossil fuels also depends on the amount of carbon that has been used in the past, since the remaining stock is increasingly harder to extract. Using data from Bauer et al., 2017, we estimate a convex relationship between cumulative emissions and the cost of extraction. Firms decide on their use of fossil fuels, which leads to carbon emissions. A standard carbon cycle model (as in IPCC, 2013) then generates global temperature dynamics.[1] Our baseline analysis matches the global temperature dynamics from 2000 to 2400 in the IPCC RCP 8.5 scenario almost exactly. To down-scale from global to local temperatures we follow Mitchell, 2003 and use a linear function with heterogeneous local factors that we estimate as a function of a large number of local characteristics.[2] The estimated down-scaling factors (the local temperature change for a one degree change in global temperature) can be as large at 2.2 in parts of Siberia and Alaska and as low as 0.5 in parts of Asia and South America.

With the quantified model in hand, we can simulate the economy forward over several centuries and evaluate the economic consequences of global warming. This phenomenon is expected to have heterogeneous effects over space, where the hottest regions in South America, Africa, India and Australia experience

---

[1]We also include exogenous CO_2 emissions from forestry and non-CO_2 greenhouse gasses from RCP 8.5.

[2]We use Chebyshev polynomials of order 10 in latitude, longitude, elevation, distance to coast, distance to ocean, distance to water, vegetation density and albedo.

welfare losses of 20% and the coldest regions in Alaska, Northern Canada, and Siberia undergo welfare gains as high as 11%. On average, the world is expected to lose 6% in terms of welfare, although the exact number depends on the yearly discount factor.[3] Global warming increases inequality across space. Welfare losses across locations are negatively correlated with current real income per capita and welfare. The poorest regions of the world, mainly located in Sub Saharan Africa and South East Asia, are the ones undergoing the highest warming losses. By 2200, the average loss in welfare is 10% and in output is 5%, although the uncertainty inherited from our estimated damage functions implies that the 95% confidence intervals include loses as high as 20% and 12%, respectively. The large uncertainty in average outcomes, however, does not translate into significant uncertainty on the spatial distribution of losses. The relative distribution of loses is very similar in our baseline case compared to the worst- or the best-case scenarios (as measured by the 95% confidence intervals of our damage functions). When we decompose the losses coming from the effect of global warming on amenities or productivity we find that about half of the average effects come from the impact of temperature rise on productivity. Effects on amenities are particularly important for loses in Africa and gains at the most northern latitudes; while losses in productivity affect almost all regions to the south of the 30° latitude.

Our evaluation of the effects of global warming emphasizes economic adaptation through migration, trade, and endogenous local innovation. We assess the importance of each of these adaptation channels using counterfactuals that increase the cost of migrating, trading, or investing by a certain percent globally. If we increase migration costs by 25% throughout the globe, the average cost of global warming rises by an additional 3% by the year 2200. Higher migration costs make global warming more costly for Africa, but also for northern regions that benefit less from the influx of migrants. Increases in migration costs lead to significantly faster population growth as more people stay in poorer areas where they have more children. Compared to migration, we find a substantially smaller impact from increases in trade costs. The reason is that the evolution of temperature is spatially correlated, and most trade is local. Furthermore, our model features trade, but only an aggregate sector and therefore no adaptation through sectoral specialization.[4] Innovation is somewhere in between, a rise in innovation costs has a large relative effect that benefits the coldest places but hurts the warmest ones significantly. On average, though, less innovation implies that regions in India and China, that will eventually be heavily affected by global warming, grow less and so the world on average loses less from the rise in temperatures.

The last part of the paper uses our quantified model to evaluate a number of environmental policies. The equilibrium allocation in the modeled economy is not efficient due to carbon emissions being a global externality, but also due to the presence of production externalities, technology diffusion, and congestion externalities. We study taxes on carbon dioxide, subsidies on clean energy, and the importance of abatement

---

[3]In our baseline scenario we use a discount factor of $\beta = 0.965$ in an economy where real GDP grows around 3% per year.

[4]See Conte et al., 2020 for a related model that incorporates an agricultural and a non-agricultural sector and where trade plays a more important role as an adaptation mechanism.

technologies that eliminate the pernicious effects of carbon. Clean energy subsidies have only a modest effect on carbon emissions and the corresponding evolution of global temperature since, although they generate substitution towards clean energy, they also lead to a reduction in the price of energy which results in more production and ultimately more energy use. These effects tend to cancel each other out.

Carbon taxes have a larger effect on CO_2 emissions and temperatures. The reduction in the use of fossil fuels leads to less carbon emissions which results in lower temperatures that persist for hundreds of years. However, the reduction in carbon use also implies that more carbon is left unexploited on Earth, which yields lower future extraction costs. The implication is that carbon taxes primarily delay the use of the carbon on Earth, rather than decreasing its total use. This has the effect of *flattening* the temperature curve, with lower temperatures for long periods of time, but with little impact over the very long-run. Hence, the effects of carbon taxes on the environment are primarily concentrated in the next 100 years or so. Of course, this result also implies that carbon taxes can be particularly effective in combination with abatement technologies. If abatement technologies are forthcoming, delaying carbon consumption has tremendously positive effects since the effect of future emissions is abated using the new technology. Thus, our results strongly suggest that carbon taxes should be combined with incentives to invent effective abatement technologies. To use an analogy from the epidemiology literature, flattening an infection curve is particularly effective if a cure is forthcoming, but much less so otherwise.[5]

Standard models of global warming use aggregate loss functions that relate the future path of the aggregate economy to the evolution of climate variables. In many cases, these loss functions fail to incorporate the behavioral responses of individuals and firms. Because those functions are not derived from micro-founded models in which optimal behavior is obtained as a response to climatic shocks, they fail to consider that households and firms can adapt, although bearing costs, to the most salient consequences of this phenomenon. Incorporating these responses is particularly important because of the vast heterogeneity that rising temperatures will have on the fundamentals of the economy. It is also essential, because only a model that explicitly takes into account these behavioural adaptation responses across regions can properly account for potential changes in aggregate loss functions in policy counterfactuals and simulations of alternative scenarios (an expression of the Lucas critique, Lucas, 1976). A quantitative dynamic model like ours, with individual behavioural responses and an explicit treatment of spatial heterogeneity at a high resolution is, therefore, a needed addition to the economics of climate change.

In the last decade there has been a surge of empirical estimates of climate damages that use panel methodologies and exploit short-run weather variation to identify the causal effect of temperature on eco-

---

[5]As we know from standard Pigovian analysis we can address the negative externality created by fossil fuels using taxes that increase their price. However, another potentially effective strategy is to increase the elasticity of substitution between fossil fuels and clean sources in the technology to produce energy. In the aggregate, this elasticity is not a fundamental parameter of technology, but rather a parameter that aggregates the many ways the world has to produce energy. As such, this parameter is not necessarily either constant or policy invariant. Although we use estimates in the literature and fix it at 1.6 in our baseline scenario, we show that increases in this elasticity can be extremely effective in reducing the use of fossil fuels over time as extraction costs rise. Such an increase in this elasticity can be achieved, for example, by switching vehicles to use energy from all sources, as electric cars do.

nomic and social outcomes. This wave of empirical papers was pioneered by the work of Deschênes and Greenstone, 2007, who study the impact of temperature on agricultural profits. This methodology has been employed to quantify the weather effects on mortality (Barreca et al., 2016, Carleton et al., 2020), amenities (Albouy et al., 2016, Baylis, 2020), crime and conflict (Burke et al., 2015a), migration (Missirian and Schlenker, 2017), crop yields (Schlenker and Roberts, 2009), GDP and GDP growth (Dell et al., 2012, Burke et al., 2015b).[6] This work has been useful to provide evidence of the link between temperature and economic outcomes, but it cannot be used to determine the future effects of temperature across regions, or to evaluate different policies.

Some of these estimates have been incorporated in economic models of global warming, also known as Integrated Assessment Models (IAM), to quantify the economic consequences of this phenomenon. The most popular models tend to consider coarse geographical units and display a limited role for adaptation mechanisms in mediating climate damages (Nordhaus, 2017, Anthoff and Tol, 2014, Hope and Hope, 2013, IPCC, 2013, Golosov et al., 2014). A notable exception is Krusell and Smith, 2017, who consider a spatial resolution similar to ours but, in contrast to us, consider the effect of global warming on local capital investments. We depart from their work, by explicitly incorporating trade, migration, innovation, and population growth, and by estimating the damage functions on productivities and amenities, rather than GDP.

These core models have been extended to analyze different dimensions of global warming. Popp, 2004, Acemoglu et al., 2012, Acemoglu et al., 2016, Acemoglu et al., 2019, Hassler et al., 2019 assess the role of clean technology investments and innovations in mitigating climate damages. Benveniste et al., 2020 explore the extent to which migration and border policies attenuate the level of exposure and vulnerability to climate change impacts. Dietz and Lanz, 2020 study the capacity to meet food demand for different climate change conditions. Fried, 2019 evaluates the role of investment in adaptation capital to reduce damages from extreme weather. Hassler et al., 2018 compare the warming-induced losses in GDP and the optimal carbon taxes, when considering extreme values for the climate sensitivity and economic damages. Costinot et al., 2016 examine the losses in the agriculture sector when trade and production patterns are allowed to adjust across different crops. Barrage, 2019 studies the optimal environmental policy in the presence of distortionary taxes.

We contribute to the development of IAMs by incorporating recent developments in spatial quantitative models. In particular, we build on Desmet et al., 2018, that develops a spatial growth theory at a fine level of geographical resolution and analyzes the evolution of the economy over several centuries. The static spatial component resembles Allen and Arkolakis, 2014, but adds costly migration, and the dynamic component follows Desmet and Rossi-Hansberg, 2014.[7] We incorporate local fertility and population dynamics, energy use, fossil fuels extraction costs, a carbon cycle, effects of temperature on productivity and amenity, among other features to these existing economic frameworks.

---

[6]Dell et al., 2014 and Auffhammer, 2018 review this body of research.

[7]See Redding and Rossi-Hansberg, 2017 for a survey of this literature.

There is an incipient literature that addresses environmental questions through the lens of spatial dynamic models. Balboni, 2019 quantifies the cost of road investment in the coasts of Vietnam under the presence of sea level rise. Desmet et al., 2021 measure the spatial shifts in population and economic activity due to sea level rise, using a highly spatially disaggregated model, closer to ours. Desmet and Rossi-Hansberg, 2015, Nath, 2020 and Conte et al., 2020 evaluate the impact of global warming across different economic sectors which is something we do not incorporate in this paper. Relative to them, we add realistic spatial heterogeneity, dynamics and high spatial resolution, and population dynamics and effects of temperature on amenities, respectively. Ultimately, our aim is to generate a model with all the necessary elements to serve as a workhorse for a new generation of IAMs models that incorporate dynamics, rich spatial heterogeneity, and micro-founded adaptation mechanisms.

The rest of the paper is structured as follows. Section 2 presents the economic and climate model. Section 3 quantifies the model and estimates the damage functions. Section 4 describes the baseline quantitative implications of global warming. Section 5 discusses the role of the different forms of adaptation in mediating the harmful effects of global warming. Section 6 analyzes the effect of a number of environmental policies. Section 7 concludes.[8]

2 The Model

The economic component of the model extends Desmet et al., 2018 among a number of dimensions. First, we incorporate an endogenous law of motion for global population. Second, we consider that production requires labor, land, and energy. Energy comes from fossil fuels or clean sources. The former type of energy generates CO_2 emissions, whereas the latter does not. Third, local climate conditions distort the fundamental amenities, productivities, and natality rates in spatially heterogeneous ways.

The carbon cycle and the global temperature modules are based on the reduced-form models in IPCC, 2013. The projection from global to local temperature follows the statistical down-scaling approach, formalized by Mitchell, 2003.

2.1 Endowment and Preferences

The world economy occupies a two-dimensional surface S, where a location is defined as a point $r \in S$ with land density $H(r)$. In each period t, L_t agents live in the world economy. Global population is time-dependent due to endogenous natality rates.

Every period, agents derive utility from consuming a set of differentiated varieties $c_t^\omega(r)$ aggregated according to a CES utility function, from local amenities, $b_t(r)$, and from their idiosyncratic preference for the location where they live, $\varepsilon_t^i(r)$. If agents move from r to s at t, utility is discounted by mobility costs,

---

[8]Replication files can be found at https://rossihansberg.economics.uchicago.edu/replication_files/Replication_EGGW.zip.

$m(r, s)$, which are paid as a permanent flow cost from t onward. Specifically, the period utility of agent i who resides in r in period t and has a location history $r_- = (r_0, \cdots, r_{t-1})$ is given by

$$u_t^i(r_-, r) = \left[\int_0^1 c_t^\omega(r)^\rho d\omega \right]^{1/\rho} b_t(r) \varepsilon_t^i(r) \prod_{s=1}^t m(r_{s-1}, r_s)^{-1}. \tag{1}$$

Agents earn income from work. They inelastically supply one unit of labor and receive a wage $w_t(r)$. They also receive a share of land rents, $H(r)R_t(r)$, which are uniformly distributed across a location's residents. Thus, per capita real income is $y_t(r) = (w_t(r) + R_t(r)/L_t(r))/P_t(r)$, where $L_t(r)$ denotes local population density (population per unit of land) and $P_t(r)$ the local ideal CES price index.

Local amenities $b_t(r)$ are affected by congestion according to $b_t(r) = \bar{b}_t(r)L_t(r)^{-\lambda}$, where $\bar{b}_t(r)$ represents a location's *fundamental* amenities and λ the congestion elasticity of amenities to population density. Fundamental amenities can be distorted by local climate conditions through the *damage* function $\Lambda^b(\cdot)$. This function denotes the percentage change in fundamental amenities when local temperature rises from $T_{t-1}(r)$ in period $t-1$ to $T_t(r) = \Delta T_t(r) + T_{t-1}(r)$ in period t. Namely,

$$\bar{b}_t(r) = \left(1 + \Lambda^b(\Delta T_t(r), T_{t-1}(r)) \right) \bar{b}_{t-1}(r). \tag{2}$$

Hence, when $\Lambda^b(\Delta T_t(r), T_{t-1}(r))$ is negative (positive), amenities in cell r are damaged (improved) by increases in local temperature. The dependence of the damage function on the level of temperature, and not only on the change in temperature, captures the heterogeneous impacts over space that global warming is expected to have. Naturally, and as we estimate in Section 3, the amenities in hot places (like Congo) decline with further increases in temperature, whereas amenities in cold places (like Siberia) benefit from warmer climate.

Households also experience idiosyncratic taste shocks, $\varepsilon_t^i(r)$, that we assume are independent and identically distributed across households, locations, and time according to a Fréchet distribution with shape parameter $1/\Omega$ and scale parameter 1. A greater value of Ω implies more dispersion in agent's tastes across locations, acting as a second congestion force.

We assume that the flow-utility cost of moving from r to s is given by the product of an origin-specific cost, $m_1(r)$, and a destination-specific cost, $m_2(s)$, so $m(r, s) = m_1(r)m_2(s)$. Since staying in the same location is costless, $m(r, r) = 1$, origin costs are simply the inverse of destination costs, namely $m_1(r) = 1/m_2(r)$. Hence, the permanent utility cost of entering a location is compensated by a permanent utility benefit when leaving, which implies that agents only pay the flow cost while residing there. This way of modelling migration costs implies that migration decisions are reversible and, therefore, the location choice of agents only depends on current variables and not on past or future ones. As is standard in discrete choice

models with idiosyncratic preferences, the fraction of households residing in r at period t is then given by

$$\frac{L_t(r)H(r)}{L_t} = \frac{u_t(r)^{1/\Omega}m_2(r)^{-1/\Omega}}{\int_S u_t(v)^{1/\Omega}m_2(v)^{-1/\Omega}dv}, \tag{3}$$

where $u_t(r)$ denotes the component of local utility that is not idiosyncratic, namely,

$$u_t(r) = b_t(r)y_t(r) = b_t(r)\left[\int_0^1 c_t^\omega(r)^\rho d\omega\right]^{1/\rho}. \tag{4}$$

At the end of period t, after the migration decisions have been made, each household has $n_t(r)$ net offsprings. Local natality rates are exogenous to the individual but endogenous to a location's real income and local temperature, $n_t(r) = \eta(y_t(r), T_t(r))$. Therefore, at the beginning of period $t + 1$, before migration decisions are made, local population density $L'_{t+1}(r)$ is determined by $L'_{t+1}(r)H(r) = (1 + n_t(r)) L_t(r)H(r)$.

Note that global population depends not only on the distribution of natality rates across space and time, and through them on the distribution of income and local temperatures, but also on the spatial distribution of population in the previous period.

2.2 Technology

In each cell there is a continuum of firms, producing differentiated varieties $\omega \in [0, 1]$. Output is produced using a constant returns to scale technology in land, labor, and energy. Output per unit of land of variety ω is given by

$$q_t^\omega(r) = \phi_t^\omega(r)^{\gamma_1} z_t^\omega(r) \left(L_t^\omega(r)^\chi e_t^\omega(r)^{1-\chi}\right)^\mu, \tag{5}$$

where $L_t^\omega(r)$ and $e_t^\omega(r)$ denote the production workers and the energy use, both per unit of land. Note that, since land is a fixed factor with share $1 - \mu$, agglomerating labor and energy in a location yields decreasing returns, which acts as a third congestion force.

A firm's productivity is determined by its innovation decision, $\phi_t^\omega(r) \geq 1$, and an idiosyncratic location-variety productivity shifter, $z_t^\omega(r)$. Firms can invest in innovation by paying a cost $\nu\phi_t^\omega(r)^\xi$, expressed in units of labor per land. The exogenous productivity shifter is the realization of a random variable which is independent and identically distributed across varieties and time according to a Fréchet distribution with cumulative distribution function $F(z, a) = e^{-a_t(r)z^{-\theta}}$. The scale parameter $a_t(r)$ governs the level of productivity in a location and is affected by agglomeration externalities as a consequence of high population density and endogenous past innovations. In particular, we let $a_t(r) = \bar{a}_t(r)L_t(r)^\alpha$ where α governs the strength of the first agglomeration force.

In turn, fundamental productivity, $\bar{a}_t(r)$, is determined by an endogenous dynamic process given by

$$\bar{a}_t(r) = (1 + \Lambda^a(\Delta T_t(r), T_{t-1}(r))) \left(\phi_{t-1}(r)^{\theta\gamma_1}\left[\int_S D(v, r)\bar{a}_{t-1}(v)dv\right]^{1-\gamma_2}\bar{a}_{t-1}(r)^{\gamma_2}\right). \tag{6}$$

9

Equation (6) has four components. The term $\phi_{t-1}(r)^{\theta \gamma_1}$ represents the shift in the local distribution of shocks that results from the last period's innovation decisions of firms, which are assumed to now be embedded in the local technology.[9] The individual contemporaneous effect of innovation affects the production function in (5) directly. The term $\left[\int_S D(v,r)\bar{a}_{t-1}(v)dv\right]^{1-\gamma_2} \bar{a}_{t-1}(r)^{\gamma_2}$ denotes the level of past technology that firms build on. It is composed of the location's own technology level $\bar{a}_{t-1}(r)$, as well as technology diffusion from other locations, where the function $D(v,r)$ denotes the spatial decay in the strength of technology diffusion. This specification follows Desmet et al., 2018 closely and all its dynamic implications are developed and discussed there. It generates a spatial endogenous growth model. Important for our purposes is that we add the term $\Lambda^a(\cdot)$, which incorporates the effect of temperature on local productivity. When the damage function $\Lambda^a(\Delta T_t(r), T_{t-1}(r))$ is negative (positive), productivity in cell r at time t declines (increases) due to temperature change. Since $\Lambda^a(\cdot)$ depends on temperature levels, it is flexible to capture the heterogeneous spatial impacts of global warming on productivity.

Unlike Desmet et al., 2018, production does not only require land and labor, but also energy. Following Golosov et al., 2014, Hassler et al., 2019, and Popp, 2006, among others, energy and other factors are aggregated through a Cobb Douglas production function where $(1-\chi)\mu$ denotes the share of energy in the production process. In turn, energy is a CES composite between fossil fuels, $e_t^{f,\omega}(r)$, and clean sources, $e_t^{c,\omega}(r)$, where the elasticity of substitution is given by ϵ.[10] The use of fossil fuels generates CO_2 emissions, which accumulate in the atmosphere intensifying the greenhouse gas effect, whereas the use of clean energy does not. Specifically, we let

$$e_t^\omega(r) = \left(\kappa e_t^{f,\omega}(r)^{\frac{\epsilon-1}{\epsilon}} + (1-\kappa)e_t^{c,\omega}(r)^{\frac{\epsilon-1}{\epsilon}}\right)^{\frac{\epsilon}{\epsilon-1}}, \tag{7}$$

where κ governs the relative productivity of both technologies in producing energy.

We assume competitive local energy markets and so the price of each type of energy is equal to its marginal production cost. Producing one unit of energy of type $j \in \{f,c\}$ requires $\mathcal{Q}_t^j(r)$ units of labor. The cost of energy varies across locations, time, and source, according to

$$\mathcal{Q}_t^f(r) = \frac{f(CumCO2_{t-1})}{\zeta_t^f(r)} \quad \text{and} \quad \mathcal{Q}_t^c(r) = \frac{1}{\zeta_t^c(r)}. \tag{8}$$

The evolution of the cost of fossil fuel, $\mathcal{Q}_t^f(r)$, is composed of two terms. The numerator denotes the cost of extracting fossil fuels from the ground, which we assume is increasing and convex in total world cumulative CO_2 emissions, $CumCO2_{t-1}$, following Nordhaus and Boyer, 2002. As cumulative emissions increase, carbon reserves shrink, which rises the cost of extraction. Cumulative emissions are simply the sum of

---

[9]As Desmet et al., 2018 shows, all firms in a given location and point in time make identical innovation decisions.

[10]This elasticity governs the extent to which energy sources might not be perfect substitutes due to their ease of use, their location, or the existence of technologies and capital designed to primarily use a particular source. We introduce it as a fixed parameter, but perform a number of counterfactual exercises to assess its impact.

cumulative emissions in the previous period plus the global CO_2 emissions released at t, E_t^f, namely

$$CumCO2_t = CumCO2_{t-1} + E_t^f = CumCO2_{t-1} + \int_S \int_0^1 e_t^{f,\omega}(v)H(v)d\omega dv. \tag{9}$$

The denominator of the energy price relates to the productivity, $\zeta_t^j(r)$, in energy generation of type j. We assume that the rate at which technology evolves over time in the fossil fuel and clean sector is related to global real GDP, y_t^w, which is endogenous in this model, as it depends on the investment decisions of firms. In particular, we consider that an increase of one percent in global real GDP rises log-productivity in energy generation by v^j, where this elasticity is allowed to vary across types of energy. That is,

$$\zeta_t^j(r) = \left(\frac{y_t^w}{y_{t-1}^w}\right)^{v^j} \zeta_{t-1}^j(r), \quad \text{where} \quad y_t^w = \int_S \left(\frac{L_t(v)H(v)}{L_t}\right) y_t(v)dv. \tag{10}$$

Consequently, firm's innovations generate an externality on energy productivity improvements with magnitude that depends on the evolution of real GDP.[11]

We also assume that land markets are competitive. Firms bid for land and the firm whose bid is the largest wins the right to produce in that parcel. This is important since past innovations, embedded in the level of the local idiosyncratic distribution of productivities, benefit all potential entrants. As proven in Desmet and Rossi-Hansberg, 2014, this implies that the solution to the dynamic innovation problem of firms is to simply choose the level of innovation that maximizes their current profits (or equivalently their bid for land), since all future gains of current innovations will accrue to land, which is the fixed factor. Future firms profits are zero independently of a firm's actions and so do not affect its decisions. Since there is a continuum of potential entrants, firms end up bidding all of their profits after covering innovation costs. Hence, in this economy, firm profits are zero and the maximum bid for land is the local land price, $R_t(r)$, every period. In sum, firms in r simply maximize

$$\max_{q,L,\phi,e^f,e^c} p_t^\omega(r,r)q_t^\omega(r) - w_t(r)L_t^\omega(r) - w_t(r)\nu\phi_t^\omega(r)^\xi - w_t(r)\mathcal{Q}_t^f(r)e_t^{f,\omega}(r) - w_t(r)\mathcal{Q}_t^c(r)e_t^{c,\omega}(r) - R_t(r)$$

where $q_t^\omega(r)$ is given by (5) and (7), and $p_t^\omega(r,r)$ is the price at location r of variety ω produced at r.

The first order conditions with respect to fossil fuel and clean energy allow us to rewrite the total energy cost in labor units as the energy composite $e_t^\omega(r)$ times its ideal price index $\mathcal{Q}_t(r)$. Namely, $\mathcal{Q}_t(r)e_t^\omega(r) = \mathcal{Q}_t^f(r)e_t^{f,\omega}(r) + \mathcal{Q}_t^c(r)e_t^{c,\omega}(r)$, where $\mathcal{Q}_t(r) = \left(\kappa^\epsilon \mathcal{Q}_t^f(r)^{1-\epsilon} + (1-\kappa)^\epsilon \mathcal{Q}_c^f(r)^{1-\epsilon}\right)^{\frac{1}{1-\epsilon}}$.

Since technology is Cobb-Douglas, a firm's energy costs are proportional to labor costs, so $\mathcal{Q}_t(r)e_t^\omega(r) = \frac{1-\chi}{\chi}L_t^\omega(r)$. Thus, the problem of the firm collapses to a problem parallel to the one posed by Desmet et al., 2018, and so all their results apply.

---

[11]An alternative approach would be to explicitly model the purposeful innovation decisions by firms that extract and distribute fossil fuels and generate clean energy, as we did for the technology of firms producing final goods. The aforementioned assumption simplifies the model and captures the reality of the many technological spillovers between industries.

2.3 Prices, Export Shares, and Trade Balance

Goods markets are competitive, so firms sell goods at marginal cost after accounting for transport costs. Let $\varsigma(s,r) \geq 1$ denote the iceberg trade cost of shipping a good from r to s. Then, $p_t^\omega(s,r) = \varsigma(s,r)mc_t(r)/z_t^\omega(r)$, where $mc_t(r)$ denotes the marginal input cost at location r, which is common across firms since they face the same prices and therefore make the same decisions. The marginal input costs is given by $mc_t(r) = \mathcal{M}\mathcal{Q}_t(r)^{(1-\chi)\mu}w_t(r)^{\mu+\gamma_1/\xi}R_t(r)^{1-\mu-\gamma_1/\xi}$, where $\mathcal{M}$ is a proportionality constant that depends on production parameters.

As is standard in trade structures based on Eaton and Kortum, 2002, the probability, $\pi_t(s,r)$, that a good produced in r is consumed at s is then given by a gravity equation of the form

$$\pi_t(s,r) = \frac{a_t(r)[mc_t(r)\varsigma(r,s)]^{-\theta}}{\int_S a_t(v)[mc_t(v)\varsigma(v,s)]^{-\theta}dv}. \tag{11}$$

And the price index, $P_t(r)$, of a location (where $\Gamma(\cdot)$ denotes the Gamma function) by

$$P_t(r) = \Gamma\left(\frac{-\rho}{(1-\rho)\theta+1}\right)^{-\frac{1-\rho}{\rho}}\left[\int_S a_t(v)[mc_t(v)\varsigma(r,v)]^{-\theta}dv\right]^{-1/\theta}. \tag{12}$$

Finally, since we are interested in outcomes over long periods of time, we impose trade balance cell by cell. Hence, total income (labor income plus land rents) at r equals total expenditure on goods from r,

$$w_t(r)L_t(r)H(r) = \int_S \pi_t(v,r)w_t(v)L_t(v)H(v)dv. \tag{13}$$

2.4 Climate and the Carbon Cycle

The burning of fossil fuels (as well as other activities, like deforestation) leads to emissions of carbon dioxide into the atmosphere. The carbon cycle defines how carbon flows accumulate in the atmosphere. The evolution of atmospheric CO_2 follows the dynamics proposed by IPCC, 2013 where the stock of carbon in the atmosphere, S_t, evolves according to

$$S_{t+1} = S_{\text{pre-ind}} + \sum_{\ell=1}^{\infty}(1-\delta_\ell)\left(E_{t+1-\ell}^f + E_{t+1-\ell}^x\right). \tag{14}$$

As defined in (9), E_t^f denotes the endogenous CO_2 emissions from fossil fuel combustion. In addition, E_t^x are exogenous CO_2 emissions from non-fuel combustion, taken from the Representative Consumer Pathway (RCP) 8.5 IPCC scenario. The parameter $S_{\text{pre-ind}}$ denotes the CO_2 stock in the pre-industrial era (1800) and $(1-\delta_\ell)$ is the share of CO_2 emissions remaining in atmosphere ℓ periods ahead. Higher concentrations of carbon dioxide rise the global radiative forcing, F_{t+1}, (net inflow of energy), which is approximated as in Myhre et al., 1998, so

$$F_{t+1} = \varphi\log_2(S_{t+1}/S_{\text{pre-ind}}) + F_{t+1}^x \tag{15}$$

where φ denotes the forcing sensitivity, that is, the increase in radiative force when carbon stock doubles with respect to its pre-industrial level. F_t^x denotes radiative forcing from non-CO_2 greenhouse gases (methane, nitrous oxide, among others). When the inflow of energy from the Sun exceeds the outflow of energy exiting the planet, global temperature rises, according to a process defined by

$$T_{t+1} = T_{\text{pre-ind}} + \sum_{\ell=0}^{\infty} \zeta_\ell F_{t+1-\ell}, \tag{16}$$

where $T_{\text{pre-ind}}$ denotes worldwide temperature over land in the pre-industrial era and ζ_ℓ is the current temperature response to an increase in radiative force ℓ periods ago.

Carbon emissions disseminate in the world quickly and affect global temperature, not local temperatures directly. This is why carbon emissions are a global externality. However, given that we want to quantify our model at a fine geographical resolution, we need to take a stand on the evolution of local temperature in response to changes in global temperatures. We follow Mitchell, 2003, who argues that a linear down-scaling relationship provides accurate results.[12] In particular, we let

$$T_t(r) - T_{t-1}(r) = g(r) \cdot (T_t - T_{t-1}), \tag{17}$$

where the coefficient $g(r)$ tells us by how much, in °C, temperature in cell r changes when global temperature changes by one °C. The coefficients $g(r)$ depend on local physical characteristics of a location, so we keep them fixed over time.

2.5 Competitive Equilibrium and Balanced Growth Path

Together the conditions defined above define a dynamic competitive equilibrium of our model. We can show that the system of equations that defines a spatial equilibrium in a given period can be reduced to a system of equations for population and wages in each location. All other variables, including firm investments, can then be directly computed using the equations presented above.[13] We can show that there exists a unique solution to the system of equations if (i) $\epsilon = 1$ or $\upsilon^f = \upsilon^c$, and (ii) $\frac{\alpha}{\theta} + \frac{\gamma_1}{\xi} \leq \lambda + (1-\mu) + \Omega$. The first condition requires that either the elasticity of substitution between fossil fuels and clean energy is one (Cobb-Douglas) or the innovation elasticity with respect to global real income growth is the same across energy types. Those assumptions allows us to keep the log-linear structure of the model.[14] The second condition is identical to the one in Desmet et al., 2018. It states that the static agglomeration economies

---

[12]More precisely, Mitchell, 2003 finds small non-linearities in the local climate response to the length of time over which warming has occurred, to the rate at which it has occurred, and to the extent to which global temperature has stabilized. Incorporating these non-linearities has only a negligible effect on our results.

[13]We present detailed proofs in the Supplementary Materials Section F.1, but they parallel the reasoning in Desmet et al., 2018.

[14]In the model quantification below, our baseline parametrization deviates from this condition slightly, but numerically we find that the solution is robust to a variation in initial conditions.

associated with the local production externalities, α/θ, and the degree of returns to innovation, γ_1/ξ, do not dominate the three congestion forces. These three congestion forces are governed by the value of the negative elasticity of amenities to density, λ, the share of land in production which determines the degree of local decreasing returns, $1 - \mu$, and the variance of taste shocks, Ω.

A spatial equilibrium in a given period determines firm innovation, energy use, and carbon emissions. Hence we can use equations (2), (6), and the climate and carbon cycle model, to determine temperatures and next period's amenities and productivities. This allows us to compute the dynamic equilibrium forward, period by period, for as many years as needed. As we show in Supplementary Materials Section F.3, eventually the distribution of population across space and the world real output growth rate converge to a balanced growth path if: (i) total natality rates $1 + n_t(r)$ converge to one as income per capita grows; (ii) the stock of carbon is finite, and $(1 - \delta_\ell), \zeta_\ell, E_\ell^x$ and F_ℓ^x converge to constant values, so eventually temperatures stabilize; (iii) $\epsilon = 1$ or $v^f = v^c$; and (iv) $\frac{\alpha}{\theta} + \frac{\gamma_1}{\xi} + \frac{\gamma_1}{\xi(1-\gamma_2)} \leq \lambda + (1 - \mu) + \Omega$. The last condition, which is identical to the one in Desmet et al., 2018, states that agglomeration forces, that now include also dynamic agglomeration forces through innovation, $\frac{\gamma_1}{\xi(1-\gamma_2)}$, are weaker than the three congestion forces. The dynamics of the model are very protracted, so convergence to a balanced growth path is not fully achieved for the four-century horizon that we consider. We now proceed to quantify our model.

3   Quantification

We quantify the model at the $1°$ latitude by $1°$ longitude spatial resolution, which is the spatial resolution of the G-Econ dataset. Our baseline year is 2000. In order to quantify the model we need values for all the economy-wide parameters, plus location specific values for initial fundamental amenities, productivities, and migration costs, as well as bilateral transport costs. We also need to parametrize the extraction cost of fossil fuels, estimate the damage functions on amenities, productivities, and natality rates, and quantify the carbon cycle and climate module.

We follow the quantification strategy in Desmet et al., 2018 for the common parts of the model. Table 3 in Appendix A summarizes the parameter values used in the baseline case. Local fundamental amenities and productivities are recovered so that the model matches exactly population and income in 2000. Migration costs are recovered so that the model matches exactly the observed change in population between 2000 and 2005. All these local characteristics are exactly identified by an inversion procedure described in detail in Desmet et al., 2018. Bilateral trade costs are based on optimal routing using the fast marching algorithm. In what follows, we describe the estimation of three families of parameters and functions, namely, the evolution of energy prices; the construction of the damage functions on amenities, productivities, and natality rates; and the carbon cycle, as well as the climate and the down-scaling factors. Appendix A provides details on the data used in the quantification.

14

3.1 Energy Prices

We split the estimation of the energy component in four steps. First, we parametrize the cost of extracting fossil fuels $f(\cdot)$ from the ground. Second, we calibrate the energy share in production, $\mu(1 - \chi)$, and the share of fossil fuels in the energy aggregator, κ. Third, we construct prices for fossil fuels and clean energy at the cell level for the year 2000 and retrieve the initial level of the productivities $\zeta_0^f(\cdot), \zeta_0^c(\cdot)$. Finally, we set υ^f, υ^c to match historical data on global CO_2 emissions and clean energy use.

To estimate the cost of extracting fossil fuels $f(\cdot)$, we employ estimates from Rogner, 1997 and Bauer et al., 2017. To construct quantity-cost relations for fossil fuel resources, Rogner, 1997 analyzed historical marginal production costs for different fossil fuel deposits and found a stable relation across regions and time: extraction costs are flat when resources are abundant, but they rise sharply as the resource gets exhausted.[15] Bauer et al., 2017 extend the work of Rogner, 1997 and formulate a database of fossil fuel quantities and extraction costs, taking into account different technological, political and economic conditions. We consider the scenario that closest resembles the most pessimistic scenario (RCP 8.5) of the IPCC, 2013.[16] Figure 1 displays, in green, the estimates by Bauer et al., 2017 as a function of cumulative CO_2 emissions. We specify the extraction cost function $f(\cdot)$ as

$$f(CumCO2_t) = \left(\frac{f_1}{f_2 + \mathrm{e}^{-f_3(CumCO2_t - f_4)}} \right) + \left(\frac{f_5}{maxCumCO2 - CumCO2_t} \right)^3, \tag{18}$$

where $CumCO2_t$ denotes the cumulative CO_2 extracted up to period t and the parameter $maxCumCO2$ denotes the total stock of carbon dioxide available to produce energy in the planet. We set the value of $maxCumCO2$ to equalize the cumulative flow of CO_2 for the next five centuries in the most pessimistic scenario (RCP 8.5) of the IPCC, 2013, that is 19,500 $GtCO_2$.[17] The rest of the parameters are chosen to fit the estimates of Bauer et al., 2017. The black curve in Figure 1 displays the estimated extraction curve, which is increasing and convex.

We calibrate the parameters χ and κ using the first order conditions of the firm's profit maximization. In particular, since technology is Cobb-Douglas, the world's average relative expenditure in fossil fuels and clean energy, and the ratio of energy expenditures to the wage bill, are constants given by

$$\left(\frac{\mathcal{Q}_0^f}{\mathcal{Q}_0^c} \right) \left(\frac{E_0^f}{E_0^c} \right)^{\frac{1}{\epsilon}} = \frac{\kappa}{1 - \kappa}, \quad \text{and} \quad \frac{w_0 \mathcal{Q}_0 E_0}{w_0 L_0} = \frac{\mu(1 - \chi)}{\mu + \gamma_1/\xi}. \tag{19}$$

---

[15]Drilling costs in the oil and gas industry increase drastically with depth and coal mining is highly sensitive to the characteristics of deep lying coal seams.

[16]Specifically, Bauer et al., 2017 present estimates for five Socio Economic Share Pathways (SSP), which consider different assumptions for the evolution of the world economy. We choose the scenario SSP5 (development based on fossil fuels), which is the one closest to RCP 8.5, and aggregate the costs of coal, natural gas, and oil into a single fossil fuel in terms of tCO_2 per usd.

[17]In comparison, Bauer et al., 2017 consider a smaller total stock of carbon dioxide of 12,550 $GtCO_2$ and Mcglade and Ekins, 2015 of 14,666 $GtCO_2$. Supplementary Materials Section G.5 presents results with a variety of alternative values for the total stock of carbon.
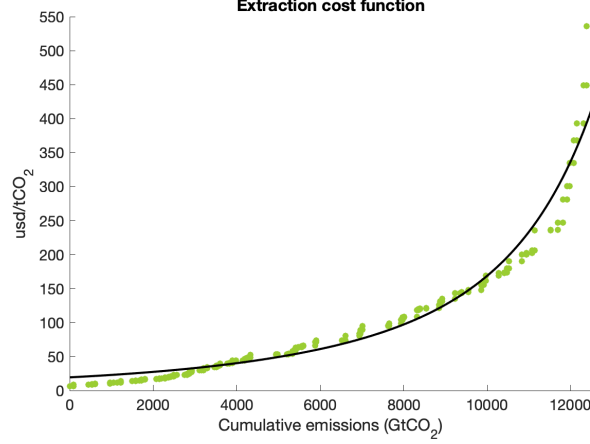
Figure 1: The extraction cost function $f(\cdot)$.

We take the elasticity of substitution ϵ from Popp, 2004,[18] who consider a value of 1.6 and obtain global income from the G-Econ database, so $w_0 L_0 = 46.59$ trillions usd for the year 2000. We construct the global price of fossil fuels by aggregating the price of coal, natural gas, and oil as in Golosov et al., 2014.[19] This procedure yields an estimate for the price of fosil fuels of $w_0 \mathcal{Q}_0^f = 72.99$ usd/tCO$_2$. Acemoglu et al., 2019 estimate the price of clean energy to be 1.15 times that of natural gas. We use that relation to obtain a price of 87.79 usd per ton of oil equivalent (toe). In turn, one ton of oil equivalent generates 2.8466 tons of CO$_2$, which is the weighted average of carbon intensities of coal, oil, and natural gas for the year 2000. With those prices and considering that the use of energy from fossil fuels is $E_0^f = 8.88$ Gtoe (IPCC, 2013) and from clean sources is $E_0^c = 1.23$ Gtoe (BP, 2019) we obtain $\kappa = 0.89$ and $\chi = 0.96$.[20]

The next step is to measure the productivity of dirty $\zeta_0^f(\cdot)$ and clean energy $\zeta_0^c(\cdot)$ in the initial period for each cell. To do so, we use the first order conditions of the firm's optimization problem in each cell, together

---

[18]Papageorgiou et al., 2017 find that the elasticity of substitution for electricity generating industries is 2 and for non-energy industries is 3. Sensitivity analysis to this parameter are conducted in Supplementary Materials Section G.4.

[19]Golosov et al., 2014 propose that energy from fossil fuels is a CES composite of coal, natural gas, and oil, with elasticity of substitution of 1.11, which corresponds to the unweighted average of the elasticity of substitution between coal and oil, coal and natual gas, and oil and natural gas, according to Stern, 2012. Acemoglu et al., 2019 focus on the electricity sector and consider an elasticity of substitution of 2, in line with Bosetti et al., 2007, so that fossil fuels are more substitutable between them than with respect to clean energy. The representative prices of oil, natural gas and coal are the average of the Brent, U.S. Henry Hub, and U.S. Central Appalachian, respectively, over the period 1983-2017 to smooth short-run fluctuations. Data on prices is taken from BP, 2019 and data on quantities from IEA, 2019.

[20]This parametrization implies that the energy share in production is 3.3%, which is slightly smaller than the values used in the literature, where Golosov et al., 2014 use 4%, Hassler et al., 2019 5.55%, and Krusell and Smith, 2017 6%.

with equation ([8](#)), to obtain

$$\zeta_0^f(r) = \left(\frac{\mu + \gamma_1/\xi}{\mu(1-\chi)\kappa}\right)\left(\frac{e_0(r)}{L_0(r)}\right)\left(\frac{e_0^f(r)}{e_0(r)}\right)^{\frac{1}{\varepsilon}} f(CumCO2_0),\tag{20}$$

$$\zeta_0^c(r) = \left(\frac{\mu + \gamma_1/\xi}{\mu(1-\chi)(1-\kappa)}\right)\left(\frac{e_0(r)}{L_0(r)}\right)\left(\frac{e_0^c(r)}{e_0(r)}\right)^{\frac{1}{\varepsilon}}.\tag{21}$$

Labor at the cell-level is directly taken from the G-Econ database. To construct cell-level energy use of fossil fuels and clean energy, we first start with data for CO_2 emissions and clean energy use at the country-level from BP, 2019, Crippa et al., 2019 and IEA, 2019. Then, we allocate energy use across cells within countries using the share of emissions in the Emissions Database for Global Atmospheric Research (EDGAR).

Finally, to estimate the elasticity of technology in the fossil fuel sector, v^f, and in the clean energy sector, v^c, with respect to global real GDP growth, we construct historical global CO_2 emissions and clean energy use from IEA, 2019 and BP, 2019. We then run the model backwards in time for 50 periods and find the elasticities that provide the best fit of the historical data on relative energy use. The resulting elasticity for clean energy is larger than the one for fossil fuels since its use has expanded faster over time ($v^c = 1.22 > 1.16 = v^f$).[21]

3.2 The Effect of Local Temperature on Amenities and Productivities

To estimate the damage functions $\Lambda^a(\cdot)$ and $\Lambda^b(\cdot)$, which determine how temperature affects the fundamentals of the economy, we first need to compute fundamental amenities and productivity in each location by *inverting the model*. The inversion of the model requires solving the system of equations in Lemma 1 for $\bar{b}_t(r)$ and $\bar{a}_t(r)$ using data on wages and population, as well as the data on the amount of land in each cell, and the energy prices we described in the previous section. We can do so for the four periods of data available in G-Econ, namely, 1990, 1995, 2000 and 2005.[22]

The model inversion exactly identifies $\bar{a}_t(r)$ and $\bar{b}_t(r)/u_t(r)$, but is unable to separate $\bar{b}_t(r)$ apart from $u_t(r)$. Intuitively, we cannot identify the numerator from the denominator since, if we observe many individuals in a poor location, it could be because amenities are high or because individuals are trapped there even though utility is very low. To disentangle a location's amenities from its initial utility, we require a measure of utility.[23] Desmet et al., 2018 use as utility measure a subjective well-being survey from the Gallup World Poll. However, this data is only available for one period and only at the country-, rather than

---

[21]Supplementary Materials Section F.4 outlines the system of equations that solve the model backwards in time and Appendix C describes, in further detail, the estimation of these elasticities.

[22]Supplementary Materials Section F.2 describes the inversion of the model in more detail. An alternative approach that would give us a longer time series would be to employ data on production from Kummu et al., 2018. This dataset spans a longer period of time, from 1990 to 2015 at a yearly frequency, but it displays a coarser geographical resolution with around 700 sub-national units.

[23]Once we identify $\bar{b}_t(r)$, we can obtain the migration costs in order to match the model-implied net migration flows with the ones observed in the data

cell-level. Thus, we use the Human Development Index (HDI) as our measure of $u_t(r)$ after transforming it into a cardinal measure of well-being that is linear in log-real income, as in our model.[24]

Once we compute the fundamentals that rationalize the observable data on wages, population and energy prices, we identify the causal effect of temperature on amenities and productivities using a panel fixed effects empirical specification, with temperature entering the regression in a flexible non-parametric way. Our main empirical specification is given by

$$\log(x_t(r)) = \sum_{j=1}^{J} \delta_j^x \cdot T_t(r) \cdot \mathbb{1}\{T_t(r) \in \mathcal{T}_j\} + \delta^z \cdot Z(r) + \iota(b) + \iota_t(s) + \varepsilon_t(r) \tag{22}$$

where $x_t(r) \in \{\bar{b}_t(r), \bar{a}_t(r)/\phi_t(r)\}$ are the fundamental amenities and the ratio of fundamental productivities to innovations at cell r in period t. We use the ratio $\bar{a}_t(r)/\phi_t(r)$ in order to account for the effect of endogenous innovation on fundamental productivity over time. The variable $T_t(r)$ denotes the average January temperature for locations in the Northern Hemisphere and the average July temperature for locations in the Southern Hemisphere over the last decade. The variable $\mathbb{1}\{T_t(r) \in \mathcal{T}_j\}$ is an indicator function of temperature $T_t(r)$ being in interval $\mathcal{T}_j$. We partition the distribution of temperatures into $J = 20$ bins, each comprising 5% of the observed temperature values.[25] Average January or July temperatures over land, respectively, range from $-50.15°\text{C}$ to $32.85°\text{C}$.

The non-parametric specification in (22) accommodates the potential non-linearities and bliss-points in the effect of temperature on these fundamentals. That is, a temperature increase of $1°\text{C}$ might have different impacts in very cold regions, like Siberia, with respect to very hot places, like the Sahara. Thus, the coefficient of interest δ_j^x, which is the semi-elasticity of $x_t(r)$ with respect to temperature, is allowed to vary according to the level of temperature. This implies that the damage function $\Lambda^x(\cdot)$ can be expressed as the semi-elasticity δ_j^x, evaluated at the current level of temperature, times the change in local temperature, namely, $\Lambda^x(\Delta T_t(r), T_{t-1}) = \delta^x(T_t(r)) \cdot \Delta T_t(r)$.

Our specification also incorporates a set of time-invariant controls at the cell-level, $Z(r)$, and a set of fixed effects, $\iota(b)$ and $\iota_t(s)$, to alleviate potential omitted variable bias. To the extent that temperature is spatially correlated, any variable not included in the estimation, that is spatially correlated, would appear in the error term and would bias our estimate of the coefficient δ_j^x. Hence, we follow Nordhaus, 2006 and include a number of geographic attributes as cell-level covariates, $Z(r)$. Alternatively, we can partition the gridded map into blocks of size 2 cells by 2 cells, denoted by $\iota(b)$. Although a bit more spatially aggregated, this specification captures any time-invariant local characteristic at the 2-cell spatial level. In addition, we

---

[24]Appendix B.1 describes the details of this calculation and compares this index to the measure used in Desmet et al., 2018.

[25]We employ decadal rather than yearly temperature to capture the long-run effects of temperature thereby exploiting also cross-sectional variation. We employ January and July, rather than yearly temperatures, because the former exhibits larger variation over space, which allows us to better identify the temperature impact on fundamentals. We perform robustness exercises in Appendix B.3 where we use average temperatures. The results are similar, but the point estimates are noisier.

consider local regional trends at the sub-national level, $\iota_t(s)$.[26] Our preferred specification for the effect of temperature on amenities considers the block time invariant fixed effects $\iota(b)$ and divides the regions of Europe in countries. Amenities are driven by many local characteristics that are hard to explicitly control for, as well as by differences in national history and cultural differences. Hence, using a flexible set of time-invariant fixed effect and trends is important. To estimate the effect of temperature on local productivity we control for geographic factors, $Z(r)$, at a detailed local level and use the slightly broader definition of European regional trends that divides Europe in four large regions. Geographic attributes have a direct impact on local productivities in agriculture, but also in other sectors through the availability of raw materials and transportation networks. Broader regional evolution in technology depends on regional specialization rather than national boundaries and so are captured through the many sub-national trends in the world and the four European regions. Appendix B.2 describes the details of the damage function estimation and Appendix B.3 presents a number of robustness exercises.

Figure 2 displays the baseline estimates of $\delta^b(T_t(r))$ and $\delta^a(T_t(r))$. We allow for spatially correlated errors as in Conley, 1999.[27] The bars in the figure denote the point estimates, the whiskers the 95% confidence intervals and the solid gray curve a logistic approximation.[28] The dashed gray lines represent the 95% confidence intervals of the logistic curves.[29]
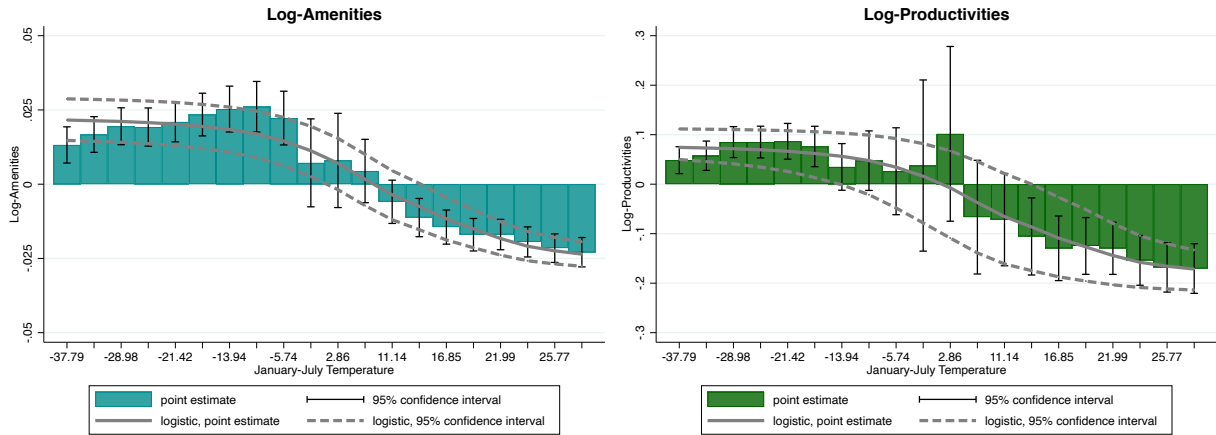

Figure 2: Effect of temperature on fundamental amenities and productivities, using January temperatures for the Northern Hemisphere and July temperatures for the Southern Hemisphere.

[26]We use two definitions of sub-national units. We start with the administrative units defined in Kummu et al., 2018 for the whole world and aggregate those in Europe at the (i) country-level and (ii) at the region-level: North, South, West and East of Europe.

[27]We consider that correlation of errors between cells declines linearly with distance, so that when distance is greater than 550 km (5 cells), correlation vanishes to zero.

[28]We opted for a logistic approximation to be conservative when extrapolating damages to temperatures that are hotter than the ones historically observed. Albouy et al., 2016 and Graff-Zivin and Neidell, 2014 argue that individuals reduce their time outdoors as temperatures become uncomfortable, reducing their sensitivity to further temperature changes.

[29]The upper (lower) confidence interval of the logistic curve is constructed using the upper (lower) confidence interval of the point estimates and fitting a logistic curve as well.

As expected, for very cold regions, increases in temperature rise both amenities and productivities. For example, in the coldest bin of January-July temperatures, centered at -37.79°C, an increase in 1°C augments local amenities by 2.16% and local productivities by 7.44%, according to the logistic smoothing. In bins with warmer temperatures, the beneficial effects of rising temperatures decline, until they reach zero and eventually turn negative. For January-July temperatures in the warmest bin, centered at 25.77°C, an increase in 1°C reduces local amenities by 2.24% and local productivities by 16.57%. These results highlight the heterogeneous effects of temperature on fundamentals across the range of temperature levels experienced in regions of the world. Extreme temperatures have negative effects and amenities and productivities have bliss-points at moderate ones. Optimal temperatures for fundamentals are given by the temperatures at which $\delta_j^x = \frac{\partial \log(x_t(r))}{\partial T_t(r)}$ equals zero. For amenities we estimate an optimal winter temperature of 8.6°C, whereas for productivities of 1.6°C.[30]

3.3 The Effect of Income and Temperature on Natality Rates

We specify local natality rates as a function of real income and temperature. In particular, we let $n_t(r) = \eta^y \left(\log(y_t(r)) \right) + \eta^T \left(T_t(r), \log(y_t^w) \right)$, where

$$\eta^y \left(\log(y_t(r)) \right) = \mathcal{B}(\log(y_t(r)); b^\ell) \cdot \mathbb{1}(\log(y_t(r)) < b^*) + \mathcal{B}(\log(y_t(r)); b^h) \cdot \mathbb{1}(\log(y_t(r)) \geq b^*), \qquad (23)$$

$$\eta^T(T_t(r), \log(y_t^w)) = \frac{\mathcal{B}(T_t(r); b^T)}{1 + e^{b_w[\log(y_t^w) - \log(y_0^w)]}}, \qquad (24)$$

with $\mathcal{B}(\log(y_t(r)); b) = b_0 + b_2 e^{-b_1 (\log(y_t(r)) - b^*)^2}$. The term $\eta^y(\cdot)$ captures the standard argument in Becker, 1960 that, as income grows, household substitutes quantity for quality by investing more in their children. Delventhal et al., 2019 analyze birth and death rates across countries and find that almost all countries in the world have experienced (or are experiencing) a demographic transition, that is, they move from a phase of high to one of low natality. Furthermore, they argue that the start of this transition occurs at roughly the same income level. Hence, the functional form in (23) specifies an inverse and asymmetric bell-shaped function, so that when income is sufficiently low, natality rates are high but, as income grows, natality rates decline until they reach negative values, as evidenced by some rich countries today. To impose that global population is stable in the long-run, natality rates tend towards zero as income rises further.[31]

The relation between temperature and natality is captured by $\eta^T(\cdot)$. Carleton et al., 2020 estimate that higher income allows households to adapt to changes in temperature, thereby flattening the mortality re-

---

[30] Although the literature estimating the impact of temperature on fundamentals, rather than endogenous outcomes, is scarce, our estimates for optimal temperatures are roughly in line with available studies. Burke et al., 2015b employ country-level data for the period 1960-2010 and, through panel methods, estimate that economic production is concave in annual temperature peaking at 13°C. Krusell and Smith, 2017 consider that a yearly temperature of 11.6°C maximizes productivity and Nordhaus, 2006 estimates that the optimal yearly temperature for output lies between 7°C and 14°C. If we translate this range to January-July temperatures, which is the temperature measure we use in our estimation, this range becomes -5°C to 6°C, which includes our bliss-point for productivity.

[31] $\mathcal{B}(\cdot)$ is a bell-shaped function where b_0 and $b_2 + b_0$ are the minimum and maximum (maximum and minimum) values if $b_2 > 0$ ($b_2 < 0$), $b_1 > 0$ governs the slope of the incline and decline, and b^* is the value that maximizes the function.

sponse to temperature. Barreca et al., 2016 argue that access to health care, electricity and, particularly, air conditioner have been important adaptation mechanisms. Thus, we specify $\eta^T(\cdot)$ as a symmetric bell-shaped function, so that when temperatures are extreme, natality rates are low, and they are maximized in temperate climates. Finally, we interact this component with a decreasing function of global income, y_t^w, to account for the remedies that a wealthier world would provide for the effect of temperature on mortality.

To estimate the parameters defining the natality rate function, b^ℓ, b^h, b^T, b_w, we run the model backwards for 50 periods and compute the endogenous historical population levels predicted by the model. Thus, we find the coefficients that maximize the model's fit with the country-level historical data on natality rates.[32] Figure 3 displays the resulting functions $\eta^y(\cdot)$ and $\eta^T(\cdot)$. They illustrate the position of the world average, a cold and rich country (United States), and a hot and poor country (Zambia), for the years 1950 and 1999.[33]
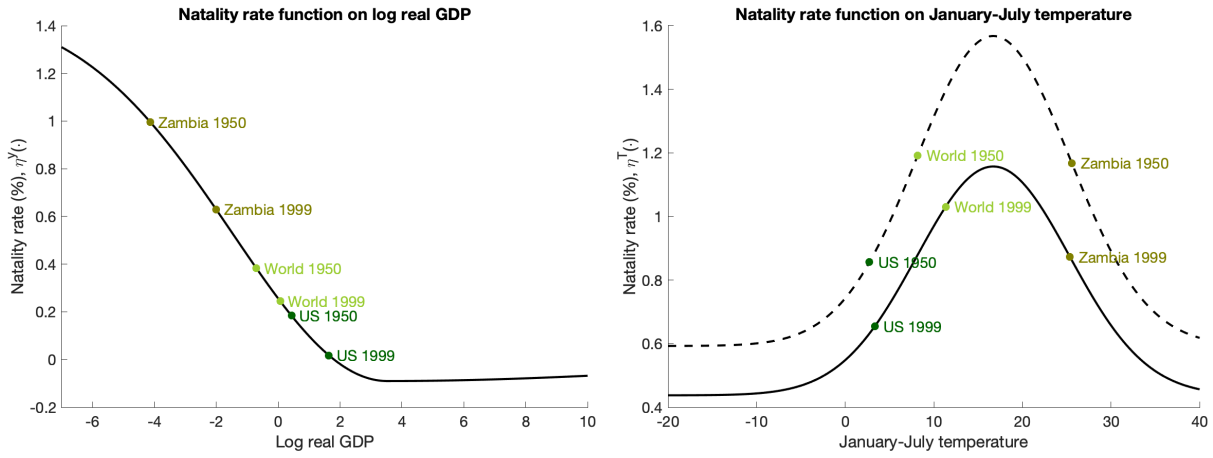
Figure 3: The natality rate function.

Finally, with the the quantified natality rate function, we compute the migration costs $m_2(\cdot)$ that make the model exactly rationalize the population levels observed in 2005. The procedure to obtain the migration costs is described in detail in Supplementary Materials Section F.5 and the procedure to estimate the natality function, as well as some additional results, are presented in Appendix C.

3.4   Carbon Cycle and Temperature Downscaling

We adopt the specification of the carbon cycle and the global climate component proposed by IPCC, 2013. We choose parameter values such that the carbon cycle in Section 2.4 exactly reproduces the values displayed in IPCC, 2013. The details and exact values used are discussed in Appendix D. As we will show below, the end result will be that the endogenous evolution of temperature in our baseline scenario will

---

[32]We weight countries by population size with additional weight for more recent observations. Additionally, we impose that the natality function $\eta(\cdot)$ matches the global natality rate in 2000 and 2020. Figures 26 and 25 compare the cross-section of country-level natality rates in 2000 and the historical global natality rates from the data and the estimation, respectively.

[33]1950 and 1999 mark the beginning and end of the time period employed in the estimation of the natality rate function.

reproduce the temperature path of the RCP 8.5 scenario almost exactly.

We use equation (17) to down-scale worldwide temperature at the cell-level. We use the Berkeley Earth Surface Temperature Database, which provides temperature data at a geographic resolution of $1° \times 1°$. In order to obtain a smooth spatial shape of the temperature scaler, $g(\cdot)$, we specify it as a function of geographical attributes of each cell. Specifically, as a Chebyshev polynomial of order 10 on latitude and longitude (including a cross term), elevation, distance to the coast, distance to non-frozen oceans, distance to water bodies, vegetation density, share of ice-covered land and albedo.[34] We estimate equation (17) by weighted OLS, with higher weight given to more recent observations. The estimation procedure yields a good fit; it captures 83% of the variation in the local temperature data. Appendix D elaborates further on the construction of the temperature scaler.

Figure 4 plots the local January-July temperatures in 2000 and the temperature scaler for every cell of the world. An increase in global temperature of $1°$C results in increases as large as $2.2°$C close to the north pole, but as low as $0.5°$C in southern locations in Central and South America, Africa, South East Asia, and Australia. Coastal regions tend to experience smaller increases in temperature compared to inland locations. This pattern is attributed to the fact that land absorbs more heat than water. These results are in line with predictions by IPCC, 2007. Overall, Figure 4 illustrates the large heterogeneity in the impact of global warming on local temperatures and underscores the importance of a high resolution spatial model.
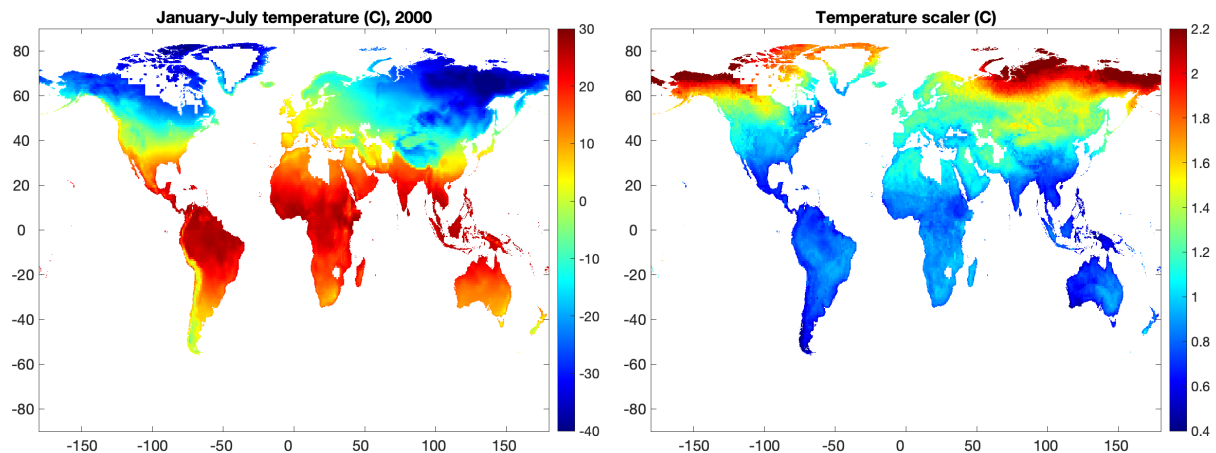

Figure 4: Local January-July temperature in 2000 and temperature scaler.

4   The Baseline Scenario

In the baseline scenario we run the quantified model and obtain predictions for 400 years, corresponding to the period 2001 to 2400. This scenario assumes that no new climate policy is put in place and that

---

[34]Albedo is the ratio of light that a surface reflects compared to the total sunlight it receives. Surfaces that reflect a lot of light are bright and have high albedo. For example, snow has a high albedo, whereas forests have a low albedo.

the evolution of clean technology follows the process described in the previous sections. We organize the exposition of the quantitative results as follows. First, we describe the endogenous evolution of aggregate CO_2 emissions and average global temperature and compare them with the projections by IPCC, 2013. Then, we explore the corresponding evolution of economic outcomes, namely, amenities, productivities and population density. Finally, we run counterfactuals where we eliminate the effect of the rise in temperatures in order to evaluate the welfare effects of global warming.

4.1 Emissions and Temperature in the Baseline Scenario

Figure 5 presents the path for CO_2 emissions predicted by the model, as well as its comparison with the two most pessimistic scenarios (RCP 8.5 and 6.0) in IPCC, 2013. Carbon dioxide emissions from fossil fuel combustion are expected to grow over the current century, since the improvements in productivity (generated by endogenous growth in global real income) overcomes the increase in the relative price of carbon-based energy that results from the larger extraction cost associated with increasing cumulative emissions. CO_2 emissions reach a peak of 117 GtCO$_2$ in 2110, a value slightly higher than the 106 GtCO$_2$ of the most pessimistic IPCC scenario. After that point, the flow of carbon dioxide declines towards zero, since extraction costs increase sharply as fossil fuels become exhausted. Note that, although the bell-shaped carbon dioxide emission path is an endogenous outcome, derived from the optimizing behavior of agents, it parallels the exogenous abatement process that makes the emission projections of IPCC, 2013 decline eventually.
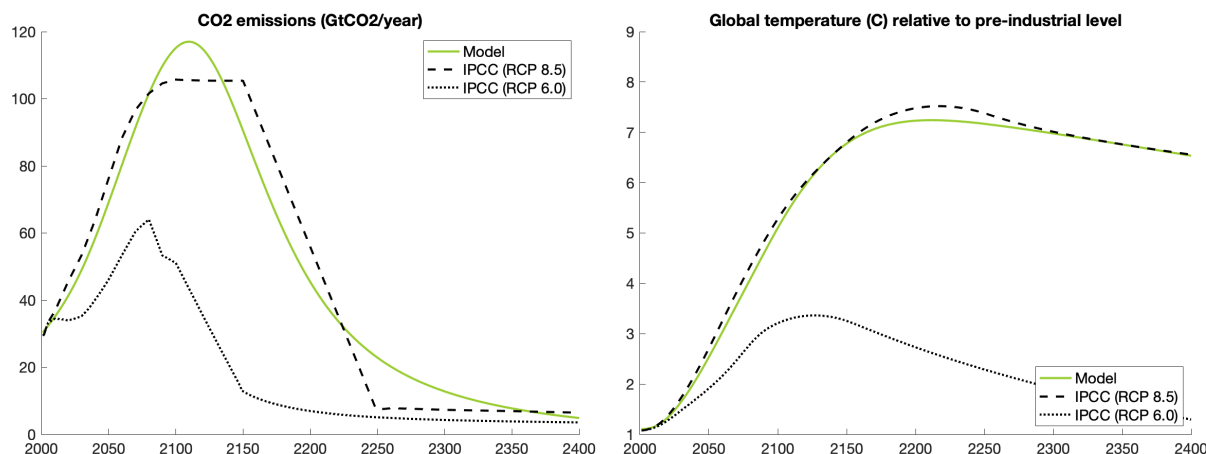

Figure 5: CO_2 emissions and global temperature.

The rise in the concentration of greenhouse gases increases global temperatures, as shown in Figure 5, so that by the end of the current century, global temperature is expect to rise 5.1°C with respect to its pre-industrial level. By 2200 the rise in global temperatures reaches 7.2°C. As carbon dioxide consumption declines towards zero, global temperature approximates its long-run level at between 6 and 7°C above pre-industrial level. As expected, given our parametrization of the carbon cycle and the close match between

the emission trajectory in our model and that in the RCP 8.5 scenario, the temperature evolution matches the RCP 8.5 almost exactly.

As illustrated in Figure 4, the increase in global temperatures yields heterogeneous increases in local temperatures across the world. In 2000, only 26.97% of the land surface experienced January-July temperatures higher that 20°C. Two hundred years later this share is predicted to increase to 40.80%, covering most of North and Central Africa, the Middle East, India, Brazil and Central America. At the other extreme, in 2000, 5.50% of the global land surface exhibited January-July temperatures below -30°C, mainly located in North Canada, Greenland, and Northern Russia. This share is expected to decline to 0.30% in 2200.[35]

4.2 Local Amenities, Productivity, and Population in the Baseline Scenario

To measure how changes in temperature distort economic outcomes, we compare two scenarios: A factual scenario, our baseline, in which temperature affects fundamental amenities, productivities, and natality rates as described in Section 3, and a counterfactual scenario, in which temperature does not disrupt these fundamentals and, therefore, has no effect on economic outcomes.

Figure 6 shows the ratio of fundamental amenities and productivities in 2200 in the scenario with global warming relative to the counterfactual scenario without global warming. Values greater (lower) than one indicate that temperature changes are predicted to increase (decrease) the respective fundamental characteristic. As we argued before, the estimated temperature damage functions, $\Lambda^b(\cdot)$ and $\Lambda^a(\cdot)$, imply that rises in temperature have differentiated effects over space depending on the level of temperature. In the year 2200, the coldest places in the world experience amenity gains as large as 38%, while the hottest places in the world are projected to suffer amenity losses of 25%. The pattern of changes in amenities depends primarily on latitude, with equatorial regions losing the most, but the geographic patterns are quite rich. Inland regions in Africa, South America, and Australia lose more than what their latitude would predict, as does the U.K., and parts of continental Europe. The average amenity losses, weighted by the 2200 population in the baseline scenario, amounts to 4.9%.

The impact of global warming on fundamental productivities by 2200 exhibits similar patterns, although more pronounced. Note that the effects on productivity are not only driven by the direct impact of temperature on the estimated damage function, $\Lambda^a(\cdot)$, but also by endogenous innovation decisions. In parts of Alaska, Northern Canada, Greenland, and Northern Russia productivity doubles relative to the scenario without global warming, and in a few areas the changes in productivity can be even larger. In contrast, in Brazil, Africa, Middle East, India, and Australia we observe declines in productivity of up to 80%. On average, and again weighting by employment in the baseline scenario, world fundamental productivity declines by 25% by 2200 due to rising temperatures.

The geographic configuration of amenities and productivites determines the desirability for residing

---

[35]Supplementary Materials Section G.1 presents additional results on the evolution of local temperature over time.
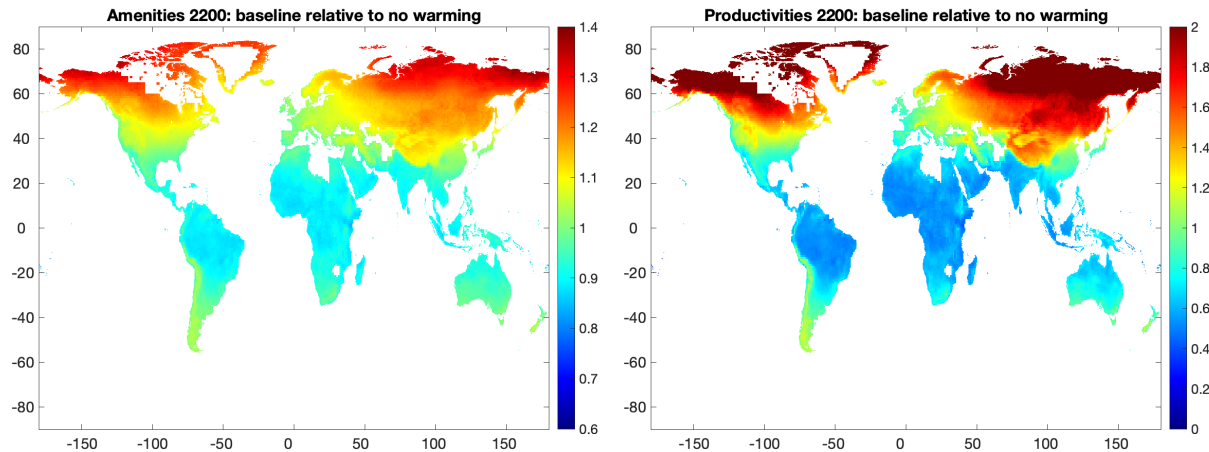
Figure 6: Gains and losses in amenities and productivities from global warming in the year 2200.

and producing in particular regions of the world. As the world becomes warmer, the regions where amenities and productivity deteriorate see their population decline. The magnitude of the decline depends on natality rates and migration costs, as well as their trade network and other local characteristics. Figure 7 presents population density in 2200 relative to the counterfactual scenario without global warming. Clearly, global warming generates migration towards colder places. Areas to the south of the 30° latitude in the Northern Hemisphere tend to lose population, while areas to the north tend to gain. Most of the developed world (U.S., Europe, and Japan) is just at the boundary and so is not greatly affected. In two centuries, population density in the north of the world is projected to increase by more than 83%, whereas locations close to the Equator are projected to experience declines in population density as large as 32%. Note that, although inflow migration to the coldest regions is large in relative terms, it is small in absolute terms, since these areas are only sparsely populated. Overall, by 2200, 4.40% of the population resides in a different location due to global warming. More than 483 million people are displaced by this dimension of climate change, namely global warming, alone!

Global warming not only affects relocation of population over space, but also its global level. In the baseline scenario, world population grows until the year 2125, reaching a peak of 11.4 billions inhabitants, as depicted in Figure 7. Afterwards, population declines as the world gets richer and natality rates decline. Since natality rates converge to zero as income grows, global population converges to a stable long-run level. The figure also presents the United Nations global population estimates. The model's population predictions for the first century are somewhat higher than the median estimate by UN, 2019, but within the 80% confidence interval. The long-run level of global population estimated by UN, 2004 at 9 billions inhabitants is close to our projection in 2400. Global warming has a relatively small impact on world population, the model predicts that higher temperatures lower population in the next 50 years by roughly 4 millions; in the next 100 years by 16 millions; and in the next 200 years by 27 millions.
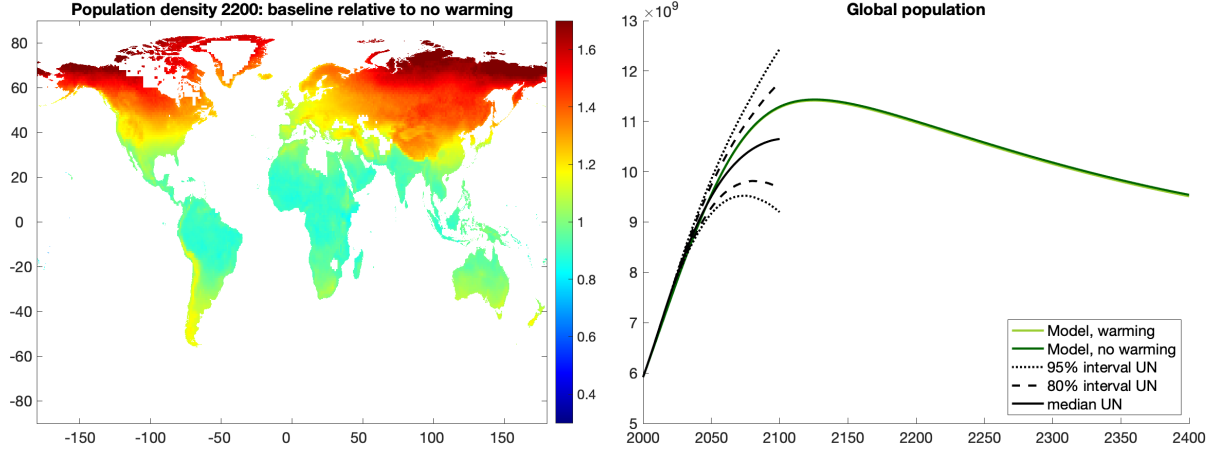
Figure 7: Spatial pattern of population and global population.

4.3 The Welfare Cost of Global Warming

To evaluate the welfare consequences of global warming, we compute the present discounted value (PDV) of local utility that is not idiosyncratic, namely, $\sum_{t=0}^{\infty} \beta^t u_t(r)$. We use a value of the discount factor of $\beta = 0.965$.[36] Our choice of the discount factor is restricted by a real output growth rate that is slightly larger than 3% per year. Clearly, to do proper comparisons we need a discount factor for which present discounted values remain finite in all exercises.

Figure 8 displays the spatial distribution of welfare gains, as well as an initial population weighted histogram of the distribution of gains and losses.[37] As before, values smaller than one indicate that the region suffers losses from global warming. The welfare effects of this phenomenon are quite heterogeneous across space. Welfare losses range from 20% in Central and Southern Africa to gains of 11% in the most northern parts of Russia. The right-hand panel of Figure 8 clearly shows that the distribution of damages is bi-modal. The left peak of the distribution, with losses of around 10%, corresponds to India, while the right peak, that experiences small effects, corresponds to parts of China, Europe, Japan, and the U.S. On average, the world is expected to experience welfare losses of 6% in our baseline scenario.[38]

Figure 9 presents a scatter-plot of the welfare losses from global warming and real GDP per capita in the year 2000. The colors indicate different areas of the world, and the size of each dot represents the population of the cell also in 2000. The dashed black line presents the population-weighted linear relationship.

---

[36]In Supplementary Materials Section G.3 we present robustness exercises with respect to the discount factor.

[37]Global average welfare losses are calculated as the population weighted average of the relative present discounted value of utility in the baseline case relative to the counterfactual without global warming.

[38]Figure 28 in Appendix E.1 presents the losses in the present discounted value of real GDP. The spatial distribution and shape of the histogram are similar than those for welfare. However, the largest losses (10%), largest gains (3%) and standard deviation (0.02) are smaller than those of welfare. This is natural, since the welfare calculation includes the effect of temperature on amenities which intensifies the magnitude and dispersion of climate damages around the world. Furthermore, as we showed in Figure 7, global warming makes people move to locations that have, at least initially, relatively low fundamental amenities.
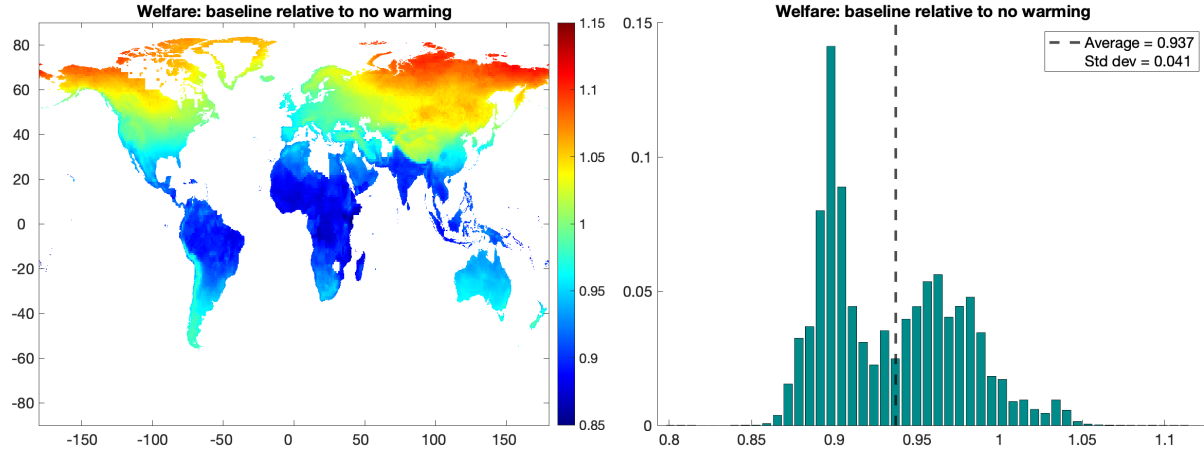
Figure 8: Welfare losses due to global warming.

The linear slope indicates that, on average, locations with double the level of real GDP exhibit welfare losses from global warming that are roughly 1.5% lower. Hence, the poorest regions of the world, mainly located in Sub Saharan Africa and South East Asia, are expected to undergo the highest warming losses. OECD countries, with initially high income, are much less affected. China, with its vast and heterogeneous territory, displays regions with both high and low levels of welfare losses. Our results show that global warming will exacerbate the already large spatial inequality in the world.
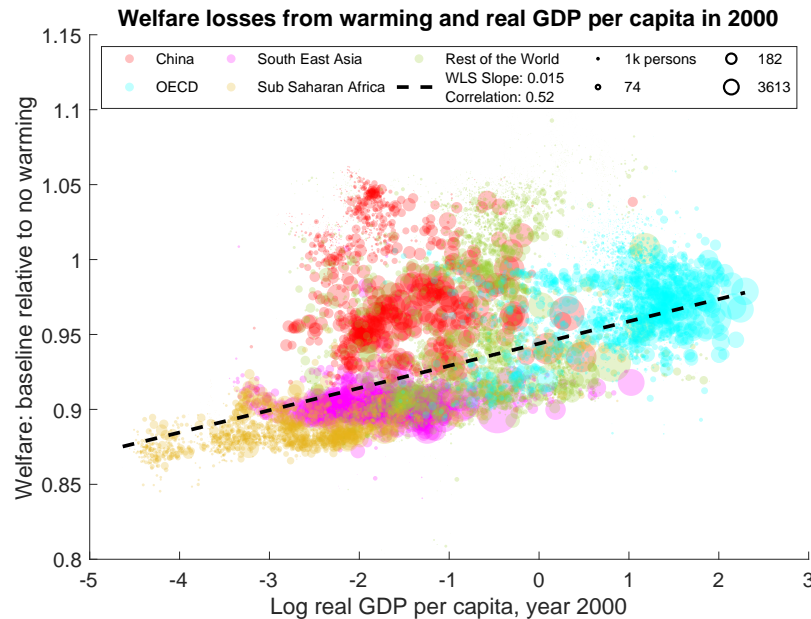
Figure 9: Correlation between welfare losses and initial real GDP per capita.

It is interesting to decompose the effect of global warming by their source: amenity or productivity effects. In Appendix E.2 we perform such exercise and show that both effects are commensurate, although

the effect on amenities is much more heterogeneous. Of course, as we underscore in the next subsection, there is tremendous uncertainty about the exact level of these aggregate losses, although there is much less uncertainty about their spatial distribution.

4.4   Uncertainty

Our baseline scenario is computed using the logistic fit of the damage coefficients by temperature bin that we estimated in Section 3.2. As we discussed there, although we find evidence of significant temperature effects on amenities and productivity for locations with low and high temperatures, the estimation also yields large confidence intervals. The implied uncertainty embedded in the imprecise estimation of the damage functions translates in uncertainty about the effect that global warming will have on the economy. Of course, we are also uncertain about many of the other parameters of the model as well as about the model specification itself. However, Desmet et al., 2018 perform a number of back-casting exercises that lend credibility to the long-run performance of the economic model and its parametrization. Hence, here we restrict attention to the parametric uncertainty related to the imprecision in the estimation of the coefficients of the temperature damage functions for fundamental amenities and productivities.

Figure 10 presents the global average welfare losses over time in the baseline estimation (solid line) and for damage functions determined by the logistic fit of the boundaries of the different confidence intervals, namely 60%, 80%, 90% and 95%. Baseline damages intensify through the next two centuries, achieving a peak of 10%. Figure 10 illustrates how uncertain we are about the aggregate effect of global warming. The 95% confidence interval includes catastrophic welfare losses of as much as 20% by 2200 but also small global gains. Confidence intervals widen during the first two centuries as temperature rises, but shrink slightly when temperature starts declining.

The large uncertainty on aggregate losses does not translate into large uncertainty on local relative effects. Figure 10 displays the spatial distribution of welfare for the baseline case, the lower 95% confidence interval (i.e. the *worst-scenario*), and the upper 95% confidence interval (i.e. the *best-scenario*). The level of the distributions are clearly different. In the worst-scenario, only a negligible part of the population, 0.003%, experiences welfare gains. Whereas, in the best-scenario, 50.51% of the population undergoes welfare losses. However, the range, standard deviation, and shape of local losses remains roughly similar in all scenarios.[39] This is the sense in which we are less uncertain about relative local effects than about the magnitude of average effects. In the baseline, as well as the best- and worst-scenarios, the losers from global warming are primarily Central America, Brazil, Africa and India.[40]

---

[39] As we move to more optimistic scenarios, the standard deviation of welfare losses tends to augment slightly. This is the result of the shape of the damage functions on amenities and productivities across different confidence levels. In the most pessimistic scenario, marginal damages are roughly constant in the hottest bins while they decline in the most optimistic scenario, as shown in Figure 2.

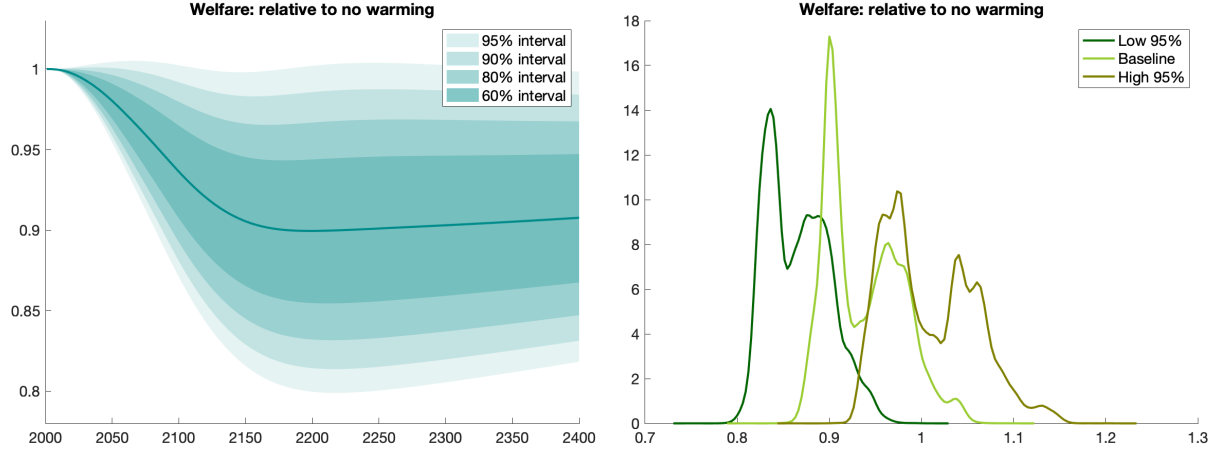[40] Appendix E.1 displays the real GDP losses by uncertainty level.

Figure 10: Welfare losses by uncertainty level.

5 Adaptation

In the model we have put forward, agents react to rises in temperatures by moving, trading, and investing in different locations on Earth. These adaptation mechanisms help agents cope with experienced changes in the economic environment. Modelling the effect of global warming using a micro-founded general equilibrium framework that incorporates these mechanisms allows us to incorporate and assess the role of economic adaptation in shaping the economy's response. Of course, the extent to which agents use these adaptation channels depends on their cost. In this section, we evaluate the importance of the different mechanisms by comparing our baseline results with counterfactual scenarios where agents face higher migration, trade, or innovation costs.[41]

5.1 Migration

In the baseline scenario we set local migration costs such that the model accounts exactly for the distribution of local population changes between 2000 and 2005. Here, we consider global increases in migration costs by raising the migration cost function $m_2(\cdot)$ to a power $\vartheta > 1$, which corresponds to a proportional increase of size $\vartheta - 1$ if $m_2(\cdot)$ is close enough to one. Larger migration frictions imply that agents migrate less to the most productive locations, leading to lower incomes, energy and fossil fuel use, CO_2 emissions, and temperatures. Lower temperatures, in turn, increase productivity and amenities in some locations. In addition, since higher migration costs imply that agents remain in poor locations, and overall incomes are lower, natality rates are higher, leading to increases in population, aggregate fossil fuel consumption, and temperatures. These feedback mechanisms make the effect of migration costs quite complex.

Figure 11 presents the welfare impact of higher migration costs across space and over time. The left panel presents relative welfare with and without global warming in the baseline case with respect to rela-

---

[41]Supplementary Materials Section I provides additional details and results.

29

tive welfare with and without global warming in the case with log migration cost that are 25% higher (the diff-and-diff effect of migration costs on the effect of temperature). Red areas in the figure represent locations where larger migration costs make global warming more costly (namely, the baseline better). Clearly, higher migration costs hurt northern regions that tend to benefit from temperature rises by attracting migrants. In contrast, it benefits regions in Latin America, and especially Oceania, that are relatively sparsely populated and, in the baseline scenario, suffer large population losses and the correspondingly lower investments in technology due to global warming. Higher migration frictions make these places keep more of their population, and associated technology growth, as temperatures rise over time. Perhaps surprisingly, Central Africa, India, and China, all have larger losses from global warming when migration costs are large. The reason is that their high density and low income imply that much of the resulting increases in population concentrate there, leading to higher productivity growth but also lower amenities due to congestion.[42] The latter effect dominates in dense developing countries, but the former dominates in sparsely populated regions, like Oceania.

The right panel of Figure 11 presents the evolution of average welfare losses over time. The dashed lines present the overall effects for two different magnitudes of ϑ. To help with the interpretation, we also present scenarios (solid lines) where we keep the evolution of temperature and population as in the baseline scenario. These exercises abstract from the feedback effect of temperatures and population on the economy. Comparing dashed and solid lines reveals the importance of these feedback effects. In the short-run, higher migration costs reduce economic activity leading to smaller temperature increases and smaller losses. In the long-run, in contrast, increases in population lead to more fossil fuel use, higher temperatures, and larger losses. Overall, larger migration costs lead to significantly larger losses from global warming. 25% larger migration costs lead to losses from temperature change that are about a third larger by 2200. Over time, these differences decline, since in all scenarios carbon reserves are eventually depleted.

These results show that migration is indeed an essential adaptation mechanism. One that is quantitatively important, but differentially so across regions in the world. Ultimately, the best way to adapt to global warming is for agents to migrate to regions that lose less or even gain from temperature increases. Many of these regions are sparsely populated today, due to their lack of amenities and productivity, but could be improved as temperatures rise and new migrants invest in them over the next centuries.

5.2 Trade

As with migration costs, we study the effect of global increases in commercial frictions that raise the bilateral iceberg trade costs $\varsigma(\cdot, \cdot)$ to some power $\vartheta > 1$. Appendix E.3 presents these results and shows that larger trade costs have only a small effect on the losses from global warming. To understand this result, remember that gravity in trade implies that most trade flows are very local. Because increases in temperatures are

---

[42]The implied increases in population that result from this large change in migration costs are as large as 5.4 billion people by 2150, stabilizing afterwards.
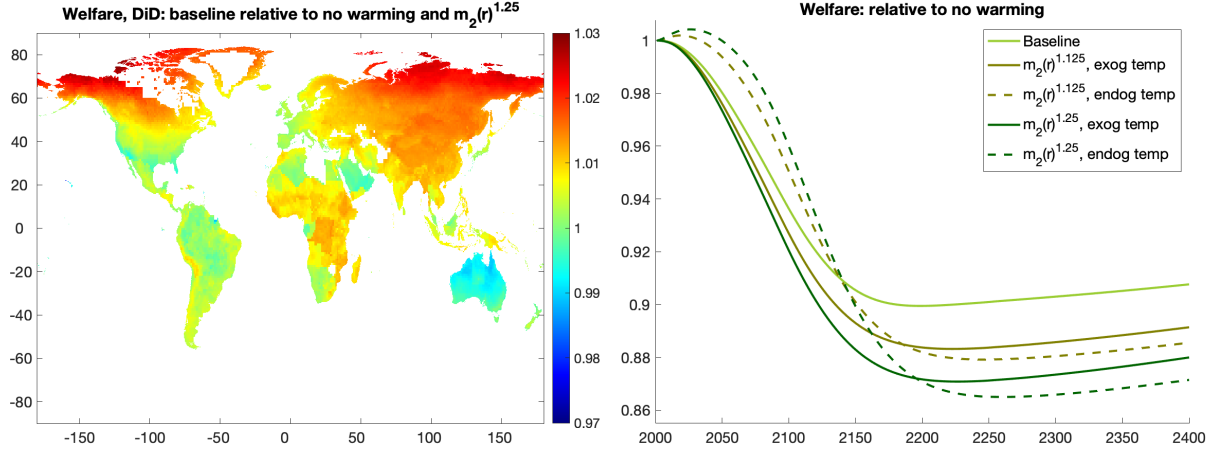
Figure 11: Welfare across different migration costs.

spatially correlated, areas that trade significantly with each other tend to experience similar shocks. Hence trade is not an effective adaptation mechanism in this model.[43]

5.3 Innovation

The final adaptation mechanism we study in this section is innovation. Firm investments respond to market size and allow a region's technology to grow relative to that of other regions. Innovation improves northern regions' productivity, as they become warmer and gain population. It also accelerates the relative losses of regions that get too warm and lose market size due to the implied lower productivity and lower amenities. We study here the effect of lowering γ_1 (or, equivalently, increasing ξ). Changes in these parameters amount to changing the returns or cost of innovation proportionally across locations. Larger costs of innovation reduce real GDP growth and, therefore, growth in CO_2 emissions, curbing the temperature path. As with trade and migration costs, the lower real GDP growth pushes upwards natality rates and global population.

Figure 12 presents the spatial and dynamic implications of lower innovation returns (or higher innovation costs). The left panel presents the diff-and-diff for the welfare consequences of global warming in the baseline relative to the exercise with high innovation costs. The spatial pattern of this measure is simpler than the one for the other mechanisms. The upmost northern regions are hurt more (benefited less) by global warming when innovation costs are higher. Developing these areas by improving their productivity and moving economic activity to the north becomes more costly. The same phenomenon is apparent in the upmost southern regions, including Oceania and the southern tip of South America and Africa.

The right panel of Figure 12 presents the dynamic evolution of the cost of global warming. In all cases, with and without feedback effects from temperature, larger innovation costs lead to smaller losses from

---

[43]Importantly, our work abstracts from trade across industries due to local comparative advantage. If temperature affects sectors differentially and therefore the comparative advantage of regions, trade can play a much more important role as an adaptation mechanism. See Desmet and Rossi-Hansberg, 2015, Nath, 2020 and Conte et al., 2020 for studies that develop this mechanism.

31

global warming. The reason is that larger innovation costs imply smaller benefits from density in locations that are eventually negatively affected by higher temperatures. In particular, Africa, India, and China experience lower technology growth and, therefore, attract less migrants from other locations. Given that these are the regions more affected by temperature rises, the average cost from this phenomenon declines. This effect builds up over time and is significant only after 2150. Once we incorporate the feedback effect through changes in the temperature and population paths, the lower temperature growth generates lower costs from global warming when innovation costs are larger even in the short-run.

These results illustrate the importance of studying the impact of adaptation mechanisms in a spatial model. The reason that higher innovation costs result in smaller costs from global warming is fundamentally spatial, as explained above. Overall, adaptation through innovation is an important mechanism, particularly in determining the spatial distribution of the welfare cost of global warming.
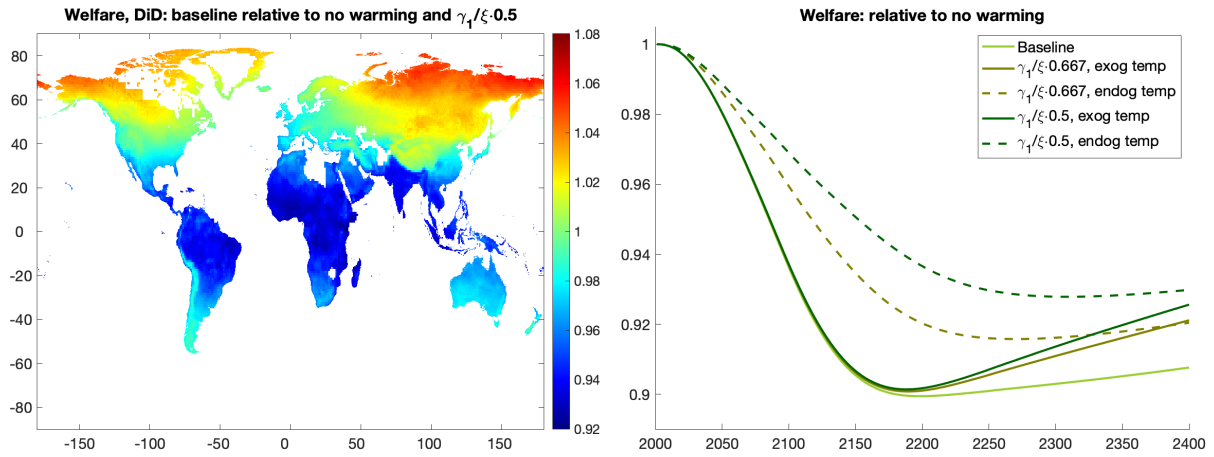

Figure 12: Welfare across different innovation costs.

6 Environmental Policies

Global warming constitutes a worldwide externality and so policy can potentially alleviate some of its negative economic impacts. Moreover, in the model we have proposed, there are local and global technological externalities, as well as congestion costs, all of which imply that the competitive equilibrium is not efficient. Hence, in this framework, achieving the first best would require a number of policies that address these other sources of inefficiencies as well. This is in general hard, since such policies would need local and global dynamic policies that are currently unknown and, therefore, neither proposed nor implemented. In fact, in our framework, the mechanisms that make the firm's innovation decision effectively static in the competitive equilibrium, do not imply the same for the planner's problem. Hence, solving for the optimal policy, even without considering global warming is, so far, beyond our capabilities. Thus, we proceed by evaluating some popular climate policies, rather than by designing optimal environmental policy.

A commonly proposed solution to the global carbon emission externality is to impose a global carbon tax, τ, to increase the cost of fossil fuels and discourage their use. This follows the standard Pigouvian logic of using taxes or subsidies to equate the social and private marginal cost of fossil fuels.[44] In the same spirit, we also consider a common and global clean energy subsidy, s, that reduces the marginal cost of renewable energy. Thus, the cost of energy per unit of land becomes $w_t(r)(1+\tau)\mathcal{Q}_t^f(r)e_t^{f,\omega}(r) + w_t(r)(1-s)\mathcal{Q}_t^c(r)e_t^{c,\omega}(r)$.[45] We assume that the balance of taxes and subsidies is taxed or rebated lump sum at each location. Because carbon taxes delay the depletion of the stock of fossil fuels on Earth, we also study the potential gains from carbon taxes when an abatement technology is forthcoming. Finally, although mostly relegated to the appendix, we study the effect of policies that increase the elasticity of substitution between fossil and clean energy; for example, by encouraging the use of electric rather than gasoline vehicles.

6.1 Carbon Taxes

Figure 13 displays the evolution of CO_2 emissions and global temperatures when considering carbon taxes of 50%, 100% and 200%, keeping clean energy subsidies at zero.[46] As expected, carbon taxes reduce current consumption of fossil fuels at impact. For instance, a tax of 200% diminishes carbon emissions by 60% with respect to the benchmark scenario in the initial period. However, as the economy grows and the productivity of energy production increases, CO_2 emissions rise. Eventually, though, extraction costs increase sharply, and the price of fossil fuels relative to clean energy rises, generating a decline in CO_2 emissions. Carbon taxes not only reduce initial emissions but they also delay the year and the magnitude of the peak in CO_2 emissions. For example, with a tax of 200% the peak is 2.53 $GtCO_2$ lower and occurs 36 years later than in the scenario with no carbon taxes.

In sum, the main effect of a carbon tax is to delay dirty energy consumption, by spreading its use over time; less current consumption but more future consumption. The more protracted path for CO_2 emissions has stark implications for the evolution of global temperatures: It *flattens* the temperature curve. A carbon tax of 200% leads to an evolution of average global temperature that is as much as 1.6°C lower in the first half of the 22nd century, peaks 46 years later at a temperature roughly 0.4°C lower, but eventually converges to the same temperature once the stock of carbon is depleted in both scenarios. This intertemporal CO_2 utilization pattern, governed in part by the convex cost of carbon extraction relative to clean energy, is essential in determining the effectiveness of carbon taxes. Carbon taxes tend to delay, not eliminate, the use of fossil fuels (even when the elasticity of substitution between fossil fuels and clean energy is rather large, $\epsilon = 1.6$, as in our calibration).

---

[44]See Hassler et al., 2019 for a modern treatment and quantification of Pigouvian logic applied to climate policy.

[45]As already imposed in the notation and although potentially superior, we leave for future research an analysis of spatially heterogeneous policies or policies that vary over time. Such analysis is certainly feasible in our framework.

[46]Given that the price of fossil fuels in the initial period is on average 73 usd/tCO_2, a carbon tax of 50% equals 37 usd/tCO_2, similar to the maximum in the E.U. Emissions Trading Scheme; a carbon tax of 200% equals 146 usd/tCO_2, close to the Swedish tax.
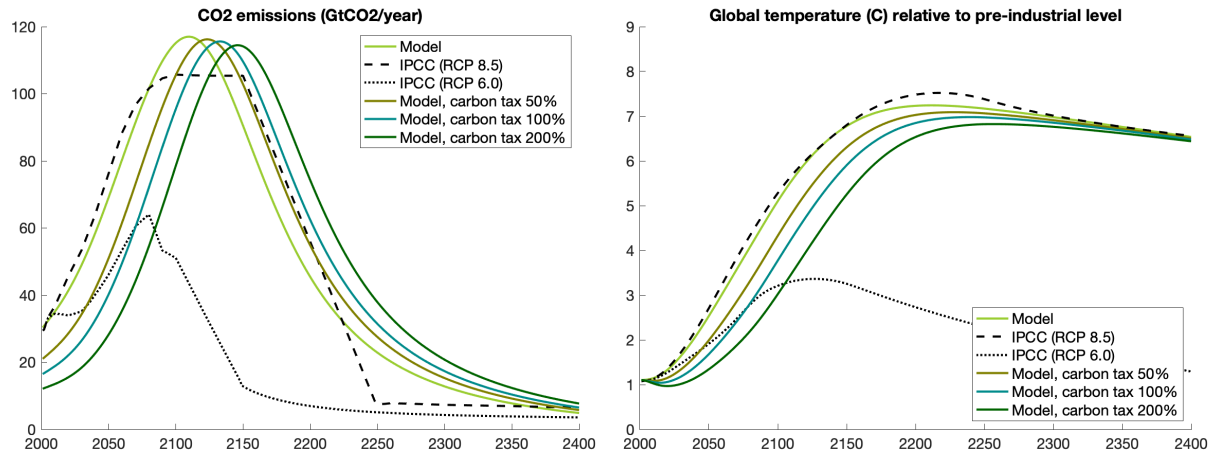
Figure 13: CO$_2$ emissions and global temperature under different carbon taxes.

Figure 14 presents global real GDP and welfare for each tax level relative to the baseline scenario with no environmental policy. At impact, the implementation of a uniform proportional carbon tax reduces the use of fossil fuels, which makes energy more expensive overall, and thus reduces income and welfare. The decline in welfare is less pronounced than that of real GDP, as welfare depends on real income which incorporates the lump sum transfer. Furthermore, initially, carbon taxes reduce firm innovation since potential current profits decline, and therefore reduce the growth rate of the economy. Of course, as time evolves, the flattening of the temperature curve has beneficial effects on amenities and productivities, leading to higher real income and welfare, as well as higher growth rates. Eventually, the curves in Figure 14 cross one, meaning that the implementation of the carbon tax is, on average, beneficial after that period. In the long-run, real GDP and welfare keep increasing due to a larger global population.[47]
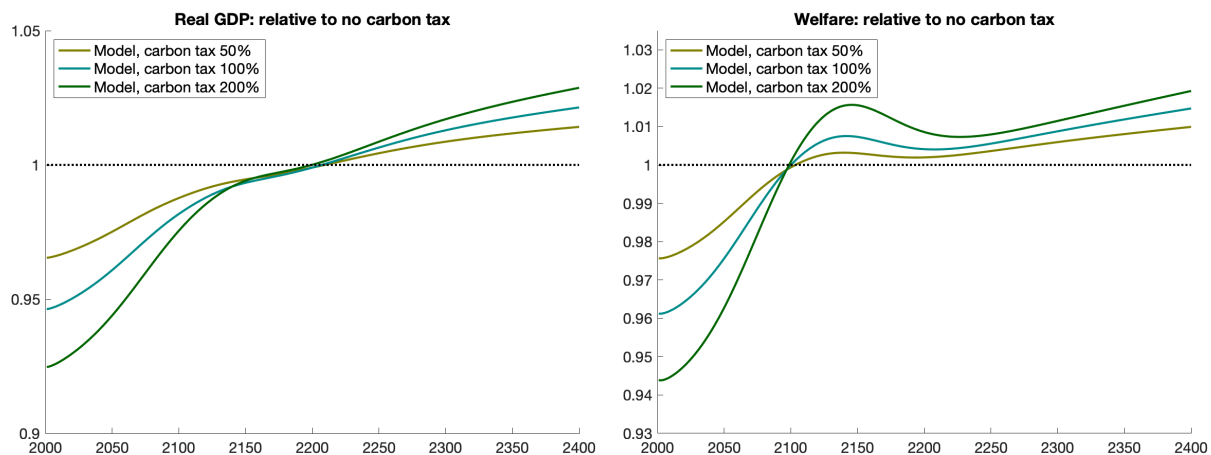

Figure 14: Real GDP and welfare under different carbon taxes.

---

[47]In the short-run, the implementation of carbon taxes reduces global income, augmenting natality rates. Consequently, global population is higher when we impose CO$_2$ levies.

The implementation of carbon taxes generates an intertemporal trade-off with short-term costs and long-term benefits. This naturally implies that any overall assessment of carbon policies depends on the chosen discount factor. Table 1 presents the global average real GDP and welfare losses from global warming across different tax levels and discount factors, with respect to a scenario in which environmental policies are absent. Our choice of discount factor is limited by the balanced-growth-path growth rate. In order to obtain finite present discounted values of welfare and real GDP for all future paths, we chose a baseline discount factor of $\beta = 0.965$.[48] For this value, carbon taxes are not desirable today. The largest present discounted value of real GDP or welfare in Table 1 is obtained for $\tau = 0$. However, if we increase the discount factor to $\beta = 0.969$, a carbon tax of 200% or more maximizes welfare and real GDP. This large sensitivity of the optimal carbon tax is natural given the path shown in Figure 14 and cautions us not to rely too heavily on PDV statistics that depend on specific values of the discount factor. Ultimately, the discount factor used determines the policy-maker's preferences for the welfare of current versus future generations.

	PDV of real GDP			Welfare		
	BGP gr	β=0.965	β=0.969	BGP gr	β=0.965	β=0.969
τ=0%	3.076%	1	1	2.971%	1	1
τ=50%	3.081%	0.993	1.028	2.974%	0.998	1.012
τ=100%	3.083%	0.990	1.044	2.977%	0.997	1.019
τ=200%	3.086%	0.986	1.063	2.979%	0.996	1.026

Table 1: PDV of real GDP and welfare gains for different carbon taxes and discount factors.

The impact of carbon taxes is not only heterogeneous over time, but also across space. Figure 15 compares the welfare impact across locations of a carbon tax of 200%. As expected, the regions that are projected to gain from imposing the carbon tax are the regions that were projected to lose the most from global warming in Figure 8. Welfare gains from the tax range from 3% in South America, Central Africa, and South Asia; to losses of 6% in the coldest places, those expected to gain from higher temperatures. Two interesting exceptions are the Middle East and Algeria. They obtain relatively low gains from the global carbon tax, compared to their projected losses from global warming. The economy of those regions relies heavily on fossil fuel, so a carbon tax generates large distortions in production.[49]

6.2 Abatement

We have shown that the main effect of carbon taxes is to delay the use of fossil fuels, without affecting the total stock of carbon released to the atmosphere, thereby *flattening* the evolution of global temperatures. Of course, delaying CO_2 emissions, and flattening the temperature curve can be extremely beneficial if, at some

---

[48]We also consider a value of $\beta = 0.969$ that, given the balanced-growth-path growth rate of 0.03, implies that we value the relative gains in all periods similarly.

[49]Supplementary Materials Section H.2 evaluates the role of carbon taxes in the worst-scenario for climate damages and J.1 develops further the discussion on the temporal and spatial effects of carbon taxes.
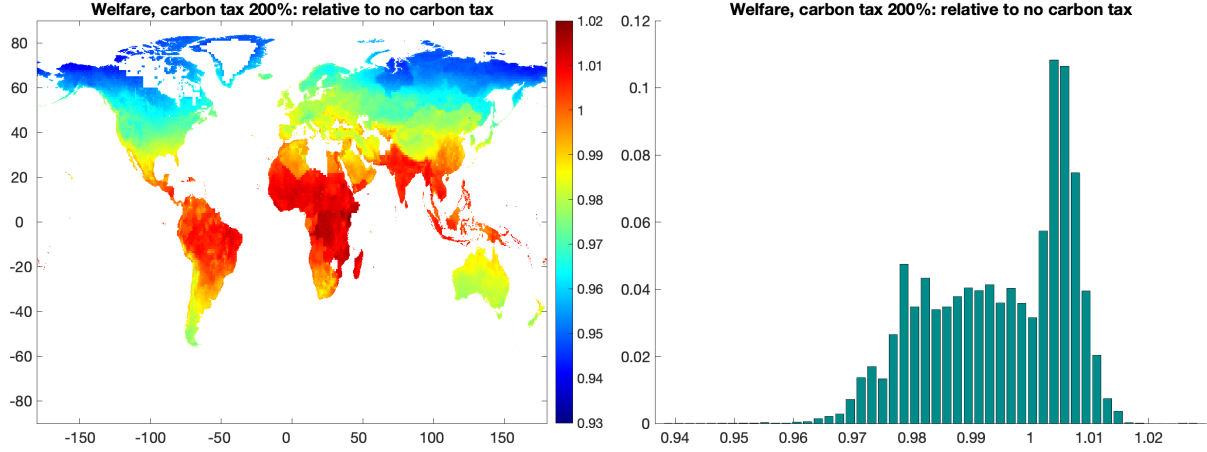
Figure 15: Local welfare effects of a carbon tax of 200% with a discount factor of $\beta = 0.965$.

point, humans invent an abatement technology that allows us to use fossil fuels without emitting CO_2 into the atmosphere (or capture CO_2 in the atmosphere through geoengineering). An abatement technology would eliminate, or reduce, the negative externality that results from the use of fossil fuels.[50] Since an abatement technology *cures* the economy from emitting CO_2 emissions after its invention, delaying the use of fossil fuels and flattening the temperature curve can become a very effective strategy, one that does affect total CO_2 emissions.[51] This is why carbon taxes and abatement technologies are complementary policies.

To illustrate this argument, here we consider a simple case in which an abatement technology becomes available at no cost in the year 2100.[52] Table 2 shows global average PDV of real GDP and welfare gains under the implementation of carbon taxes when an abatement technology becomes available in 2100. When comparing it with Table 1, we observe that, when an abatement technology is forthcoming, large carbon taxes are beneficial for the economy for both discount factors. With $\beta = 0.969$, the impact of this policy is very large and can yield gains in real GDP of 8% and in welfare of 7%. These results illustrate how the abatement technology and carbon taxes are complementary policies. That is, a forthcoming abatement technology makes carbon taxes a much more effective policy. In fact, this combination of policies is the most effective one we have found in our analysis.[53]

---

[50]More precisely, if we denote by $\nu_t(r)$ the share of CO_2 emissions abated in region r at period t, the evolution of atmospheric CO_2, given by equation (14), becomes $S_{t+1} = S_{\text{pre-ind}} + \sum_{\ell=1}^{\infty}(1 - \delta_\ell)\left(E_{t+1-\ell}^{\prime f} + E_{t+1-\ell}^x\right)$, where $E_t^{\prime f} = \int_S \int_0^1 (1 - \nu_t(v))\, e_t^{f,\omega}(v) H(v) d\omega dv$. The law of motion of fossil fuel extraction is still given by equation (9).

[51]The interaction of carbon taxes and an abatement technology within our framework is analogous to lockdowns and the introduction of a vaccine in a pandemia: a lockdown delays current infections at an economic cost, but reduces total infections only if a vaccine is forthcoming.

[52]As in Nordhaus, 2015, we could alternatively assume that preventing a share $\nu_t(r)$ of CO_2 emissions in region r at period t costs a fraction, $(1 - \varpi_{1,t}(r) \cdot \nu_t(r)^{\varpi_2})$, of household's income. We could assume that $\varpi_{1,t}(r)$ declines over time to reflect the widening menu of technological alternatives and that it varies across regions depending on their carbon intensity. The parameter ϖ_2 controls the degree of non-linearity in costs. At a global scale, Nordhaus, 2015 considers $\varpi_{1,t} = 0.0334$ and $\varpi_2 = 2$. Of course, because of well-understood free-rider problems, the abatement policy would still need to be imposed by a global agreement.

[53]Appendix E.4 presents the evolution of CO_2, temperature, real GDP and welfare with carbon taxes and an abatement technology

	PDV of real GDP			Welfare		
	BGP gr	β=0.965	β=0.969	BGP gr	β=0.965	β=0.969
τ=0%	3.076%	1	1	2.971%	1	1
τ=50%	3.081%	0.997	1.044	2.974%	1.004	1.032
τ=100%	3.083%	0.996	1.072	2.977%	1.008	1.053
τ=200%	3.086%	0.995	1.107	2.979%	1.011	1.080

Table 2: PDV of real GDP and welfare gains for different carbon taxes and discount factors with an abatement technology introduced in 2100.

6.3 Clean Energy Subsidies

Clean energy subsidies have two countervailing effects. First, they make clean energy less expensive, thereby creating incentives for agents to produce energy with clean sources. The magnitude of this effect is governed by the elasticity of substitution in energy production which we set at $\epsilon = 1.6$, as well as by the initial relative productivity of clean energy, which is heterogeneous across locations and chosen to match relative energy use. Second, clean energy subsidies reduce the price of the energy composite. This additional effect is also governed by the share of clean energy in the energy composite, which is initially about 11%. Figure 16 shows that in the quantitative model we have put forward, these two effects roughly cancel out. Subsidies as large as 75% yield only a minuscule reduction in CO_2 emissions and temperatures. We conclude that clean energy subsidies are not an effective way to combat global warming.[54]
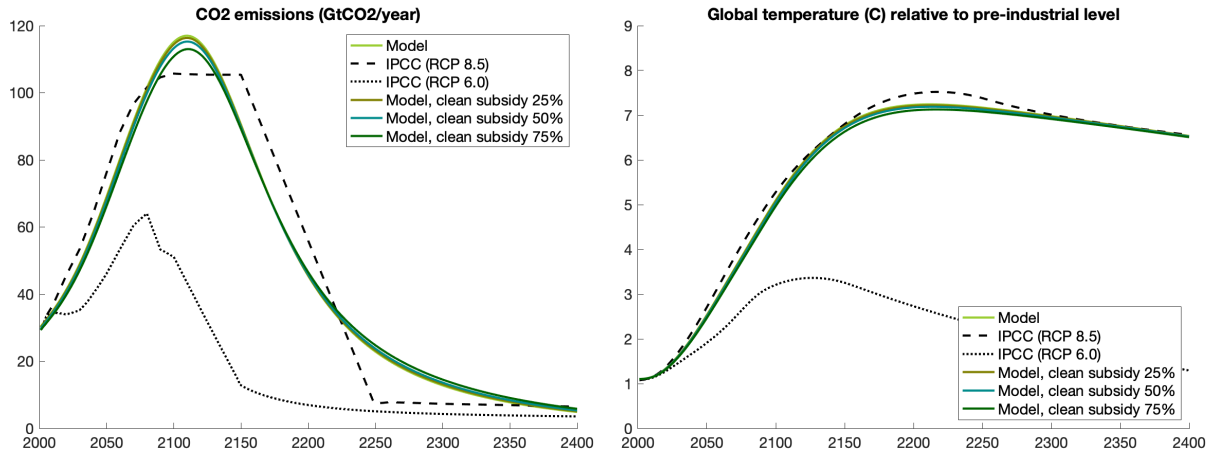

Figure 16: CO_2 emissions and global temperature for different clean energy subsidies.

that appears in 2100. Supplementary Materials Sections J.3 and J.4 show exercises with alternative measurements and timing.

[54]Appendix E.5 presents additional results on clean energy subsidies including welfare effect across locations and over time, as well as their impact on welfare. Supplementary Materials Section J.2 evaluates the joint effect of carbon taxes and clean energy subsidies.

7 Conclusions

The goal of this paper is to propose a novel geographically detailed integrated assessment model of the effect of global warming on economic outcomes and welfare. The large heterogeneity in projected temperature changes across regions of the world, and the heterogeneous effects of these changes across locations and over time, underscore the need for assessment models that feature a realistic geography with many locations and agents that make decisions to live, move, trade, and invest across them. The micro-founded spatial dynamic model that forms the core of the proposed framework features local population growth, costly migration and trade, endogenous technology investments, as well as local fossil and energy use and its impact on local temperature and, correspondingly, its heterogeneous effect on amenities and productivity. Thus, the proposed model allows us to incorporate a number of endogenous adaptation mechanisms that have been mostly absent in assessment models so far. Furthermore, it allows us to estimate the impact of global warming on economic outcomes by explicitly aggregating the dynamic effects on local outcomes.

When we quantify the proposed economic model for the world economy at a fine level of spatial resolution we obtain local effects of global warming on welfare that range from losses of 20% to gains of 12%. Our results show that global warming will increase spatial inequality since, on average, countries with double the level of current real income experience welfare losses that are about 1.5% lower. We find that the distribution of relative losses across locations is fairly robust to the damage functions we estimate but, in contrast, our estimates imply large uncertainty about overall welfare losses. The 95% confidence interval of average welfare losses in 2200 ranges from losses of 20% to small gains. This wide range reflects that, although the data allows us to estimate significant effects from temperature on fundamental productivity and amenities, the estimates are still imprecise given that the rise in temperatures has only recently started to affect economic outcomes more severely.

The model we propose can be used as a workhorse model to study a number of additional dimensions of climate change as well as alternative policies. A few examples are coastal flooding, as analyzed in Desmet et al., 2021, the increased likelihood of extreme weather events, or the political economy of climate policy as determined by the spatially heterogeneous effects we have uncovered.

Inevitably, our model abstracts from some important aspects. First, the model we propose does not introduce multiple sectors and the effect of temperature on relative sectoral productivity. Conte et al., 2020 show how this can be done in a related framework. Second, we have abstracted from purposeful innovations in green, fossil, and abatement technologies. In our model these technologies only evolve through spillovers from other innovations. Third, the model we develop gains tractability from assuming an economic structure in which anticipatory effects from future shocks or policy only affect land rents, but do not affect allocations. That is, future events do not affect the spatial evolution of the economy. Incorporating anticipatory effects in rich spatial model with endogenous investments and growth is still infeasible, although potentially interesting. Of course, the importance of anticipatory effects to evaluate

protracted phenomena, like global warming, is debatable.

Global warming presents a daunting challenge for humanity. Designing the best tools to address it requires modern micro-founded economic models that incorporate multiple forms of adaptation and the rich spatial heterogeneity of the world. Our hope is that this paper contributes to this effort.

References

Acemoglu, D., Aghion, P., Barrage, L., & Hemous, D. (2019). *Climate change, directed innovation, and energy transition: The long-run consequences of the shale gas revolution.*

Acemoglu, D., Aghion, P., Bursztyn, L., & Hemous, D. (2012). The environment and directed technical change. *American Economic Review*, *102*(1), 131–66. https://doi.org/10.1257/aer.102.1.131

Acemoglu, D., Akcigit, U., Hanley, D., & Kerr, W. (2016). Transition to clean technology. *Journal of Political Economy*, *124*(1), 52–104. https://doi.org/10.1086/684511

Albouy, D., Graf, W., Kellogg, R., & Wolff, H. (2016). Climate amenities, climate change, and american quality of life. *Journal of the Association of Environmental and Resource Economists*, *3*(1), 205–246. https://doi.org/10.1086/684573

Allen, T., & Arkolakis, C. (2014). Trade and the topography of the spatial economy. *The Quarterly Journal of Economics*, *129*(3), 1085–1140. https://doi.org/10.1093/qje/qju016

Anthoff, D., & Tol, R. (2014). The climate framework for uncertainty, negotiation and distribution (fund), technical description, version 3.9.

Auffhammer, M. (2018). Quantifying economic damages from climate change. *Journal of Economic Perspectives*, *32*(4), 33–52. https://doi.org/10.1257/jep.32.4.33

Balboni, C. (2019). *In harm's way? infrastructure investments and the persistence of coastal cities* (Doctoral dissertation).

Barrage, L. (2019). Optimal Dynamic Carbon Taxes in a Climate–Economy Model with Distortionary Fiscal Policy. *The Review of Economic Studies*, *87*(1), 1–39. https://doi.org/10.1093/restud/rdz055

Barreca, A., Clay, K., Deschenes, O., Greenstone, M., & Shapiro, J. S. (2016). Adapting to climate change: The remarkable decline in the us temperature-mortality relationship over the twentieth century. *Journal of Political Economy*, *124*(1), 105–159. https://doi.org/10.1086/684582

Bauer, N., Hilaire, J., Brecha, R. J., Edmonds, J., Jiang, K., Kriegler, E., Rogner, H.-H., & Sferra, F. (2017). Data on fossil fuel availability for shared socioeconomic pathways. *Data in Brief*, *10*, 44–46. https://doi.org/https://doi.org/10.1016/j.dib.2016.11.043

Baylis, P. (2020). Temperature and temperament: Evidence from twitter. *Journal of Public Economics*, *184*, 104161. https://doi.org/https://doi.org/10.1016/j.jpubeco.2020.104161

Becker, G. (1960). An economic analysis of fertility. *Demographic and economic change in developed countries* (pp. 209–240). National Bureau of Economic Research, Inc. https://EconPapers.repec.org/RePEc:nbr:nberch:2387

Benveniste, H., Oppenheimer, M., & Fleurbaey, M. (2020). Effect of border policy on exposure and vulnerability to climate change. *Proceedings of the National Academy of Sciences*. https://doi.org/10.1073/pnas.2007597117

Bernard, A. B., Eaton, J., Jensen, J. B., & Kortum, S. (2003). Plants and productivity in international trade. *American Economic Review*, *93*(4), 1268–1290. https://doi.org/10.1257/000282803769206296

Bosetti, V., Massetti, E., & Tavoni, M. (2007). *The WITCH Model. Structure, Baseline, Solutions* (Climate Change Modelling and Policy Working Papers No. 12064). Fondazione Eni Enrico Mattei (FEEM). https://doi.org/10.22004/ag.econ.12064

Boucher, O., & Reddy, M. (2008). Climate trade-off between black carbon and carbon dioxide emissions. *Energy Policy*, *36*(1), 193–200. https://EconPapers.repec.org/RePEc:eee:enepol:v:36:y:2008:i:1:p:193-200

BP. (2019). Bp statistical review of world energy. https://doi.org/https://www.bp.com/en/global/corporate/energy-economics/statistical-review-of-world-energy.html

Burke, M., Hsiang, S. M., & Miguel, E. (2015a). Climate and conflict. *Annual Review of Economics*, *7*(1), 577–617. https://doi.org/10.1146/annurev-economics-080614-115430

Burke, M., Hsiang, S. M., & Miguel, E. (2015b). Global non-linear effect of temperature on economic production. *Nature*, *527*, 235–239.

Carleton, T. A., Jina, A., Delgado, M. T., Greenstone, M., Houser, T., Hsiang, S. M., Hultgren, A., Kopp, R. E., McCusker, K. E., Nath, I. B., Rising, J., Rode, A., Seo, H. K., Viaene, A., Yuan, J., & Zhang, A. T. (2020). *Valuing the global mortality consequences of climate change accounting for adaptation costs and benefits* (Working Paper No. 27599). National Bureau of Economic Research. https://doi.org/10.3386/w27599

Carlino, G. A., Chatterjee, S., & Hunt, R. M. (2007). Urban density and the rate of invention. *Journal of Urban Economics*, *61*(3), 389–419. https://doi.org/https://doi.org/10.1016/j.jue.2006.08.003

Carrea, L., Embury, O., & Merchant, C. J. (2015). Datasets related to in-land water for limnology and remote sensing applications: Distance-to-land, distance-to-water, water-body identifier and lake-centre coordinates. *Geoscience Data Journal*, *2*(2), 83–97. https://doi.org/10.1002/gdj3.32

Colella, F., Lalive, R., Sakalli, S. O., & Thoenig, M. (2019). *Inference with arbitrary clustering*.

Conley, T. (1999). Gmm estimation with cross sectional dependence. *Journal of Econometrics*, *92*(1), 1–45. https://doi.org/https://doi.org/10.1016/S0304-4076(98)00084-0

Conte, B., Desmet, K., Krisztián, D., & Rossi-Hansberg, E. (2020). *Local sectoral specialization in a warming world* (tech. rep.).

Correia, S. (2016). *Linear models with high-dimensional fixed effects: An efficient and feasible estimator* (tech. rep.) [Working Paper].

Costinot, A., Donaldson, D., & Smith, C. (2016). Evolving Comparative Advantage and the Impact of Climate Change in Agricultural Markets: Evidence from 1.7 Million Fields around the World. *Journal of Political Economy*, *124*(1), 205–248. https://doi.org/10.1086/684719

Crippa, M., Guizzardi, D., Muntean, M., Olivier, J., Schaaf, E., Solazzo, E., & Vignati, E. (2019). *Fossil co2 and ghg emissions of all world countries*.

Dell, M., Jones, B. F., & Olken, B. A. (2012). Temperature shocks and economic growth: Evidence from the last half century. *American Economic Journal: Macroeconomics*, *4*(3), 66–95. https://doi.org/10.1257/mac.4.3.66

Dell, M., Jones, B. F., & Olken, B. A. (2014). What do we learn from the weather? the new climate–economy literature. *Journal of Economic Literature*, *52*(3), 740–798. http://www.jstor.org/stable/24434109

Delventhal, M. J., Fernández-Villaverde, J., & Guner, N. (2019). Demographic transitions across time and space.

Deschênes, O., & Greenstone, M. (2007). The economic impacts of climate change: Evidence from agricultural output and random fluctuations in weather. *American Economic Review*, *97*(1), 354–385. https://doi.org/10.1257/aer.97.1.354

Desmet, K., Kopp, R. E., Kulp, S. A., Nagy, D. K., Oppenheimer, M., Rossi-Hansberg, E., & Strauss, B. H. (2021). Evaluating the economic cost of coastal flooding. *American Economic Journal: Macroeconomics*.

Desmet, K., Nagy, D., & Rossi-Hansberg, E. (2018). The geography of development. *Journal of Political Economy*, *126*(3), 903–983. https://doi.org/10.1086/697084

Desmet, K., & Rappaport, J. (2017). The settlement of the United States, 1800–2000: The long transition towards Gibrat's law. *Journal of Urban Economics*, *98*(100), 50–68. https://doi.org/10.1016/j.jue.2015.03.004

Desmet, K., & Rossi-Hansberg, E. (2014). Spatial development. *American Economic Review*, *104*(4), 1211–43. https://doi.org/10.1257/aer.104.4.1211

Desmet, K., & Rossi-Hansberg, E. (2015). On the spatial economic impact of global warming. *Journal of Urban Economics*, *88*(100), 16–37. https://EconPapers.repec.org/RePEc:eee:juecon:v:88:y:2015:i:c:p:16-37

Dietz, S., & Lanz, B. (2020). *Can a growing world be fed when the climate is changing?* (Tech. rep.).

Eaton, J., & Kortum, S. (2002). Technology, geography, and trade. *Econometrica*, *70*(5), 1741–1779. http://www.jstor.org/stable/3082019

Etminan, M., Myhre, G., Highwood, E. J., & Shine, K. P. (2016). Radiative forcing of carbon dioxide, methane, and nitrous oxide: A significant revision of the methane radiative forcing. *Geophysical Research Letters*, *43*(24), 12, 614–12, 623. https://doi.org/10.1002/2016GL071930

Forster, P., Ramaswamy, V., Artaxo, P., Berntsen, T., Betts, R., Fahey, D., Haywood, J., Lean, J., Lowe, D., Myhre, G., Nganga, J., Prinn, R., Raga, G., Schulz, M., Dorland, R., Bodeker, G., Boucher, O., Collins, W., Conway, T., & Whorf, T. (2007). Changes in atmospheric constituents and in radiative forcing.

Fried, S. (2019). *Seawalls and stilts: A quantitative macro study of climate adaptation* (2019 Meeting Papers No. 898). Society for Economic Dynamics. https://EconPapers.repec.org/RePEc:red:sed019:898

Gaedicke, C., Franke, D., Ladage, S., Lutz, R., Pein, M., Rebscher, D., Schauer, M., Schmidt, S., & von Goerne, G. (2020). *Data and developments concerning german and global energy supplies* (tech. rep.).

Golosov, M., Hassler, J., Krusell, P., & Tsyvinski, A. (2014). Optimal taxes on fossil fuel in general equilibrium. *Econometrica*, *82*(1), 41–88. https://doi.org/10.3982/ECTA10217

Graff-Zivin, J., & Neidell, M. (2014). Temperature and the allocation of time: Implications for climate change. *Journal of Labor Economics*, *32*(1), 1–26. http://www.jstor.org/stable/10.1086/671766

Greenwood, J., Hercowitz, Z., & Krusell, P. (1997). Long-run implications of investment-specific technological change. *American Economic Review*, *87*(3), 342–62. https://EconPapers.repec.org/RePEc:aea:aecrev:v:87:y:1997:i:3:p:342-62

Hassler, J., Krusell, P., & Olovsson, C. (2018). The consequences of uncertainty: Climate sensitivity and economic sensitivity to the climate. *Annual Review of Economics*, *10*(1), 189–205. https://doi.org/10.1146/annurev-economics-080217-053229

Hassler, J., Krusell, P., & Olovsson, C. (2019). *Directed technical change as a response to natural-resource scarcity* (Working Paper Series No. 375). Sveriges Riksbank (Central Bank of Sweden). https://ideas.repec.org/p/hhs/rbnkwp/0375.html

Hope, C., & Hope, M. (2013). The social cost of co 2 in a low-growth world. *Nature Climate Change*, *3*, 722–724.

IEA. (2019). *World energy outlook 2019*. https://doi.org/https://doi.org/https://doi.org/10.1787/caf32f3b-en

IEA. (2020). *Co2 emissions from fuel combustion* (tech. rep.) [Database Documentation].

IPCC. (2007). Climate change 2007: Synthesis report. contribution of working groups i, ii and iii to the fourth assessment report of the intergovernmental pan on climate change. *Cambridge University Press*.

IPCC. (2013). Climate change 2013: The physical science basis. contribution of working group i to the fifth assessment report of the intergovernmental panel on climate change. *Cambridge University Press*.

Joos, F., Roth, R., Fuglestvedt, J. S., Peters, G. P., Enting, I. G., von Bloh, W., Brovkin, V., Burke, E. J., Eby, M., Edwards, N. R., Friedrich, T., Frölicher, T. L., Halloran, P. R., Holden, P. B., Jones, C., Kleinen, T., Mackenzie, F. T., Matsumoto, K., Meinshausen, M., . . . Weaver, A. J. (2013). Carbon dioxide and climate impulse response functions for the computation of greenhouse gas metrics: A multi-model analysis. *Atmospheric Chemistry and Physics*, *13*(5), 2793–2825. https://doi.org/10.5194/acp-13-2793-2013

Krusell, P., & Smith, A. (2017). *Climate change around the world* (2017 Meeting Papers No. 1582). Society for Economic Dynamics. https://EconPapers.repec.org/RePEc:red:sed017:1582

Kummu, M., Taka, M., & Guillaume, J. (2018). Gridded global datasets for gross domestic product and human development index over 1990–2015. *Scientific Data*, *5*, 180004. https://doi.org/10.1038/sdata.2018.4

Lucas, R. E. (1976). Econometric policy evaluation: A critique. *Carnegie-Rochester Conference Series on Public Policy*, *1*, 19–46. https://doi.org/https://doi.org/10.1016/S0167-2231(76)80003-6

Mcglade, C., & Ekins, P. (2015). The geographical distribution of fossil fuels unused when limiting global warming to 2¬c. *Nature*, *517*, 187–90. https://doi.org/10.1038/nature14016

Missirian, A., & Schlenker, W. (2017). Asylum applications respond to temperature fluctuations. *Science*, *358*(6370), 1610–1614. https://doi.org/10.1126/science.aao0432

Mitchell, T. (2003). Pattern scaling: An examination of the accuracy of the technique for describing future climates. *Climatic Change*, *60*, 217–242.

Monte, F., Redding, S. J., & Rossi-Hansberg, E. (2018). Commuting, migration, and local employment elasticities. *American Economic Review*, *108*(12), 3855–90. https://doi.org/10.1257/aer.20151507

Myhre, G., Highwood, E. J., Shine, K. P., & Stordal, F. (1998). New estimates of radiative forcing due to well mixed greenhouse gases. *Geophysical Research Letters*, *25*(14), 2715–2718. https://doi.org/10.1029/98GL01908

Nath, I. (2020). The food problem and the aggregate productivity consequences of climate change. *Job Market Paper*.

Nordhaus, W. (2006). Geography and macroeconomics: New data and new findings. *Proceedings of the National Academy of Sciences*, *103*(10), 3510–3517. https://doi.org/10.1073/pnas.0509842103

Nordhaus, W. (2015). Climate clubs: Overcoming free-riding in international climate policy. *American Economic Review*, *105*(4), 1339–70. https://doi.org/10.1257/aer.15000001

Nordhaus, W. (2017). Revisiting the social cost of carbon. *Proceedings of the National Academy of Sciences*, *114*(7), 1518–1523. https://doi.org/10.1073/pnas.1609244114

Nordhaus, W., & Boyer, J. (2002). Economic models of global warming. mit press, cambridge mass., 2000. isbn 0 262 14071 3. *Environment and Development Economics*, *7*(3), 593–601. https://doi.org/10.1017/S1355770X02240346

Papageorgiou, C., Saam, M., & Schulte, P. (2017). Substitution between clean and dirty energy inputs: A macroeconomic perspective. *The Review of Economics and Statistics*, *99*(2), 281–290. https://doi.org/10.1162/REST_a_00592

Popp, D. (2004). Entice: Endogenous technological change in the dice model of global warming. *Journal of Environmental Economics and Management*, *48*(1), 742–768. https://doi.org/https://doi.org/10.1016/j.jeem.2003.09.002

Popp, D. (2006). Entice-br: The effects of backstop technology rd on climate policy models. *Energy Economics*, *28*(2), 188–222. https://doi.org/https://doi.org/10.1016/j.eneco.2005.10.004

Redding, S. J., & Rossi-Hansberg, E. (2017). Quantitative spatial economics. *Annual Review of Economics*, *9*(1), 21–58. https://doi.org/10.1146/annurev-economics-063016-103713

Rogner, H.-H. (1997). An assessment of world hydrocarbon resources. *Annual Review of Energy and the Environment*, *22*(1), 217–262. https://doi.org/10.1146/annurev.energy.22.1.217

Schlenker, W., & Roberts, M. J. (2009). Nonlinear temperature effects indicate severe damages to u.s. crop yields under climate change. *Proceedings of the National Academy of Sciences*, *106*(37), 15594–15598. https://doi.org/10.1073/pnas.0906865106

Schwerhoff, G., & Stuermer, M. (2020). *Non-renewable resources, extraction technology, and endogenous growth* (Working Papers No. 1506). https://doi.org/10.24149/wp1506r1

Simonovska, I., & Waugh, M. (2014). The elasticity of trade: Estimates and evidence. *Journal of International Economics*, *92*(1), 34–50. https://EconPapers.repec.org/RePEc:eee:inecon:v:92:y:2014:i:1:p:34-50

Stern, D. I. (2012). Interfuel substitution: A meta-analysis. *Journal of Economic Surveys*, *26*(2), 307–331. https://doi.org/10.1111/j.1467-6419.2010.00646.x

UN. (2004). The united nations on world population in 2300. *Population and Development Review*, *30*(1), 181–187. http://www.jstor.org/stable/3401513

UN. (2019). *World population prospects 2019: Data booklet*. https://www.un-ilibrary.org/content/publication/3e9d869f-en

Zabreyko, P. P., Koshelev, A., Krasnoselskii, M., Mikhlin, S., Rakovshchik, L. S., Stet'senko, V., Shaposhnikova, T., & Anderssen, R. (1975). Integral equations: A reference text.

Online Appendix

A   Parameters and Data

Table 3 summarizes the parameters we use in the baseline scenario. The rest of this section discusses the sources and construction of our data.

Population and GDP at $1° \times 1°$. Data on population and GDP, in Power Purchasing Parities, for $1° \times 1°$ cells across the entire world come from the G-Econ 4.0 research project. For the estimation of fundamental amenities and productivities, we use data for the years 1990, 1995, 2000, 2005. We consider the same 17,048 cells that in 2000 have positive population, GDP and land. If some of these cells display missing values for 1990, 1995 or 2005, we linearly extrapolate the missing data, and, in each period, we cap GDP per capita at the percentile 97.13.

Human Development Index at $1° \times 1°$. Kummu et al., 2018 provide data on the Human Development Index at a yearly frequency, from 1990 to 2015, at a subnational level, considering around 700 geographic units. This data is presented at a resolution of 5 arc-min, so we aggregate it at a resolution of 60 minutes by considering the mode across cells.

Geographical attributes at $1° \times 1°$. Elevation data, measured as meters above the sea level at a resolution of $1° \times 1°$ is taken from the University of Washington, Join Institute for the Study of the Atmosphere and the Ocean, http://research.jisao.washington.edu/data_sets/elevation/. In order to construct the standard deviation and the mean absolute error, also known as *roughness*, within each $1° \times 1°$ cell, we use the afore-mentioned dataset at a resolution of $0.25° \times 0.25°$ and compute these statistics over the cells with positive land.

Distance to the coast is taken from the NASA Ocean Biology Processing Group https://oceancolor.gsfc.nasa.gov/docs/distfromcoast/. This data is provided at a resolution of $0.1° \times 0.1°$, so we compute the average distance within each $1° \times 1°$ cell. Distance to non-frozen oceans is taken from G-Econ database and displayed at a resolution of $1° \times 1°$. Distance to nearest water body either inland or sealand (ice-covered land areas are not considered as water bodies) is taken from Carrea et al., 2015, which presents data at $1° \times 1°$.

The following data are obtained from the NASA Earth Observations, https://neo.sci.gsfc.nasa.gov at a geographical resolution of $1° \times 1°$. Vegetation density is taken as the average over the period 1951-1980.[55] Share of ice-covered land is taken over April of 2010. Albedo, which is the ratio of light that a surface reflects compared to the total sunlight that falls, is taken over April of 2010.[56] Land cover classification

---

[55]The vegetation index ranges from -0.1 to 0.9 and have no unit. Rather, they are index values in which higher values (0.4 to 0.9) show lands covered by green, leafy vegetation and lower values (0 to 0.4) show lands where there is little or no vegetation.

[56]Surfaces that reflect a large share of the light falling on them are bright, and have high albedo, like snow. Surfaces that do not

1. Energy: $q_t^\omega(r) = \phi_t^\omega(r)^{\gamma_1} z_t^\omega(r) \left(L_t^\omega(r)^\chi e_t^\omega(r)^{1-\chi}\right)^\mu$, $e_t^\omega(r) = (\kappa e_t^{f,\omega}(r)^{\frac{\epsilon-1}{\epsilon}} + (1-\kappa)e_t^{c,\omega}(r)^{\frac{\epsilon-1}{\epsilon}})^{\frac{\epsilon}{\epsilon-1}}$	
$\mathcal{Q}_t^f(r) = f(CumCO2_t)/\zeta_t^f(r)$, $\mathcal{Q}_t^c(r) = 1/\zeta_t^c(r)$, $\zeta_t^j(r) = \left(y_t^w/y_{t-1}^w\right)^{v^j} \zeta_{t-1}^j(r)$	
$\chi = 0.96$	Relation between global GDP, CO_2 emissions flow and price
$\epsilon = 1.6$	Elasticity of substitution (Popp, 2004)
$\kappa = 0.89$	Relation between prices and quantities of fossil fuels and clean energy
$f(\cdot)$	Extraction costs (Rogner, 1997; Bauer et al., 2017)
$\zeta_0^f(\cdot), \zeta_0^c(\cdot)$	Target current cell-level energy use
$v^f = 1.16$	Target historical global CO_2 emissions
$v^c = 1.22$	Target historical global clean energy use
2. Damage functions: $\Lambda^a(\Delta T_t(r), T_t(r))$, $\Lambda^b(\Delta T_t(r), T_t(r))$, $n_t(r) = \eta(y_t(r), L_t(r))$	
$\Lambda^a(\cdot), \Lambda^b(\cdot)$	Relation between temperature and productivities and amenities
$\eta(\cdot)$	Relation between real GDP and temperature and natalities
3. Carbon cycle and climate	
$g(\cdot)$	IPCC, 2013 and statistical down-scaling
4. Preferences: $\sum_t \beta^t u_t(r)$, $u_t(r) = \left(1 + \Lambda_t^b(r)\right) \bar{b}_{t-1}(r) L_t(r)^{-\lambda}[\int_0^1 c_t^\omega(r)^\rho d\omega]^{1/\rho}$, $u_0(r) = e^{HDI_0(r)^3/\psi}$	
$\beta = 0.965$	Discount factor
$\rho = 0.75$	Elasticity of substitution of 4 (Bernard et al., 2003)
$\lambda = 0.32$	Relation between amenities and population (Desmet et al., 2018)
$\Omega = 0.5$	Elasticity of migration flows wrt income (Monte et al., 2018)
$\psi = 0.05$	Relation between utility and HDI (Kummu et al., 2018)
5. Technology: $q_t^\omega(r) = \phi_t^\omega(r)^{\gamma_1} z_t^\omega(r) \left(L_t^\omega(r)^\chi e_t^\omega(r)^{1-\chi}\right)^\mu$, $F_{r,t}^\omega(z) = e^{a_t^\omega(r)z^{-\theta}}, a_t^\omega(r) = \bar{a}_t(r) L_t(r)^\alpha$	
$\alpha = 0.06$	Static elasticity of productivity to density (Carlino et al., 2007)
$\theta = 6.5$	Trade elasticity (Eaton and Kortum, 2002; Simonovska and Waugh, 2014)
$\mu = 0.8$	Non-land share in production (Greenwood et al., 1997; Desmet and Rappaport, 2017)
$\gamma_1 = 0.319$	Relation between population distribution and growth (Desmet et al., 2018)
6. Productivity evolution: $\bar{a}_t(r) = (1 + \Lambda_t^a(r)) \left(\phi_{t-1}(r)^{\theta\gamma_1} \left[\int \bar{a}_{t-1}(v)dv\right]^{1-\gamma_2} \bar{a}_{t-1}(r)^{\gamma_2}\right)$, $\varphi(\phi) = \nu\phi^\xi$	
$\gamma_2 = 0.993$	Relation between population distribution and growth (Desmet et al., 2018)
$\xi = 125$	Desmet and Rossi-Hansberg, 2015
$\nu = 0.15$	Initial growth rate of real GDP of 1.75%
7. Trade costs	
$\varsigma(\cdot, \cdot)$	Allen and Arkolakis, 2014 and Fast Marching Algorithm
8. Migration costs	
$m_2(\cdot)$	Match population change between 2000 and 2005 (Desmet et al., 2018)

Table 3: Summary of parametrization.

considers the year 2010.[57]

Land density at $1° \times 1°$. Data on land comes from the Global Land One-km Base Elevation (GLOBE) Digital Elevation Model (DEM), a raster elevation data set from the National Oceanic and Atmospheric Administration covering all $30'' \times 30''$ (arcsecond) cells that are located on land. Using this information, we compute for each $1° \times 1°$ cell on the globe the share of the $30'' \times 30''$ cells that are on land.

Since the size of a $1° \times 1°$ cell is larger in the Equator than in the poles, we adjust the land density by the size of each cell. Finally, we normalize this measure, so that the cell with the largest amount of land has a land density of one.

Temperature at $1° \times 1°$. Gridded temperature data comes from the Berkeley Earth Surface Temperature (http://berkeleyearth.org/data-new/). This dataset provides information as far as 1750, as frequent as daily maximum, minimum and average temperature and as fine as $0.25° \times 0.25°$. We employ the database that provides annual temperature at a resolution of $1° \times 1°$.

For the cells with missing temperature, we take the simple average temperature across the nine surrounding cells, that is, we create a block of cells of size 3×3 centered at the cell with missing data. If there are still cells with missing temperature (which occurs in the case of small islands), we create a block of cells of size 5×5 centered at the cell with missing data and take the simple average temperature. We continue with this procedure until the cell is filled with temperature data.

Historical CO_2 emissions and clean energy at country-level. Crippa et al., 2019 (https://edgar.jrc.ec.europa. eu/overview.php?v=booklet2020) provide CO_2 emissions for all countries considered in this analysis, except for Greenland. We supplement this observation with data from the World Bank. Additionally, Crippa et al., 2019 consider international marine and international aviation. We split those emissions across countries according to the distribution provided in IEA, 2020.

Since IEA, 2020 provides information for aggregate regions that comprise several countries, like Former Soviet Union or Other Africa, we partition the emissions of those aggregate regions across countries according to the pattern displayed in Crippa et al., 2019 for total emissions.

As for the use of clean energy, expressed in tons of oil equivalent (toe), we use information from BP, 2019 and define clean energy as the sum of nuclear, hydroelectricity and renewables (wind, solar, among others). Since this database provides information for some aggregate regions, like Other South America and Other Middle East, we partition the energy use of those aggregate regions across countries according to the pattern for CO_2 emissions presented in Crippa et al., 2019. In order to make comparable CO_2 emissions and use of clean energy, we take the ratio of tons of CO_2 per ton of oil equivalent to be 2.8466.

---

reflect much light are dark, and have low albedo, like forests.

[57]This dataset partitions land based on characteristics of the surface that satellites can detect, such as water, soil, and vegetation types. There are 17 categories of land cover: 9 classes of natural vegetation, 3 classes of developed lands, 2 classes of mosaic lands, and 3 classes of non-vegetated lands (snow/ice, bare soil/rocks, water).

CO_2 emissions and clean energy at $1° \times 1°$. The Emission Database for Global Atmospheric Research (EDGAR) v4.0 https://jeodpp.jrc.ec.europa.eu/ftp/jrc-opendata/EDGAR/datasets/v40/ contains global emission inventories for greenhouse gases and air pollutants. These emissions are calculated as totals by country from 1970 to 2008, and distributed at a resolution of $0.1° \times 0.1°$ using proxy data. We aggregate thi data at $1° \times 1°$ by considering the sum across cells.

We employ the CO_2 distribution from residential emissions. We prefer this specification over total emissions or emissions from production, because the former considers emissions that occur over cells with no land and the latter displays high level of CO_2 in cells scarcely populated and with low income levels (due to presence of plants producing steel or cement, for instance), we consider that such pattern does not represent the long-run trend of CO_2 emissions.

In order to define carbon dioxide emissions at the cell-level, we disaggregate the country-level emissions according to the spatial pattern displayed in the EDGAR database. As no gridded data for clean energy exists, we split the country-level clean energy use using the spatial pattern of the EDGAR database. Figure 17 displays the spatial distribution of CO_2 emissions and clean energy in 2000.
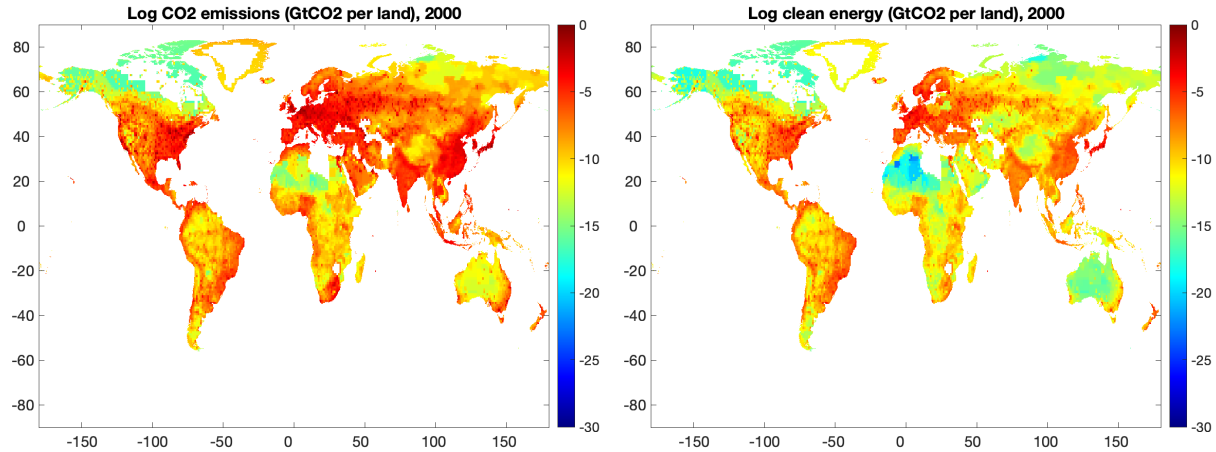
Figure 17: Spatial distribution of CO_2 emissions and clean energy in 2000.

Historical net natality at country-level. Crude birth rates and crude death rates at the country-level since 1950 at a yearly frequency are taken from the World Population Prospects of the United Nations (https://population.un.org/wpp/Download/Standard/Population/).

Projections of non-fuel combustion CO_2 emissions and non-CO_2 forcing. Forecasts up to 2500 for CO_2 flow and forcing for RCP 8.5, 6.0, 4.5 and 2.6 are taken from the RCP Database version 2.0 (http://www.iiasa.ac.at/web-apps/tnt/RcpDb). Carbon dioxide from deforestation is considered as *OtherCO2* and we consider that 1 GtC equals 44/12 $GtCO_2$. Non-CO_2 forcing is considered as *Total anthropogenic and natural radiative forcing* minus *CO2 forcing*.

Projections of global population. Global population levels at a quinquenial frequency for the medium

scenario, as well as 80% and 95% confidence intervals are taken from the World Population Prospects of the United Nations (https://population.un.org/wpp/Download/Standard/Population/). In order to make consistent total population from United Nations and G-Econ in the year 2000, from the former dataset I substract the total population of the initial period and add the total population of the year 2000 displayed in the G-Econ database.[58]

Cost of extracting fossil fuel. Bauer et al., 2017 estimate the cost of extracting fossil fuels and present estimates for different Socio Economic Share Pathways (SSP), which consider alternative assumption regarding the evolution of the world economy. We choose the scenario SSP5 (development based on fossil fuels), which is the one that closest resembles the RCP 8.5. Then, we aggregate the costs of hard coal and lignite into a single fossil fuel in terms of tCO_2 per usd, considering the conversion factors of 0.0946 and 0.1012 $GtCO_2$ per EJ, respectively. Finally, we rank costs from the least to the most expensive.

B   Damage Functions on Amenities and Productivities

In this section, we detail how we employ the Human Development Index (HDI) as our measure of utility, how we estimate our main empirical specification for the damage function on amenities and productivities, and perform some robustness exercises of these functions.

B.1   HDI as a Measure of Utility

The HDI is constructed as a geometric mean of indices evaluating three dimensions of human development: a long and healthy life, being knowledgeable and have a decent standard of living. The health dimension is assessed by life expectancy at birth; the education dimension by mean of years of schooling for adults aged 25 years and more and expected years of schooling for children of school entering age; and the standard of living dimension by Gross National Income (GNI) per capita. The HDI uses the logarithm of income, to reflect the diminishing importance of income with increasing GNI.

$$HDI_t(r) = \left(I_t^{\text{Health}}(r) \cdot I_t^{\text{Educ}}(r) \cdot I_t^{\text{Income}}(r) \right)^{1/3} \tag{25}$$

$$I_t^{\text{Income}}(r) = \begin{cases} 1 & \text{if} \quad GNI_t(r) > 75,000 \\ \frac{\log(GNI_t(r)) - \log(100)}{\log(75,000) - \log(100)} & \text{if} \quad 100 \leq GNI_t(r) \leq 75,000 \\ 0 & \text{if} \quad GNI_t(r) < 100 \end{cases} \tag{26}$$

---

[58]This adjustment is performed since the G-Econ database does not display information for some regions of the world, like Libya and some parts of Africa and Asia.

To obtain a measure of well-being that is log-linear in real income, we combine equations (25) and (26)

$$HDI_t(r)^3 = \psi_{0,t}(r) + \psi_{1,t}(r) \log\left(GNI_t(r)\right) + \log\left(\varepsilon_t^i(r)\right). \tag{27}$$

Consequently, there is a direct relationship between equation (27) and the definition of utility in our model, given by equation (1). Ignoring migration costs, the flow utility of an individual i residing in location r in the model is given by: $\log\left(u_t^i(r)\right) = \log\left(b_t(r)\right) + \log\left(y_t(r)\right) + \log\left(\varepsilon_t^i(r)\right)$. Accordingly, we estimate the following regression.

$$HDI_t(r)^3 = \psi_0 + \psi \log\left(y_t(r)\right) + \epsilon_t^i(r) \tag{28}$$

Where the HDI is obtained from Kummu et al., 2018, which present this index at a yearly frequency, from 1990 to 2015 at a subnational level, considering around 700 geographic units. Real-income, $y_t(r) = L_t(r)u_t(r)/\bar{b}_t(r)$, is computed using data on population and the ratio of utility in terms of amenities, derived from the model inversion. We estimate equation (28) aggregating cells at the subnational level and weighting observations by population size.

Table 4 shows the results of the estimation. Column (1) denotes the specification of equation (28). Column (2) allows the intercept to be time-dependent, $\psi_{0,t}$. Column (3) allows the intercept and the slope to be time-dependent, $\psi_{0,t}$ and ψ_t. As can be observed, the estimates of ψ_t are relatively stable over time. Columns (4)-(6) repeat the aforementioned exercises weighting each subnational unit by land size rather than population size as in Columns (1)-(3). We take the central estimate of $\psi = 0.045$, given by Column (2).

Finally, we compare the spatial pattern of the HDI with that of the Cantril ladder. This measure of subjective well-being is employed in Desmet et al., 2018. Figure 18 evidences that both measures of utility display a similar spatial configuration for the year 2000. However, we prefer the HDI as it provides more cross-sectional and temporal variation, which allows to better identify the effect of temperature on fundamentals.

B.2 Estimation of Damage Functions

In order to estimate the effect of temperature on amenities and productivities, we employ equation (22) as our main empirical specification. The variable $T_t(r)$ denotes the average temperature over the last decade for January in the Northern Hemisphere and July in the Southern Hemisphere, and $\mathbb{1}\{T_t(r) \in \mathcal{T}_j\}$ is an indicator function for temperature $T_t(r)$ being in interval $\mathcal{T}_j$. We partition the distribution of temperature into $J = 20$ bins, each comprising 5% of the observed temperature values.

The variable $Z(r)$ is a vector of cell-level geographic attributes. Namely, mean, standard deviation and average deviation of elevation, distance to the coast, to a water body and to non-frozen oceans. Each of these six covariates, $Z_i(r)$, is transformed by means of a Chebyshev polynomial, $Z_i^j(r)$, $j \in \{1, \cdots, 5\}$.

	(1)	(2)	(3)	(4)	(5)	(6)
logrealgdp	0.107***	0.0450***		0.0974***	0.0447***	
	(0.00391)	(0.00442)		(0.00783)	(0.00478)	
1990×logrealgdp			0.0338***			0.0360***
			(0.00400)			(0.00551)
1995×logrealgdp			0.0412***			0.0407***
			(0.00379)			(0.00507)
2000×logrealgdp			0.0459***			0.0424***
			(0.00381)			(0.00507)
2005×logrealgdp			0.0510***			0.0427***
			(0.00396)			(0.00537)
subcountry fe	X	X	X	X	X	X
year fe		X	X		X	X
weight pop	X	X	X			
weight area				X	X	X
N	2,952	2,952	2,952	2,952	2,952	2,952
R^2	0.9822	0.9880	0.9910	0.9863	0.9927	0.9933
RMSE	0.0297	0.0245	0.0211	0.0300	0.0219	0.0211

Standard errors in parentheses, clustered by country

* $p < 0.10$, ** $p < 0.05$, *** $p < 0.01$

Table 4: Estimation of utility measure from HDI.
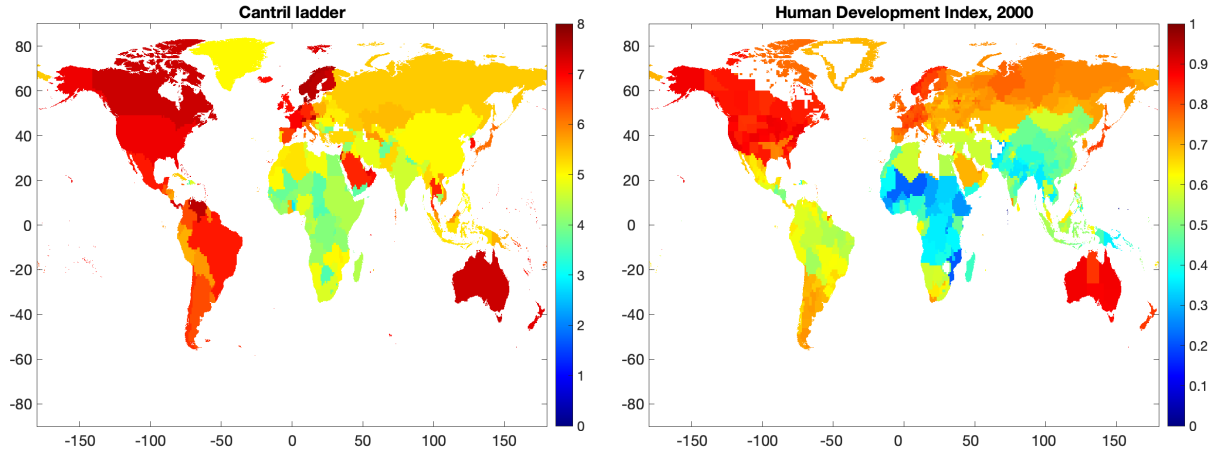
Figure 18: Cantril ladder and Human Development Index in 2000.

Accordingly, the vector $Z(r)$ comprises the 30 elements of $Z_i^j(r)$. Additionally, we consider an indicator

function for 16 different types of land.[59]

$$Z_i^j(r) = \cos\left(j \cdot \arccos\left(\frac{\tilde{Z}_i(r)}{\max_{s \in S} |\tilde{Z}_i(s)|} \right) \right)$$

$$\tilde{Z}_i(r) = \left(Z_i(r) - \frac{1}{2} \left(\min_{s \in S} Z_i(s) + \max_{s \in S} Z_i(s) \right) \right)$$

With respect to the time-invariant fixed effects, $\iota(b)$, we partition the $180° \times 360°$ gridded map into blocks of size $2° \times 2°$. As for the time-varying fixed effects at the subnational level, $\iota_t(s)$, we take as basis the subnational levels, as delimited in Kummu et al., 2018, and aggregate the subnational units in Europe at the (i) country-level, as defined in Desmet et al., 2018, and (ii) at the region level, considering North, South, West and East. Figure 19 displays the spatial demarcations of the subnational units.[60]
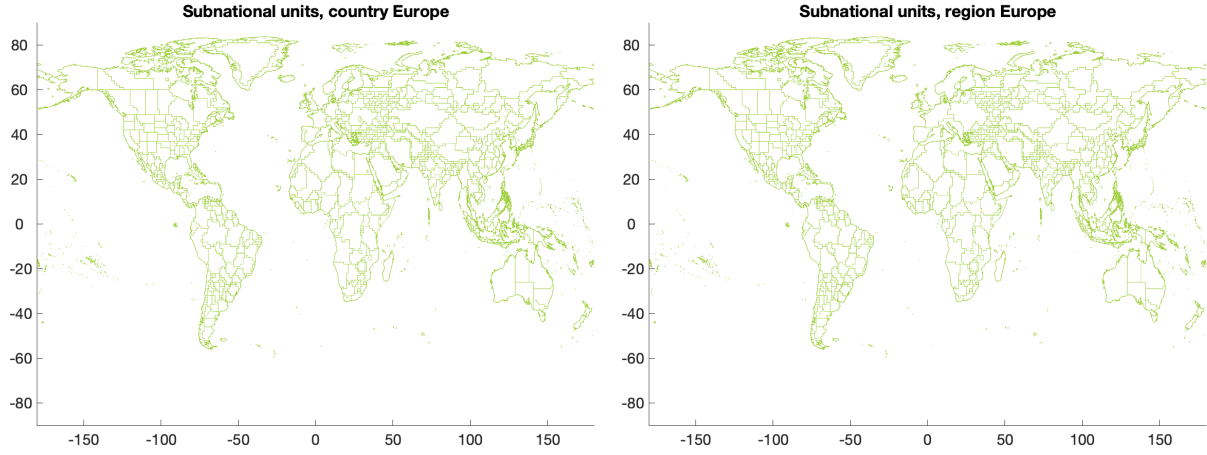
Figure 19: Time-varying fixed effects at the subnational level, $\iota_t(s)$.

We estimate equation (22), modeling the error term as in Conley, 1999. That is, we consider that errors are spatially correlated, so that correlation linearly declines from one to zero as distance increases. When distance is greater or equal than 550 km (5 cells) correlation equals zero, as in Schlenker and Roberts, 2009. We implement this error structure through the Stata package `acreg`, developed by Colella et al., 2019.

To smooth the behavior of the point estimates across temperature bins, $\hat{\delta}_j^x$, we fit the logistic curve $\delta^x(T)$, given by equation (30), across the point estimates of each bin, weighting them by the inverse of their standard errors, $se(\hat{\delta}_j^x)$, to provide a greater weight to the more accurate estimates. In other words, we

---

[59] $Z_i(r)$ denotes the variable in raw units (for instance, in meters when considering elevation) and $Z_i^j(r)$ the Chebyshev transformation for the j-th polynomial so that it lies between minus one and one.

[60] We aggregate the subnational units in Europe, because some of them have a size of one cell, precluding a proper identification.

estimate the coefficients $(\delta^x_{\min}, \delta^x_{\max}, \delta^x_{\text{center}})$ that solve (29).[61]

$$\min \quad \sum_{j=1}^{J} \frac{1}{se(\hat{\delta}_j)} \left(\hat{\delta}_j - \delta^x(T_j) \right)^2 \tag{29}$$

$$\text{st} \quad \delta^x(T) = \delta^x_{\min} + \frac{\delta^x_{\max} - \delta^x_{\min}}{1 + e^{0.1 \cdot (T - \delta^x_{\text{center}})}} \tag{30}$$

Where T_j is the $(2j-1)/(2J)$-th percentile of the temperature observations, $j \in \{1, \cdots, J = 20\}$. To estimate the upper and lower $\alpha\%$ confidence interval of the logistic function, we solve (29), but replace the point estimates of each bin j by their upper and lower $\alpha\%$ confidence intervals, respectively.

B.3 Robustness Exercises

In this subsection, we present robustness exercises with regard to the estimation of the damage functions $\Lambda^a(\cdot), \Lambda^b(\cdot)$. Figure 20 presents the damage function considering January temperature for all cells in the world, rather than January temperatures in the Northern Hemisphere and July temperatures in the Southern Hemisphere. The quantitative results are in line with those of the main specification.
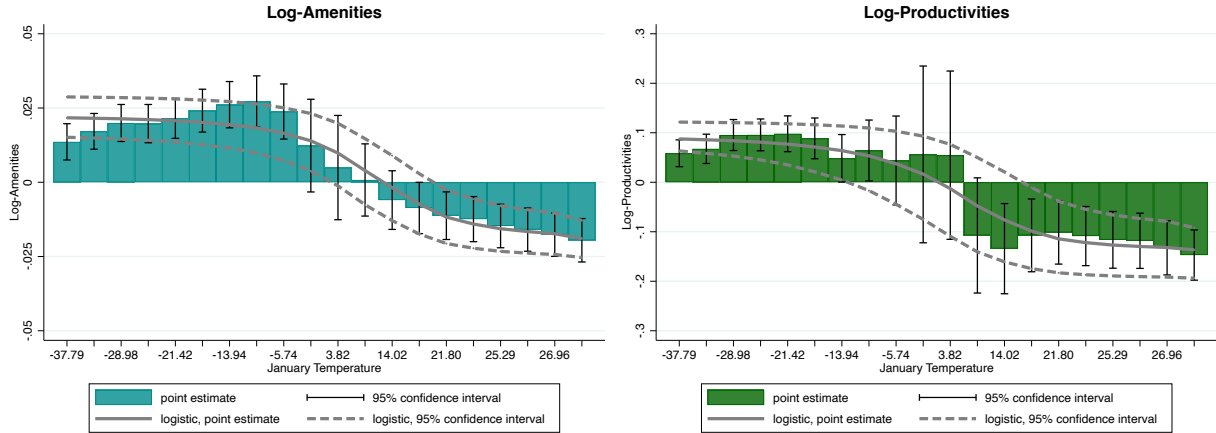
Figure 20: Effect of temperature on fundamental amenities and productivities, using January temperature.

Figure 21 plots the main specification using January-July temperatures for one year, rather than the ten-year average. Although the results are similar to the main specification, the use of only one year provides noisier results in terms of the standard errors, and the transition from benefits in cold regions to damages in warm places is less smooth.

Figure 22 implements a finer partition of the temperature observations, by considering 50 bins, each comprising 2% of the observed temperature values. Given the finer partition of the data, there are less observations in each bin and therefore the standard errors tend to be larger with respect to the baseline

---

[61]To achieve convergence of the non linear estimation, we exogenously set to 0.1 the slope coefficient of the logistic function.
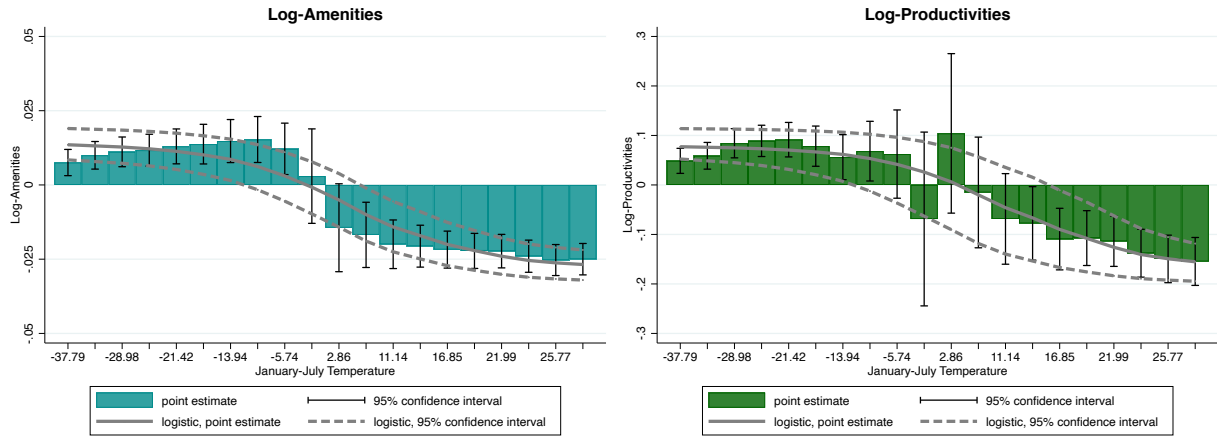
Figure 21: Effect of temperature on fundamental amenities and productivities, using one-year variation of January-July temperature.

estimation. This behavior is more pronounced at the middle of the temperature distribution. However, the logistic smoothing is similar to that in the main specification.
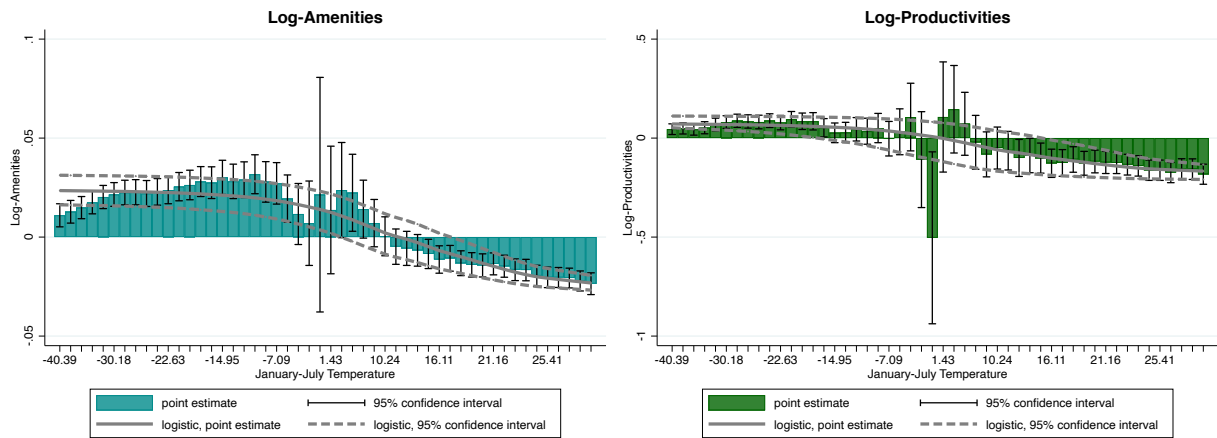
Figure 22: Effect of temperature on fundamental amenities and productivities, using 50 temperature bins.

Tables 5 and 6 evaluate how the standard errors of the main specification of the damage functions vary under different assumptions of the errors. Columns (1) and (2) consider that errors are spatially correlated with a cutoff of 550km, as in the main specification, and 1,100km, respectively. Columns (3) and (4) assume that errors are homoskedastic and heteroskedastic, respectively, with no correlation between observations. Column (5) clusters the errors within subnational units, as defined in Kummu et al., 2018. The last three columns are estimated with the stata package `reghdfe`, implemented by Correia, 2016.

Coefficients	Standard Errors				
	(1)	(2)	(3)	(4)	(5)
0.0132	(0.0031)***	(0.0039)***	(0.0013)***	(0.0014)***	(0.0076)*
0.0167	(0.0031)***	(0.0039)***	(0.0014)***	(0.0015)***	(0.0073)**
0.0195	(0.0032)***	(0.0040)***	(0.0014)***	(0.0016)***	(0.0072)***
0.0192	(0.0033)***	(0.0041)***	(0.0015)***	(0.0017)***	(0.0074)***
0.0210	(0.0034)***	(0.0042)***	(0.0016)***	(0.0018)***	(0.0078)***
0.0234	(0.0037)***	(0.0045)***	(0.0017)***	(0.002)***	(0.0084)***
0.0253	(0.0039)***	(0.0047)***	(0.0019)***	(0.0023)***	(0.0092)***
0.0261	(0.0043)***	(0.0049)***	(0.0023)***	(0.0029)***	(0.0092)***
0.0223	(0.0046)***	(0.0051)***	(0.0032)***	(0.0038)***	(0.0088)**
0.0072	(0.0076)	(0.0083)	(0.0060)	(0.0069)	(0.0110)
0.0080	(0.0081)	(0.0081)	(0.0047)*	(0.0060)	(0.0095)
0.0044	(0.0054)	(0.0057)	(0.0028)	(0.0033)	(0.0086)
-0.0059	(0.0037)	(0.0039)	(0.0023)**	(0.0026)**	(0.0060)
-0.0112	(0.0033)***	(0.0035)***	(0.0021)***	(0.0023)***	(0.0055)**
-0.0144	(0.0029)***	(0.0031)***	(0.0019)***	(0.0021)***	(0.0048)***
-0.0170	(0.0028)***	(0.0029)***	(0.0018)***	(0.0019)***	(0.0045)***
-0.0170	(0.0026)***	(0.0027)***	(0.0017)***	(0.0018)***	(0.0042)***
-0.0194	(0.0026)***	(0.0026)***	(0.0016)***	(0.0017)***	(0.0043)***
-0.0215	(0.0025)***	(0.0025)***	(0.0016)***	(0.0016)***	(0.0042)***
-0.0229	(0.0025)***	(0.0026)***	(0.0016)***	(0.0016)***	(0.0044)***

* $p < 0.10$, ** $p < 0.05$, *** $p < 0.01$

Columns: (1) spatially correlated up to 550 km, (2) spatially correlated up to 1100 km,

(3) homoskedastic, (4) heteroskedastic and (5) clustered at the subnational level

Table 5: Standard errors of the damage function on amenities under different specifications of the error.

C Natality Rates, Energy Elasticities and Migration Costs

In this section, we outline the procedure to estimate the parameters of the natality rate function, b^ℓ, b^h, b^T, b^w, the elasticities of energy productivity growth to global real GDP growth, υ^f, υ^c and the migration cost function, $m_2(\cdot)$. To construct the natality rate function $\eta(\cdot)$, we set the parameter b_0^T to target the global natality rate observed in the year 2000, n_0^w, and we impose the functional form of equation (24).

$$n_0^w L_0 - \int_S \eta^y(y_0(v); b^\ell, b^h) L_0(v) H(v) dv = \int_S \eta^T(T_0(v), \log(y_0^w); b^T, b_w) L_0(v) H(v) dv$$

$$= 0.5 \int_S \left(b_0^T + b_2^T e^{-b_1^T \left(T_0(v) - b^{*T} \right)^2} \right) L_0(v) H(v) dv$$

$$= (0.5) b_0^T L_0 + (0.5) b_2^T \int_S \left(e^{-b_1^T \left(T_0(v) - b^{*T} \right)^2} \right) L_0(v) H(v) dv$$

Hence, we can define b_0^T as a function of the remaining parameters $\flat = (b^\ell, b^h, b_1^T, b_2^T, b^{*T})$ and data on the initial period $x_0 = (n_0^w, L_0(\cdot), y_0(\cdot), T_0(\cdot))$. Where local population is obtained from the G-Econ database, local real income is constructed as $y_0(r) = L_0(r)^\lambda u_0(r)/\bar{b}_0(r)$ so that the ratio of utility to amenities is

<div align="center">Damage Function on Productivities</div>

Coefficients	Standard Errors				
	(1)	(2)	(3)	(4)	(5)
0.0485	(0.0139)***	(0.0168)***	(0.0049)***	(0.0056)***	(0.0286)*
0.0575	(0.0151)***	(0.0181)***	(0.0054)***	(0.0063)***	(0.0315)*
0.0850	(0.016)***	(0.0193)***	(0.0056)***	(0.0066)***	(0.0315)***
0.0852	(0.0163)***	(0.0193)***	(0.0059)***	(0.0071)***	(0.0325)***
0.0867	(0.0184)***	(0.0217)***	(0.0065)***	(0.0078)***	(0.0351)**
0.0762	(0.0208)***	(0.0235)***	(0.0075)***	(0.0090)***	(0.0351)**
0.0349	(0.0240)	(0.0270)	(0.0089)***	(0.0104)***	(0.0398)
0.0475	(0.0307)	(0.0346)	(0.0115)***	(0.0134)***	(0.0438)
0.0262	(0.0448)	(0.0512)	(0.0177)	(0.0206)	(0.0666)
0.0377	(0.0882)	(0.0978)	(0.0416)	(0.0469)	(0.1000)
0.1017	(0.0901)	(0.0395)**	(0.0283)***	(0.0342)***	(0.1569)
-0.0666	(0.0586)	(0.0417)	(0.0145)***	(0.0183)***	(0.1421)
-0.0716	(0.0476)	(0.0388)*	(0.0112)***	(0.0141)***	(0.1186)
-0.1056	(0.0397)***	(0.0362)***	(0.0097)***	(0.012)***	(0.1084)
-0.1296	(0.0333)***	(0.0308)***	(0.0085)***	(0.0104)***	(0.0914)
-0.1248	(0.0293)***	(0.0264)***	(0.0078)***	(0.0093)***	(0.0801)
-0.1295	(0.0269)***	(0.0251)***	(0.0071)***	(0.0086)***	(0.0755)*
-0.1539	(0.0256)***	(0.025)***	(0.0068)***	(0.0082)***	(0.0728)**
-0.1681	(0.0255)***	(0.0256)***	(0.0068)***	(0.0084)***	(0.0720)**
-0.1703	(0.0256)***	(0.0274)***	(0.0070)***	(0.0086)***	(0.0714)**

$* \ p < 0.10, ** \ p < 0.05, *** \ p < 0.01$

Columns: (1) spatially correlated up to 550 km, (2) spatially correlated up to 1100 km,

(3) homoskedastic, (4) heteroskedastic and (5) clustered at the subnational level

Table 6: Standard errors of the damage function on productivities under different specifications of the error.

computed as in Supplementary Materials Section F.2,[62] and local temperature comes from the Berkeley Earth Surface Temperature Database (BEST).

$$b_0^T(\flat, x_0) = 2n_0^w - \frac{1}{L_0} \int_S \left(2\eta^y(y_0(v); b^\ell, b^h) + b_2^T e^{-b_1^T \left(T_0(v) - b^{*T} \right)^2} \right) L_0(v) H(v) dv \tag{31}$$

Analogously, we set the parameter b_w to target the global natality rate observed in the year 2020, n_{20}^w. The natality rates n_0^w and n_{20}^w are taken from the World Population Prospects of the United Nations.

$$n_{20}^w L_{20} - \int_S \eta^y(y_{20}(v); b^\ell, b^h) L_{20}(v) H(v) dv$$
$$= \int_S \eta^T(T_{20}(v), \log(y_{20}^w); b^T, b_w) L_{20}(v) H(v) dv$$
$$= \frac{1}{1 + e^{b_w [\log(y_{20}^w / y_0^w)]}} \int_S \left(b_0^T(\flat, x_0) + b_2^T e^{-b_1^T \left(T_{20}(v) - b^{*T} \right)^2} \right) L_{20}(v) H(v) dv \tag{32}$$

---

[62]To solve for this ratio we require data on local wages and energy prices, which come from G-Econ, EDGAR and BP databases. Further details of the data are described in Appendix A.

Hence, we can define b_w as a function of the parameters $\flat$ and data on the initial and twentieth period.

$$b_w(\flat, x_0, x_{20}) = \frac{1}{\log(y_{20}^w/y_0^w)} \log \left(\frac{\int_S \left(b_0^T(\flat, x_0) + b_2^T e^{-b_1^T \left(T_{20}(v) - b^{*T} \right)^2} \right) L_{20}(v) H(v) dv}{n_{20}^w L_{20} - \int_S \eta^y(y_{20}(v); b^\ell, b^h) L_{20}(v) H(v) dv} - 1 \right) \tag{33}$$

Now, we describe the algorithm employed to jointly solve for the parameters and functions of interest.

1. Guess $m_2(\cdot), \flat, \upsilon^f, \upsilon^c$ and x_{20}.

2. Run the model backwards for 50 periods using equation (87) of Supplementary Materials Section F.4, taking the behavior of local historical temperature as in the BEST data,[63] and retrieve $L_t(\cdot)$ and $y_t(\cdot)$.

3. Compute the natality rates at the country-level induced from the model.[64] If the difference between the model induced and the historical natality rates is small enough, go to the next step. Otherwise, use the solution of (34) to update $\flat$ and go back to step 2.

$$\min_{\flat} \quad SSR(\flat) = \sum_{c=1}^{168} \sum_{t=1950}^{1999} L_t^c \left(u_t^c \right)^2 \tag{34}$$

$$\text{st} \quad u_t^c = \left(n_t^{c,data} - n_t^{c,model}(\flat) \right)^2, \quad n_t^{c,model}(\flat) = \frac{\int_{v \in c} \eta(y_t(v), T_t(v); \flat) L_t(v) H(v) dv}{\int_{v \in c} L_t(v) H(v) dv} \tag{35}$$

Where c denotes countries, t periods of time, L_t^c is the weight given to each observation, based on historical country-level population data, and u_t^c is the error between the model and the data for each observation. Let B be the number of elements in the vector $\flat$.

We solve (34) as follows: If $SSR(\cdot)$, evaluated at the guess, is small enough, the procedure ends. Otherwise, we update $\flat$ in the j-th iteration as shown below.

$$\flat_{j+1} = \flat_j + \varrho(X_j'DX_j)^{-1}(X_j'Du_j) \tag{36}$$

Where X_j is a matrix of size $(168 \cdot 50) \times B$ comprising the derivatives of $n_t^{c,model}(\cdot)$ evaluated at $\flat_j$, D is a matrix of size $(168 \cdot 50) \times (168 \cdot 50)$ comprising the population weights, and u_j is a matrix of size $B \times (168 \cdot 50)$ comprising the errors evaluated at $\flat_j$. Additionally, ϱ is *step size* scalar parameter chosen at each iteration to improve convergence.

At each iteration, ϱ is set to one, and a candidate $\flat_{j+1}^*$ is compute from (36). If $SSR(\flat_{j+1}^*) < SSR(\flat_j)$, then $\flat_{j+1} = \flat_{j+1}^*$ and the iteration is completed. Otherwise, ϱ is halved, a new $\flat_{j+1}^*$ is computed, and the process is repeated. The NLLS estimation concludes when $SSR(\flat_{j+1})$ is small enough.

---

[63]The backward solution of the climatic model does not provide very accurate results with respect to the historical observations. Therefore, we prefer to employ observed past data.

[64]We consider 168 countries, following the classification of Desmet et al., 2018.

4. Compute the migration costs that target population distribution in the year 2005 using equation (91) of Supplementary Materials Section F.5. If the difference between the guess and the targeted migration costs is small enough, run the model 20 periods in the future, update x_{20} and go to the next step. Otherwise, use the targeted migration costs to update $m_2(\cdot)$ and go back to step 2. Figure 23 displays the logarithm of migration costs of the last iteration of the algorithm.
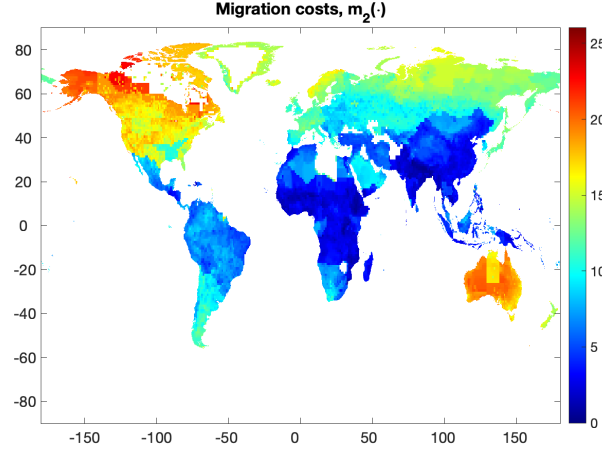
Figure 23: Log-Migration costs.

5. If the difference between the model induced, $E_t^{f,model}$, and historical data on global emissions, $E_t^{f,data}$, from 1950 to 1999 is small enough, run the model 20 periods in the future, update x_{20} and go to the next step. Otherwise, update $\upsilon^f = (E_{1999}^{f,data} - E_{1950}^{f,data})/(E_{1999}^{f,model} - E_{1950}^{f,model})$ and go back to step 2.

6. If the difference between the model induced, $E_t^{c,model}$, and historical data on global clean energy use, $E_t^{c,data}$, from 1965 to 1999 is small enough, run the model 20 periods in the future, update x_{20} and the algorithm concludes.[65] Otherwise, update $\upsilon^c = (E_{1999}^{c,data} - E_{1965}^{c,data})/(E_{1999}^{c,model} - E_{1965}^{c,model})$ and go back to step 2. Figure 24 compares the historical and model estimated flow of global CO_2 emissions and clean energy use.[66]

Figure 25 compares the evolution of global population and natality rates in the data and the model. Figure 26 plots the cross-section of the country-level natality rates in the data and the cell-level natality rates estimated by the algorithm for the year 2000. Figure 27 displays in solid black curves the natality rate functions on log real GDP and temperature, and in green bubbles the observed relationships between country-level natality rates, temperature and model induced log real GDP, where the size of the bubbles depends on population levels.[67]

---

[65]The BP database does not contain information on clean energy use for the years 1950-1964.

[66]The dashed black curve in Figure 24 represents the 11-year moving average of global CO_2 emissions.

[67]We consider the model-induced log real GDP, because it is challenging to construct a measure of real income from the data that
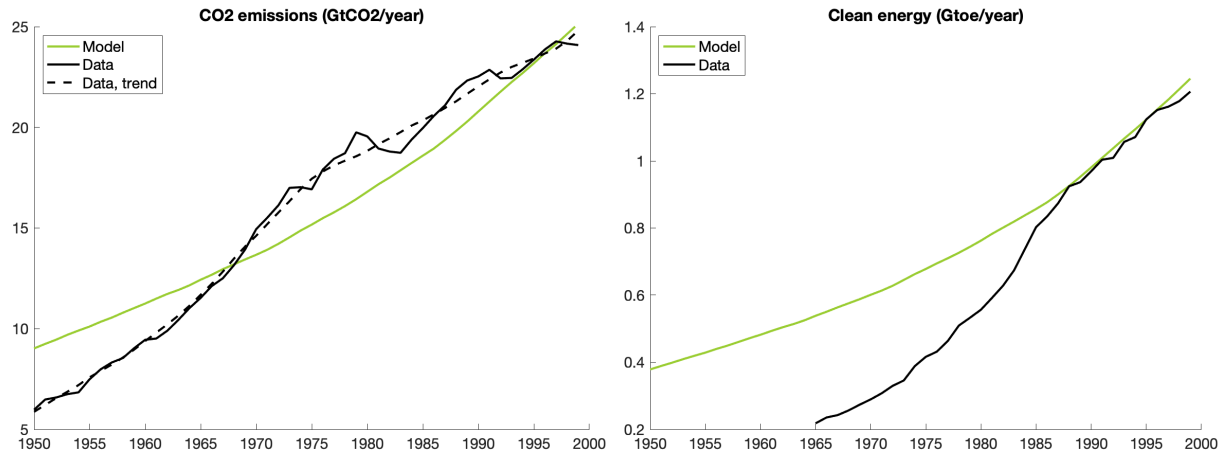
Figure 24: Historical global CO_2 emissions and clean energy use.

These figures reveal that the model predicts lower dispersion in natality rates with respect to the data. Steeper natality rate functions might exacerbate the long-run effects of shocks to the economy. For instance, a rise in iceberg trade costs that reduces income at impact would generate a huge increase in the natality rates of the subsequent periods, generating greater levels of population in the long-run and therefore higher growth rates in the BGP. In other words, the direct effect of higher commercial frictions would be overshadowed by the evolution of global population.
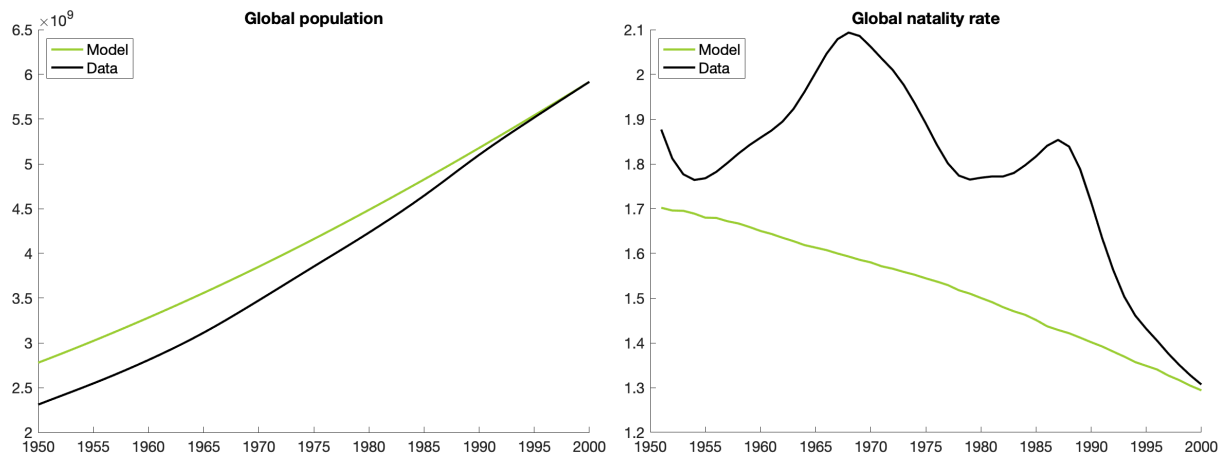
Figure 25: Historical global population and natality rates: model and data.

captures the same elements of this model for every year of the period 1950-1999.
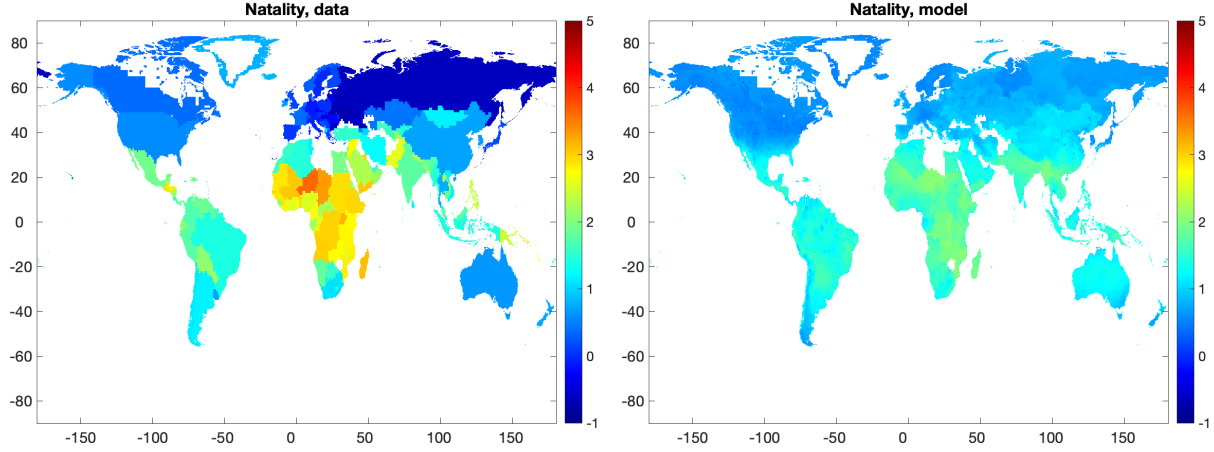
Figure 26: Natality rates in 2000: country-level data and cell-level model fit.
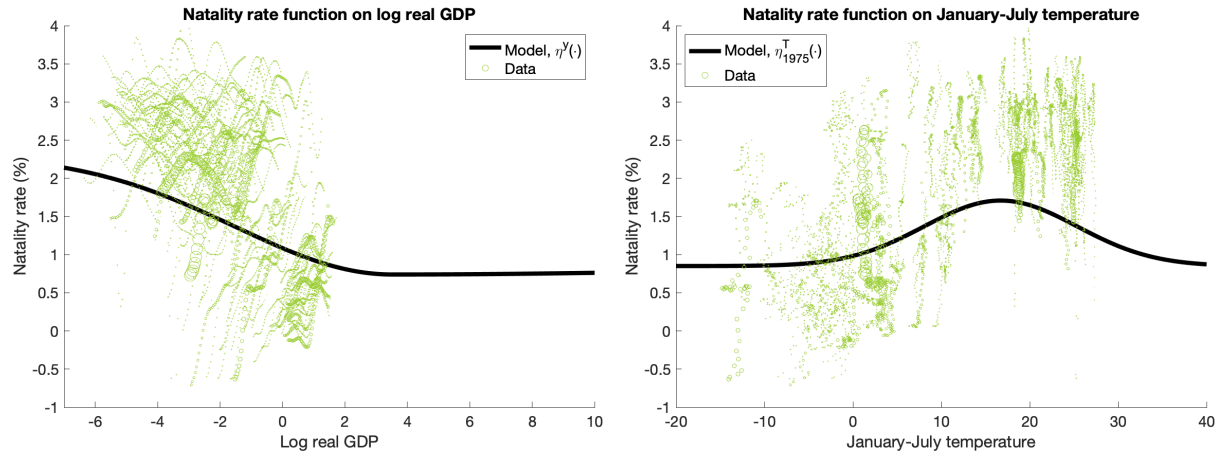
Figure 27: Natality rate function on real GDP and temperature: model and data.

D   Carbon Cycle and Temperature Down-scaling

In this section, we describe the parametrization of the carbon cycle and the temperature down-scaling. Regarding the evolution of the stock of carbon dioxide, displayed in equation (14), the share of CO_2 remaining in the atmosphere ℓ periods ahead, $(1 - \delta_\ell) = a_0 + \sum_{i=1}^{3}(a_i \cdot e^{-\ell/b_i})$, is approximated by a sum of exponentials, as in Forster et al., 2007 and Joos et al., 2013. According to IPCC, 2013, we set $a_0 = 0.2173, a_1 = 0.2240, a_2 = 0.2824, a_3 = 0.2763, b_1 = 394.4, b_2 = 36.54, b_3 = 4.304$. To simplify the

evolution of carbon stock, we rewrite the law of motion as follows:

$$S_{t+1} = S_{0,t+1} + \sum_{i=1}^{3} S_{i,t+1} \tag{37}$$

$$S_{0,t+1} = S_{0,t} + a_0(E_t^f + E_t^x) \tag{38}$$

$$S_{i,t+1} = (e^{-1/b_i})S_{i,t} + a_i(E_t^f + E_t^x), \quad i \in \{1,2,3\} \tag{39}$$

Thus, the model requires the initial values of the four layers, $S_{0,i}, i \in \{0,1,2,3\}$. Following Golosov et al., 2014, we consider $S_{0,2000} = 2,429$ GtCO$_2$ as the sum of the pre-industrial stock, $S_{\text{pre-ind}} = 2,200$ GtCO$_2$, plus a share a_0 of the historical cumulative carbon emissions, $\sum_{\ell=1945}^{1999}(E_\ell^f + E_\ell^x) = 1,054$ GtCO$_2$. The remaining three layers, $S_{1,2000} = 224, S_{2,2000} = 178, S_{3,2000} = 37$ GtCO$_2$, are computed as the discounted sum of past emissions.[68]

With respect to the effect of forcing on global temperature, the response to a unit forcing can be represented by a sum of two exponentials, $\zeta_\ell = \sum_{j=1}^{2}(c_j/d_j) \cdot e^{-\ell/d_j}$, as in Boucher and Reddy, 2008. We take the forcing sensitivity to be $\varphi = 5.35$ and the climate parameters to be $c_1 = 0.631, c_2 = 0.429, d_1 = 8.4, d_2 = 409.5$.[69] Analogously to the carbon circulation, we rewrite the temperature module as shown below:

$$T_{t+1} = T_{1,t+1} + T_{2,t+1} \tag{40}$$

$$T_{j,t+1} = (e^{-1/d_j})T_{j,t} + \frac{c_j}{d_j}F_{t+1}, \quad j \in \{1,2\} \tag{41}$$

Where $T_{1,2000} = 1.01°C$ is the discounted sum of past forcings (from 1825 to 2000) and $T_{2,2000} = 8.19°C$ is the discounted sum of past forcings plus the pre-industrial temperature $T_{\text{pre-ind}} = 8.1°C$. We interpret temperature as that over land, excluding that over water.

To construct the mapping from global to local temperature, we estimate equation (17), where the object of interest is the temperature scaler function, $g(\cdot)$. We parametrize this function as an additive separable Chebyshev polynomial of order 10 in the following arguments: latitude, longitude, product of latitude and longitude, mean elevation, distance to the coast, distance to the ocean, distance to a water body, vegetation density, albedo and share of land covered by ice.

Therefore, we can define the function $g(\cdot)$ as shown in equation (42), where $Z_i(\cdot)$ denotes each of the ten covarites mentioned in the previous paragraph, $Z_i^j(\cdot)$ is the Chebyshev polynomial of order $j \in \{1, \cdots, 10\}$

---

[68]Historical data for CO$_2$ stock and projections for CO$_2$ emissions and forcing for every RCP are taken from http://www.iiasa.ac.at/web-apps/tnt/RcpDb.

[69]Etminan et al., 2016 provide new calculations of the radiative force with respect to Myhre et al., 1998. They propose a GHG concentration-dependence for the forcing sensitivity, so that it can be expressed as $\varphi = 5.35 + \varphi_1|S_t - S_{\text{pre-ind}}| + \varphi_2(S_t - S_{\text{pre-ind}})^2 + \varphi_N(N_t + N_{\text{pre-ind}})/2$, where N_t denotes the stock of nitrous oxide.

of covariate i and β_i^j is the set of coefficients to be estimated by OLS.[70]

$$g(r) = \sum_{i=1}^{10} \sum_{j=1}^{10} \beta_i^j Z_i^j(r) \tag{42}$$

$$Z_i^j(r) = \cos\left(j \cdot \arccos\left(\frac{\tilde{Z}_i(r)}{\max_{s \in S} |\tilde{Z}_i(s)|} \right) \right)$$

$$\tilde{Z}_i(r) = \left(Z_i(r) - \frac{1}{2} \left(\min_{s \in S} Z_i(s) + \max_{s \in S} Z_i(s) \right) \right)$$

To estimate (17) and (42), we construct the temperature variables as follows: $T_{\text{base}}(r)$ is the average temperature from 1950 to 1979 in cell r, $T_t(r)$ is the yearly temperature from 1980 to 2017 in cell r, and T_{base} is the global average of $T_{\text{base}}(r)$, where each cell is weighted by land size. Finally, we provide more weight to the more recent observations, according to $\omega_t = (2018 - t)^{-1}$. The estimation procedure is able to capture 83% of the variance of the data.

E   Additional Baseline and Policy Results

E.1   Real GDP losses from Global Warming

Figure 28 displays the baseline losses in real GDP and Figure 29 the losses by uncertainty level.[71]
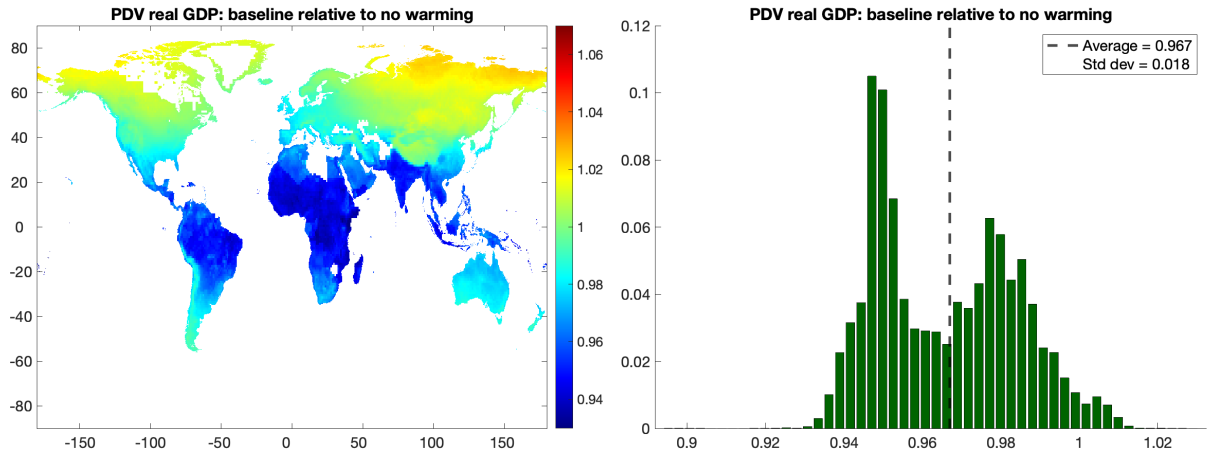
Figure 28: Real GDP losses due to global warming.

---

[70]When constructing the product of latitude and longitude, we first normalize latitude and longitude so that they lie between minus one and one, and then we multiply them. That is, we define this product as $Z_{\text{lat}}^j(\cdot) \times Z_{\text{lon}}^j(\cdot)$.

[71]Baseline average damages in real GDP and welfare rise until the years 2164 and 2199, respectively. The more prolonged path of welfare damages is attributed to the damage function on amenities having a greater slope than that of productivities for relatively warm temperatures, so that population keeps moving to locations with relatively low fundamental amenities.
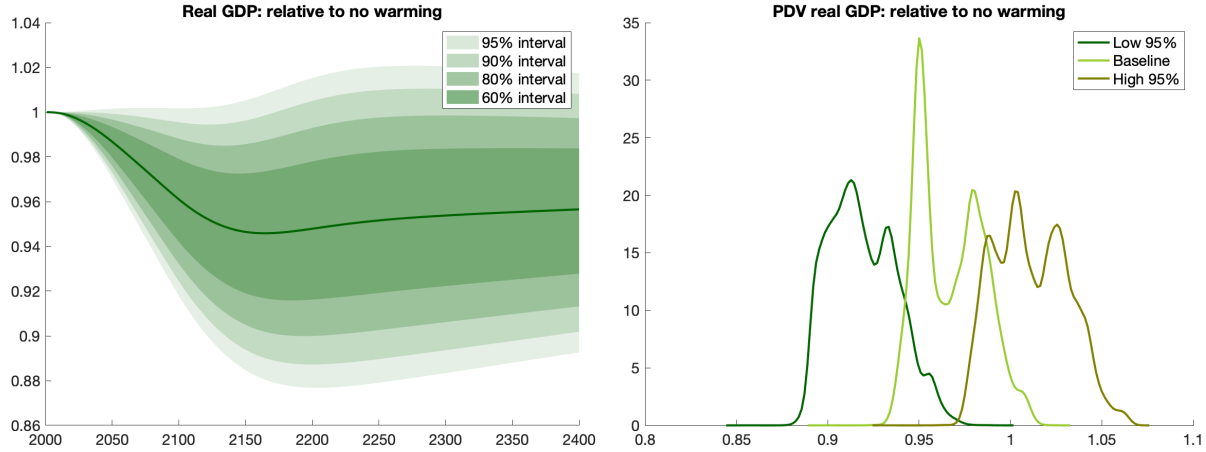
Figure 29: Real GDP losses by uncertainty level.

E.2 Decomposing the Losses from Global Warming by Source

As we argued in the main text, the two main direct channels through which global warming affects economic outcomes are the effects on amenities and productivities. In fact, incorporating the effect of temperature on amenities at this level of spatial disaggregation is, we believe, novel to our study. To understand the contribution of each of these two sources of economic effects, we decompose the warming damages as those arising exclusively from the effect of temperature on local amenities and those arising exclusively from the effect of temperature on local productivities. That is, we calculate two additional counterfactual scenarios setting each of the damage functions to zero for every period and cell, respectively.
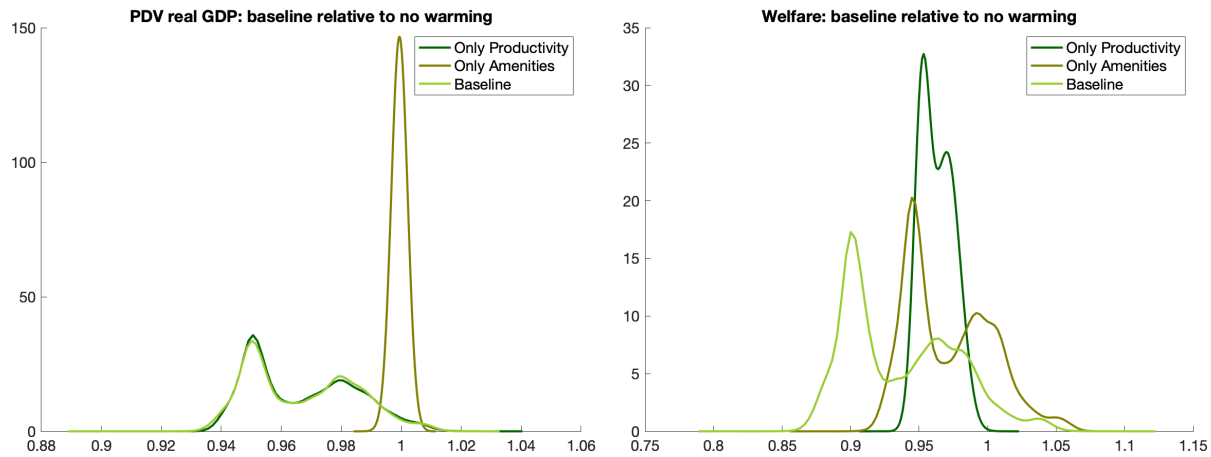
Figure 30: Distribution of real GDP and welfare losses by damage source.

Figure 30 compares the cross-section of losses in the PDV of real GDP and welfare across damage sources. The spatial distribution of real GDP losses is mainly driven by the productivity component. The amenity component affects real GDP through its effect on the spatial distribution of population and the

corresponding effects of investment. However, the effects are small compared to the direct impact of productivity. In contrast, when we analyze the cross-sectional distribution of welfare, the role of amenities is very large and governs the overall shape of the distribution. For welfare, the productivity component is more uniform across regions with implied losses for almost all locations. This exercise highlights the importance of incorporating the effect of changes in temperature on amenities when assessing the local welfare impact of global warming.

Figure 31 displays the spatial composition of losses in welfare when the damage function only takes into account damages on amenities or productivities, respectively. The large dispersion in the effect coming exclusively from amenities implies large gains in Russia, Canada, and Alaska, and losses in South America, Africa, and India. In contrast, the spatial distribution of the effects coming exclusively through the productivity channel implies losses in most of the southern regions. All southern regions, including Australia, suffer, and the losses reach further north to Mexico and the Southern part of the U.S., as well as India and China. Clearly, the spatial distribution of the losses from global warming that result from each source are quite different.
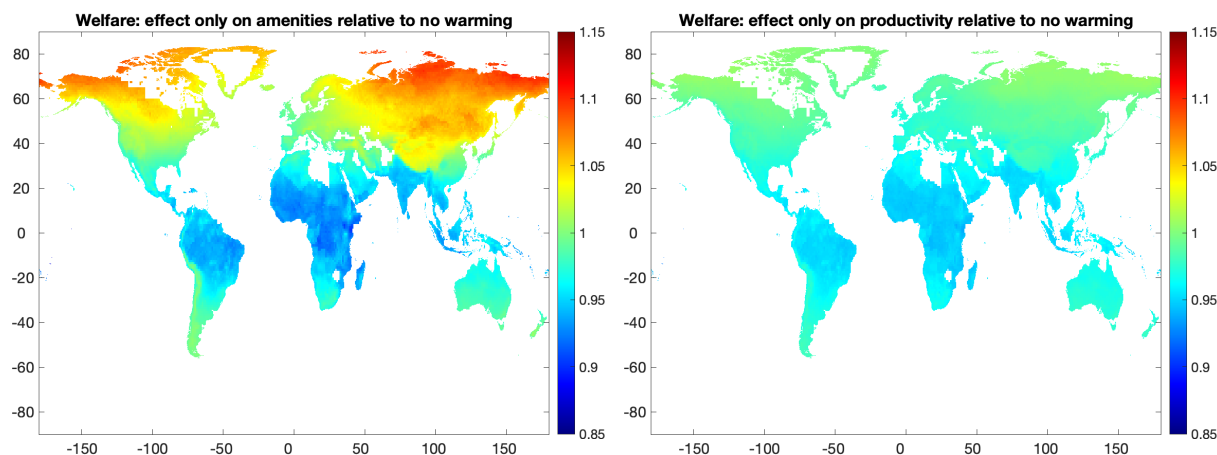
Figure 31: Spatial distribution of real GDP and welfare losses due to global warming by damage source.

To end this subsection, Figure 32 decomposes the evolution of economic losses over time. When we consider damages on amenities only, cold regions become more amenable for living, which creates an incentive for people to move to some of the most productive places in the world. This migration boosts agglomeration and thus rises global average real GDP slightly for the first 200 years. Eventually, as temperatures decline due to the rising cost of extracting fossil fuels, this process reverses. Welfare, in contrast, exhibits only losses that accelerate as rising temperatures deteriorate amenities in the developing world. When we isolate the damages from warming coming from changes in local fundamental productivity, the evolution of losses in real GDP is similar to the benchmark scenario for the first century. Without the impact of climate on amenities, however, less people move north which results in less agglomeration and slightly

larger real GDP losses. The difference is much larger when considering welfare. The effect on amenities essentially doubles the impact of global warming on welfare throughout. Overall, Figure 32 shows that the effect of temperature on fundamental productivity and the effect of temperature on amenities, each account for about half of the total welfare losses from global warming.
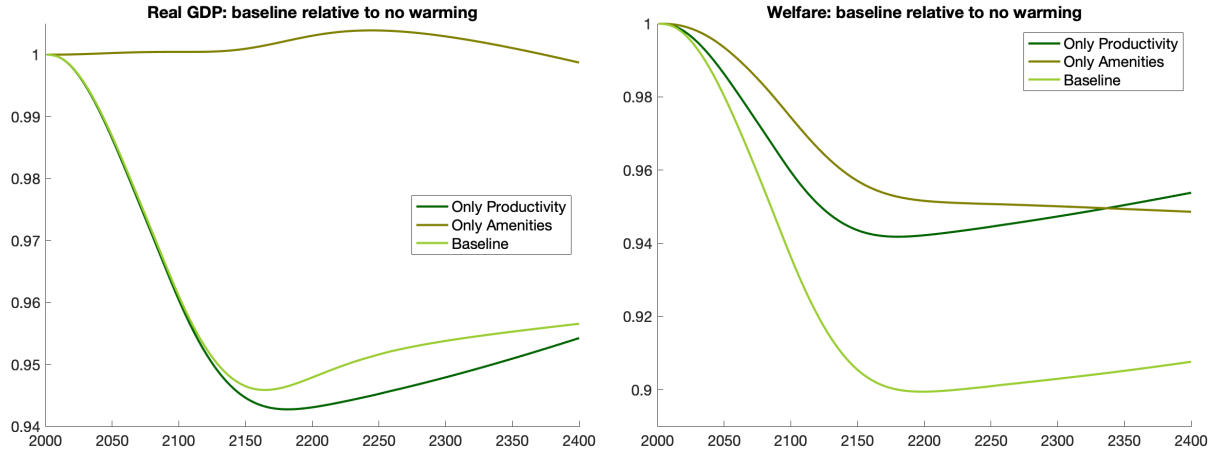
Figure 32: Real GDP and welfare losses by damage source over time.

E.3 Trade as an Adaptation Mechanism: Additional Results

Figure 33 presents the spatial and dynamic effect on welfare for values of ϑ of 1.5 and 2. The left panel presents the spatial distribution of the relative effect of global warming on welfare in the baseline scenario with respect to the same relative effect in the scenario with higher trade costs. In this diff-and-diff calculation, large values, represented in red, identify areas that are hurt by larger trade costs. As is evident in Figure 33 trade costs have a negligible effect on the cost of global warming.

The spatial pattern in Figure 33 is markedly different than the one for migration. As with migration, larger trade costs make warming more harmful in Africa, India, and China. However, it also makes warming more harmful in Central and South America, as well as Europe, and less harmful in northern regions in Canada, Scandinavia, and Russia. Trade has little impact on northern regions since their relative isolation implies that they trade little with the rest of the world anyway. In contrast, regions in more central, well connected geographies, rely more on trade and so they suffer from the double impact of higher trade costs and higher temperatures. In addition, as with migration, higher trade costs reduce incomes which results in higher natality rates, particularly in the developed world, leading to additional congestion. Brazil, Africa, and India are affected the most.

The right panel of Figure 33 shows the temporal evolution of average welfare. As with migration, we plot cases keeping the evolution of temperatures and population constant, as well as the full equilibrium evolution. The small effect of trade is evident, particularly when conditioning on the temperature path.

65

Once we take the effect of changes in income and population on the evolution of temperature into account, we get smaller losses from global warming with higher trade costs in the short-run, but larger ones in the long-run. Similar to the case of changes in migration costs, lower incomes lead to smaller increases in temperature in the short-run, but larger population leads to greater losses from temperature rises in the long-run.[72] Overall, adaptation through trade seems to play only a minor role in our results.
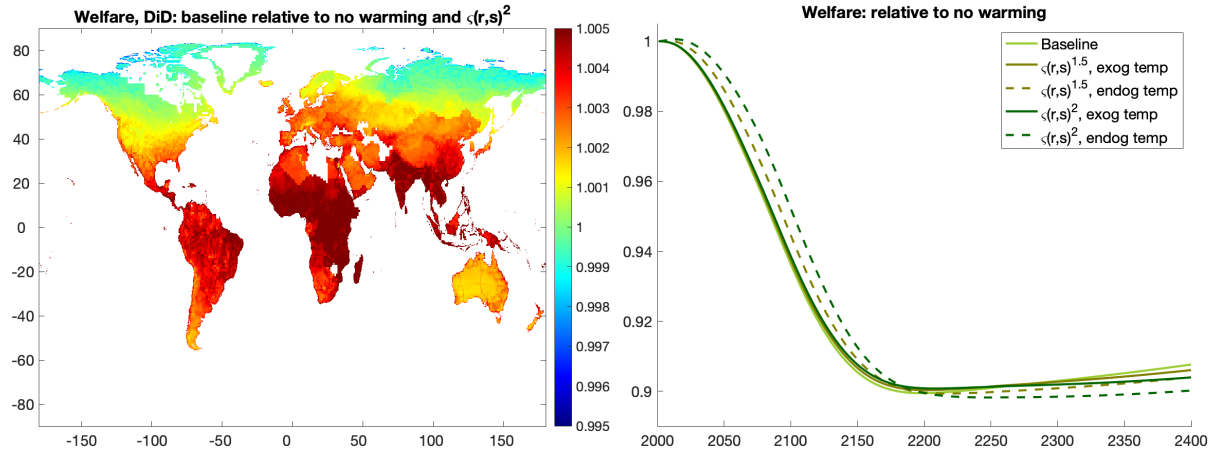
Figure 33: Welfare across different iceberg trade costs.

E.4 Abatement: Additional Results

Here, we present the evolution of emission, temperature, real GDP and welfare over time with carbon taxes and an abatement technology that appears in 2100. Figure 34 introduces the abatement technology to the exercises represented in Figure 13. The solid curves present CO_2 emissions and global temperature under different carbon taxes when the abatement technology is not available. The dashed curves, present the results with the introduction of a perfect abatement technology in 2100. When the abatement technology is introduced, the flow of CO_2 into the atmosphere drops discontinuously and permanently to zero. The cut in the cumulative carbon dioxide emissions has transcendental consequences in the temperature path, which declines until it reaches a new and much lower steady-state.

Figure 35 replicates Figure 14 but includes, in dashed lines, the global average real GDP and welfare effects of the implementation of a carbon tax relative to a scenario with no carbon taxes, when we introduce the abatement technology in 2100. Since the abatement technology eliminates the effect of carbon emission on temperatures, and therefore on amenities and productivity, the deceleration of growth caused by global warming that we observe after 2100 without an abatement technology is now avoided.[73]

---

[72]World population increases as much as 6.5 billions by 2200 when $\vartheta = 2$.

[73]Note that relative real GDP and welfare can be slightly lower in the abatement case for a couple of decades after the invention of the abatement technology. The reason is that the difference in temperatures between the benchmark scenario with and without
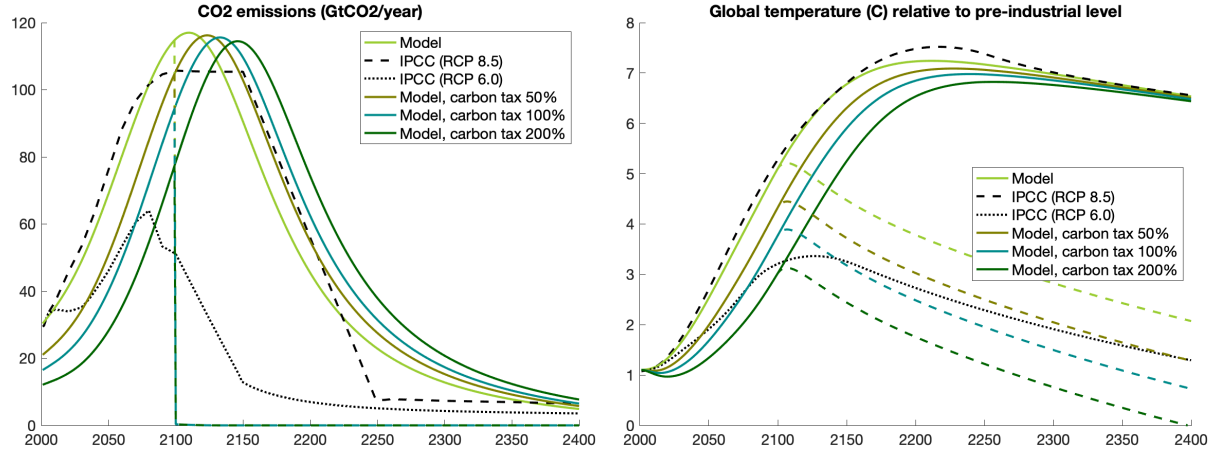
Figure 34: CO_2 emissions and global temperature for different carbon taxes with an abatement technology introduced in 2100.
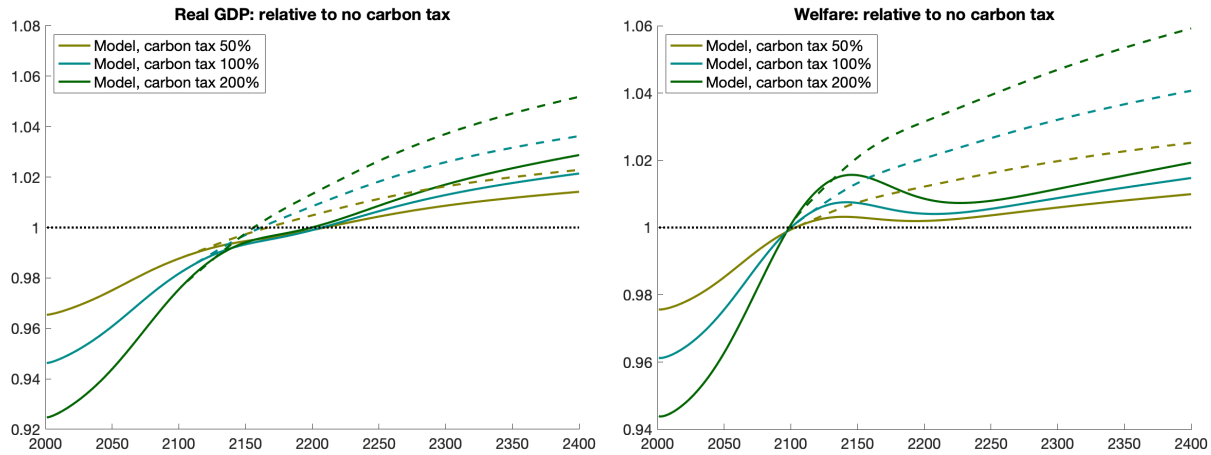
Figure 35: Real GDP and welfare for different carbon taxes with an abatement technology introduced in 2100.

E.5 Clean Energy Subsidies: Additional Results

At impact, the subsidy on clean energy leads to a reduction in the composite price of energy. Given our Cobb-Douglas production function, the subsidy acts like a positive production subsidy that increases output and encourages innovation, which accelerates growth. Given that the model features dynamic spillovers that are not internalized in equilibrium, such a subsidy is potentially beneficial. Furthermore, the subsidy leads to declines in energy costs that vary across locations. Areas using more clean energy relatively to fossil fuels undergo greater declines in the composite price of energy. On average, developed

---

abatement can be larger than the difference in temperature with and without abatement in the scenario with a carbon tax, depending on the second derivative of the temperature function at the time the abatement technology arrives. After a few decades, this effect is always dominated by the faster increases in temperature in the case without abatement.

countries tend to be more intensive in clean energy, attracting more households to those places. The re-location of people towards the most productive places rises global real GDP and welfare, but also lowers natality rates and world population in the long-run. A lower population in the balanced growth path leads to lower long-run growth rates. In sum, subsidies increase output and welfare in the short-run, but eventually reduce them in the long-run. As with carbon taxes, the overall economic effects from the subsidy depend on the discount factor. In this case, however, the sign of the short- and long-run effects are reversed relative to the carbon tax. Larger discount factors result in smaller gains. Table 7 presents these results.

	PDV of real GDP			Welfare		
	BGP gr	β=0.965	β=0.969	BGP gr	β=0.965	β=0.969
s=0%	3.076%	1	1	2.971%	1	1
s=25%	3.073%	1.012	1.005	2.967%	1.007	1.003
s=50%	3.066%	1.034	1.008	2.959%	1.021	1.006
s=75%	3.044%	1.098	1.007	2.935%	1.053	1.000

Table 7: PDV of real GDP and welfare gains for different clean energy subsidies and discount factors.

Figure 36 presents the spatial distribution of welfare gains from a 75% clean energy subsidy relative to the baseline. The left panel shows the heterogeneous spatial effects from the subsidy. As we discussed above, the subsidy has only a small impact on the temperature path. The main source of spatial heterogeneity comes from the differences in the relative price of fossil fuels and clean energy. Remember that, in the quantification of our model, we infer this relative price using the relative use of energy sources, which is available at the country level only (which explains the national demarcations in the figure). Scandinavia has a large relative price of fossil fuels (partly because of other prevailing policies) and so it benefits more from the subsidy than the Arabian peninsula or Australia, where fossil fuels are relatively cheap. Paraguay benefits significantly, since clean energy is cheap there due to the abundance of hydroelectric power. The right panel presents the distribution of welfare gains. Parts of Africa and South America gain in welfare 7%, while some regions in North Africa or the Arabian peninsula gain only 3%. Higher discount factors would make some of these regions lose.
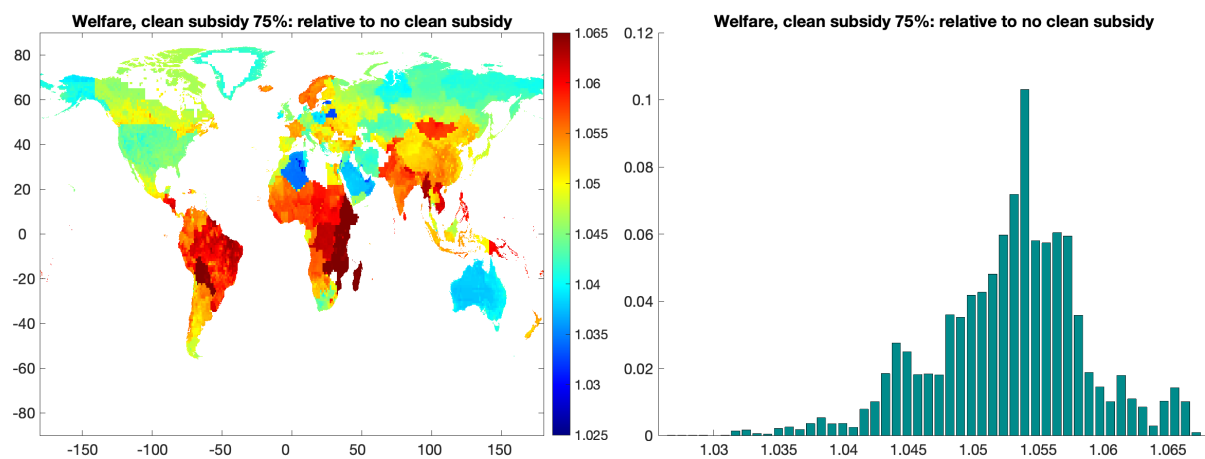
Figure 36: Local welfare effects of a clean energy subsidy of 75% with a discount factor of $\beta = 0.965$.

The Economic Geography of Global Warming

José-Luis Cruz and Esteban Rossi-Hansberg

Supplementary Materials: Not for Publication

F Proofs

In this section, we discuss the solution of the model, as well as the existence and uniqueness of a balanced growth path. Additionally, we outline the solution of the model backwards in time and the system of equations that solve for fundamental amenities, productivities and migration costs.

F.1 Forward Solution

In this subsection, we compute the forward solution of the model under the presence of proportional carbon taxes, $\tau_t(r)$, and clean energy subsidies, $s_t(r)$. Those taxes are charged to the firm and uniformly rebated to the households residing in region r itself through a lump-sum transfer, $\Phi_t(r)$.

The firm's cost minimization problem, in terms of fossil fuels and clean energy, is given by:

$$w_t(r)\mathcal{Q}_t(r)e_t^\omega(r) = \min_{e^f,e^c} \quad w_t(r)(1+\tau_t(r))\mathcal{Q}_t^f(r)e_t^{f,\omega}(r) + w_t(r)(1-s_t(r))\mathcal{Q}_t^c(r)e_t^{c,\omega}(r)$$

$$\text{st} \quad \left(\kappa e_t^{f,\omega}(r)^{\frac{\epsilon-1}{\epsilon}} + (1-\kappa)e_t^{c,\omega}(r)^{\frac{\epsilon-1}{\epsilon}}\right)^{\frac{\epsilon}{\epsilon-1}} = e_t^\omega(r)$$

The First Order Conditions with respect to $e_t^{f,\omega}(r)$ and $e_t^{c,\omega}(r)$ imply the following relations, where $\mathcal{Q}_t(r)$ is the ideal energy price index.

$$\frac{e_t^{c,\omega}(r)}{e_t^{f,\omega}(r)} = \left(\frac{1-\kappa}{\kappa}\frac{1+\tau_t(r)}{1-s_t(r)}\frac{\mathcal{Q}_t^f(r)}{\mathcal{Q}_t^c(r)}\right)^\epsilon \tag{43}$$

$$\mathcal{Q}_t(r) = \left(\kappa^\epsilon(1+\tau_t(r))^{1-\epsilon}\mathcal{Q}_t^f(r)^{1-\epsilon} + (1-\kappa)^\epsilon(1-s_t(r))^{1-\epsilon}\mathcal{Q}_t^c(r)^{1-\epsilon}\right)^{\frac{1}{1-\epsilon}} \tag{44}$$

We define the lump-sum transfer, per unit of land, as shown in equation (45).

$$\Phi_t(r) = \int_0^1 \Phi_t^\omega(r)d\omega$$

$$\Phi_t^\omega(r) = \left(\tau_t(r)\mathcal{Q}_t^f(r)e_t^{f,\omega}(r) - s_t(r)\mathcal{Q}_t^c(r)e_t^{c,\omega}(r)\right) \tag{45}$$

$$= \mathcal{Q}_t(r)e_t^\omega(r) - \left(\mathcal{Q}_t^f(r)e_t^{f,\omega}(r) + \mathcal{Q}_t^c(r)e_t^{f,\omega}(r)\right)$$

$$= \mathcal{Q}_t(r)e_t^\omega(r) - \tilde{\mathcal{Q}}_t(r)^{1-\epsilon}\mathcal{Q}_t(r)^\epsilon e_t^\omega(r)$$

$$\tilde{\mathcal{Q}}_t(r) = \left(\kappa^\epsilon(1+\tau_t(r))^{-\epsilon}\mathcal{Q}_t^f(r)^{1-\epsilon} + (1-\kappa)^\epsilon(1-s_t(r))^{-\epsilon}\mathcal{Q}_t^c(r)^{1-\epsilon}\right)^{\frac{1}{1-\epsilon}} \tag{46}$$

Equation (44) reduces the firm's problem to:

$$\max_{q,L,\phi,e} \quad p_t^\omega(r,r)\phi_t^\omega(r)^{\gamma_1}z_t^\omega(r)\left(L_t^\omega(r)^\chi e_t^\omega(r)^{1-\chi}\right)^\mu - w_t(r)L_t^\omega(r)$$

$$- w_t(r)\nu\phi_t^\omega(r)^\xi - w_t(r)\mathcal{Q}_t(r)e_t^\omega(r) - R_t(r)$$

The First Order Conditions with respect to $e_t^\omega(r)$ and $L_t^\omega(r)$ imply:

$$\mathcal{Q}_t(r)e_t^\omega(r) = \left(\frac{1-\chi}{\chi}\right)L_t^\omega(r) \tag{47}$$

Equation (47) collapses the firm's problem to:

$$\max_{L,\phi} \quad p_t^\omega(r,r)\left(\frac{1-\chi}{\chi}\frac{1}{\mathcal{Q}_t(r)}\right)^{(1-\chi)\mu}\phi_t^\omega(r)^{\gamma_1}z_t^\omega(r)L_t^\omega(r)^\mu - \frac{w_t(r)L_t^\omega(r)}{\chi} - w_t(r)\nu\phi_t^\omega(r)^\xi - R_t(r)$$

The First Order Conditions with respect to $\phi_t^\omega(r)$ and $L_t^\omega(r)$ imply:

$$w_t(r)L_t^\omega(r) = \mu\chi\left(p_t^\omega(r,r)q_t^\omega(r)\right) \tag{48}$$

$$\chi\mu\nu\phi_t^\omega(r)^\xi = (\gamma_1/\xi)L_t^\omega(r) \tag{49}$$

We define total labor demand, $\bar{L}_t^\omega(r)$, as the demand from production, $L_t^\omega(r)$; innovation, $L_t^{\phi,\omega}(r)$; fossil fuel energy, $L_t^{f,\omega}(r)$; and clean energy, $L_t^{c,\omega}(r)$. Then, we insert equations (46), (47) and (49).

$$\bar{L}_t^\omega(r) = L_t^\omega(r) + L_t^{\phi,\omega}(r) + L_t^{f,\omega}(r) + L_t^{c,\omega}(r)$$

$$= L_t^\omega(r) + \nu\phi_t^\omega(r)^\xi + \mathcal{Q}_t^f(r)e_t^{f,\omega}(r) + \mathcal{Q}_t^c(r)e_t^{c,\omega}(r)$$

$$= L_t^\omega(r) + \frac{\gamma_1/\xi}{\mu\chi}L_t^\omega(r) + \left(\frac{\tilde{\mathcal{Q}}_t(r)}{\mathcal{Q}_t(r)}\right)^{1-\epsilon}\mathcal{Q}_t(r)e_t(r)$$

$$= L_t^\omega(r) + \frac{\gamma_1/\xi}{\mu\chi}L_t^\omega(r) + \left(\frac{\tilde{\mathcal{Q}}_t(r)}{\mathcal{Q}_t(r)}\right)^{1-\epsilon}\left(\frac{1-\chi}{\chi}\right)L_t^\omega(r)$$

$$= \frac{\mu\chi + \gamma_1/\xi + \mu(1-\chi)(\tilde{\mathcal{Q}}_t(r)/\mathcal{Q}_t(r))^{1-\epsilon}}{\mu\chi}L_t^\omega(r)$$

To ease notation, define $\varphi_t(r)$ as shown in (50). Note that when taxes and subsidies are zero, $\varphi_t(r) = 1$.

$$\varphi_t(r) = \frac{\mu\chi + \gamma_1/\xi + \mu(1-\chi)(\tilde{\mathcal{Q}}_t(r)/\mathcal{Q}_t(r))^{1-\epsilon}}{\mu + \gamma_1/\xi} \tag{50}$$

$$\bar{L}_t^\omega(r) = \left(\frac{\mu + \gamma_1/\xi}{\mu\chi}\right)\varphi_t(r)L_t^\omega(r) \tag{51}$$

Combine equations (7), (43), (47), (51) and rewrite fossil fuel and clean energy use as:

$$e_t^{f,\omega}(r) = \left(\frac{(1-\chi)\mu}{\mu + \gamma_1/\xi}\right) \left(\frac{\bar{L}_t^\omega(r)}{\varphi_t(r)\mathcal{Q}_t(r)}\right) \left(\frac{\kappa \mathcal{Q}_t(r)}{(1+\tau_t(r))\mathcal{Q}_t^f(r)}\right)^\epsilon \tag{52}$$

$$e_t^{c,\omega}(r) = \left(\frac{(1-\chi)\mu}{\mu + \gamma_1/\xi}\right) \left(\frac{\bar{L}_t^\omega(r)}{\varphi_t(r)\mathcal{Q}_t(r)}\right) \left(\frac{(1-\kappa)\mathcal{Q}_t(r)}{(1-s_t(r))\mathcal{Q}_t^c(r)}\right)^\epsilon \tag{53}$$

Due to the Cobb Douglas formulation of the production function, rents $R_t(r)$ can be expressed as a constant fraction of revenue, by inserting equations (48) and (49).

$$R_t(r) = p_t^\omega(r,r)q_t^\omega(r) - \frac{w_t(r)L_t^\omega(r)}{\chi} - w_t(r)\nu\phi_t^\omega(r)^\xi$$

$$= (1 - \mu - \gamma_1/\xi)p_t^\omega(r,r)q_t^\omega(r) \tag{54}$$

Since in equilibrium $R_t(r)$ is taken as given by firms producing at r, the decisions of how much to innovate, $\phi_t^\omega(r)$, how many workers to hire per unit of land, $L_t^\omega(r)$, and how much energy to use from fossil fuels, $e_t^{f,\omega}(r)$, and clean energy, $e_t^{c,\omega}(r)$, are independent of the local idiosyncratic productivity shocks, $z_t^\omega(r)$, and so are identical across varieties ω. Hereinafter, we drop the superscript ω, except from production labor, $L_t^\omega(r)$, to differentiate it from total labor demand, $L_t(r)$.

We arrange firm sales by inserting equations (48) and (49).

$$p_t(r,r)q_t(r) = p_t(r,r)\left(\frac{1-\chi}{\chi}\frac{1}{\mathcal{Q}_t(r)}\right)^{(1-\chi)\mu}\phi_t(r)^{\gamma_1}z_t(r)L_t^\omega(r)^\mu$$

$$= p_t(r,r)z_t(r)\left(\frac{1-\chi}{\chi}\frac{1}{\mathcal{Q}_t(r)}\right)^{(1-\chi)\mu}\left(\frac{\gamma_1\chi}{\xi\nu}\frac{p_t(r,r)q_t(r)}{w_t(r)}\right)^{\frac{\gamma_1}{\xi}}\left(\mu\chi\frac{p_t(r,r)q_t(r)}{w_t(r)}\right)^\mu$$

$$(p_t(r,r)q_t(r))^{1-\mu-\gamma_1/\xi} = p_t(r,r)z_t(r)\left(\frac{1-\chi}{\chi}\frac{1}{\mathcal{Q}_t(r)}\right)^{(1-\chi)\mu}\left(\frac{\gamma_1\chi}{\xi\nu}\right)^{\frac{\gamma_1}{\xi}}(\mu\chi)^\mu w_t(r)^{-\mu-\gamma_1/\xi} \tag{55}$$

We define marginal cost, $mc_t(r)$, as shown below and insert equations (48) and (51) in equation (55).

$$mc_t(r) = p_t(r,r)z_t(r)$$

$$= \left(\frac{1-\chi}{\chi}\frac{1}{\mathcal{Q}_t(r)}\right)^{-(1-\chi)\mu}\left(\frac{\gamma_1\chi}{\xi\nu}\right)^{-\frac{\gamma_1}{\xi}}(\mu\chi)^{-\mu}w_t(r)^{\mu+\gamma_1/\xi}(p_t(r,r)q_t(r))^{1-\mu-\gamma_1/\xi}$$

$$= \left(\frac{1-\chi}{\chi}\frac{1}{\mathcal{Q}_t(r)}\right)^{-(1-\chi)\mu}\left(\frac{\gamma_1\chi}{\xi\nu}\right)^{-\frac{\gamma_1}{\xi}}(\mu\chi)^{\gamma_1/\xi-1}w_t(r)L_t^\omega(r)^{1-\mu-\gamma_1/\xi}$$

$$= \left(\frac{1-\chi}{\chi}\right)^{-(1-\chi)\mu}\left(\frac{\gamma_1\chi}{\xi\nu}\right)^{-\frac{\gamma_1}{\xi}}\mu^{-\mu}\chi^{-(\mu+\gamma_1/\xi)}$$

$$\times \varphi_t(r)^{-(1-\mu-\gamma_1/\xi)}\mathcal{Q}_t(r)^{(1-\chi)\mu}w_t(r)L_t(r)^{1-\mu-\gamma_1/\xi} \tag{56}$$

We define total revenue per unit of land, $\mathcal{R}_t(r)$, as the sum of labor revenue, rents and lump sum transfer.

$$\mathcal{R}_t(r) = w_t(r)L_t(r) + R_t(r) + w_t(r)\Phi_t(r)$$

$$= w_t(r)L_t(r) + (1 - \mu - \gamma_1/\xi)y_t(r) + w_t(r)\left[1 - \left(\frac{\tilde{\mathcal{Q}}_t(r)}{\mathcal{Q}_t(r)}\right)^{1-\epsilon}\right]\mathcal{Q}_t(r)e_t(r)$$

$$= w_t(r)L_t(r) + \left(\frac{1 - \mu - \gamma_1/\xi}{\mu\chi}\right)w_t(r)L_t(r) + w_t(r)\left[1 - \left(\frac{\tilde{\mathcal{Q}}_t(r)}{\mathcal{Q}_t(r)}\right)^{1-\epsilon}\right]\left(\frac{1-\chi}{\chi}\right)L_t^\omega(r)$$

$$= \left(\frac{1 - \mu - \gamma_1/\xi + \mu\chi}{\mu\chi}\right)w_t(r)L_t(r) + w_t(r)\left[1 - \left(\frac{\tilde{\mathcal{Q}}_t(r)}{\mathcal{Q}_t(r)}\right)^{1-\epsilon}\right]\left(\frac{\mu(1-\chi)}{\mu+\gamma_1/\xi}\right)\frac{1}{\varphi_t(r)}L_t(r)$$

$$= \left(\frac{1}{\mu + \gamma_1/\xi}\right)\left(\frac{w_t(r)L_t(r)}{\varphi_t(r)}\right) \tag{57}$$

Now, we combine equations (4) and (57), where $y_t(r) = \mathcal{R}_t(r)/(L_t(r)P_t(r))$.

$$u_t(r) = \bar{b}_t(r)L_t(r)^{-\lambda}\frac{\mathcal{R}_t(r)}{L_t(r)P_t(r)}$$

$$= \bar{b}_t(r)L_t(r)^{-\lambda}\left(\frac{1}{\mu + \gamma_1/\xi}\right)\left(\frac{w_t(r)}{\varphi_t(r)}\right)\left(\frac{1}{P_t(r)}\right) \tag{58}$$

We solve for $P_t(r)$ and employ equations (12) and (56).

$$P_t(r) = \frac{\bar{b}_t(r)}{u_t(r)}L_t(r)^{-\lambda}\left(\frac{1}{\mu + \gamma_1/\xi}\right)\left(\frac{w_t(r)}{\varphi_t(r)}\right) \tag{59}$$

$$= \Gamma\left(\frac{-\rho}{(1-\rho)\theta + 1}\right)^{-\frac{1-\rho}{\rho}}\left(\int_S a_t(v)[mc_t(v)\varsigma(r,v)]^{-\theta}dv\right)^{-\frac{1}{\theta}}$$

$$= (\bar{p}\bar{\kappa})\left(\int_S \bar{a}_t(v)L_t(v)^{\alpha - (1-\mu-\gamma_1/\xi)\theta}\varphi_t(v)^{(1-\mu-\gamma_1/\xi)\theta}\mathcal{Q}_t(v)^{-(1-\chi)\mu\theta}w_t(v)^{-\theta}\varsigma(r,v)^{-\theta}dv\right)^{-\frac{1}{\theta}} \tag{60}$$

And we define $\bar{p}$ and $\bar{\kappa}$ as shown below.

$$\bar{p} = \Gamma\left(\frac{-\rho}{(1-\rho)\theta + 1}\right)^{-\frac{1-\rho}{\rho}}$$

$$\bar{\kappa} = \left(\frac{1-\chi}{\chi}\right)^{-(1-\chi)\mu}\left(\frac{\gamma_1\chi}{\xi\nu}\right)^{-\frac{\gamma_1}{\xi}}\mu^{-\mu}\chi^{-(\mu+\gamma_1/\xi)}$$

We manipulate the equation (60) to obtain (61).

$$\left(\frac{\bar{b}_t(r)}{u_t(r)}\right)^{-\theta}L_t(r)^{\lambda\theta}\left(\frac{w_t(r)}{\varphi_t(r)}\right)^{-\theta} = \kappa_1$$

$$\times \left(\int_S \bar{a}_t(v)L_t(v)^{\alpha - (1-\mu-\gamma_1/\xi)\theta}\varphi_t(v)^{(1-\mu-\gamma_1/\xi)\theta}\mathcal{Q}_t(v)^{-(1-\chi)\mu\theta}w_t(v)^{-\theta}\varsigma(r,v)^{-\theta}dv\right) \tag{61}$$

Where $\kappa_1 = ((\mu + \gamma_1/\xi)\bar{p}\bar{\kappa})^{-\theta}$. Now, we use the condition that trade is balanced cell by cell, given by equation (13), considering the expression of revenue per unit of land found in equation (57), and insert the

expression for trade shares, given by equation (11).

$$\frac{w_t(r)H(r)L_t(r)}{\varphi_t(r)} = \int_S \frac{\pi_t(v,r)w_t(v)H(v)L_t(v)}{\varphi_t(v)}dv$$

$$= \bar{p}^{-\theta} \int_S \frac{a_t(r)[mc_t(r)\varsigma(r,v)]^{-\theta}P_t(v)^{\theta}w_t(v)H(v)L_t(v)}{\varphi_t(v)}dv \tag{62}$$

We insert equation (56) in the left-hand side of equation (62).

$$\frac{w_t(r)H(r)L_t(r)}{\varphi_t(r)a_t(r)}mc_t(r)^{\theta}$$

$$= \frac{w_t(r)H(r)L_t(r)^{1-\alpha}}{\varphi_t(r)\bar{a}_t(r)}\left(\bar{\kappa}\varphi_t(r)^{-(1-\mu-\gamma_1/\xi)}\mathcal{Q}_t(r)^{(1-\chi)\mu}w_t(r)L_t(r)^{1-\mu-\gamma_1/\xi}\right)^{\theta} \tag{63}$$

We insert equation (59) in the right-hand side of equation (62).

$$\int_S P_t(v)^{\theta}\left(\frac{w_t(v)H(v)L_t(v)}{\varphi_t(v)}\right)\varsigma(r,v)^{-\theta}dv$$

$$= \int_S \left(\frac{\bar{b}_t(v)}{u_t(v)}L_t(v)^{-\lambda}\left(\frac{1}{\mu+\gamma_1/\xi}\right)\left(\frac{w_t(v)}{\varphi_t(v)}\right)\right)^{\theta}\left(\frac{w_t(v)H(v)L_t(v)}{\varphi_t(v)}\right)\varsigma(r,v)^{-\theta}dv \tag{64}$$

We manipulate equations (63) and (64) to obtain equation (65).

$$\bar{a}_t(r)^{-1}w_t(r)^{1+\theta}L_t(r)^{1-\alpha+(1-\mu-\gamma_1/\xi)\theta}\mathcal{Q}_t(r)^{(1-\chi)\mu\theta}\varphi_t(r)^{-(1+(1-\mu-\gamma_1/\xi)\theta)}H(r)$$

$$= \kappa_1 \int_S \left(\frac{\bar{b}_t(v)}{u_t(v)}\right)^{\theta}L_t(v)^{1-\lambda\theta}\varphi_t(v)^{-(1+\theta)}w_t(v)^{1+\theta}H(v)\varsigma(r,v)^{-\theta}dv \tag{65}$$

Equations (3), (4), (8), (10), (44), (61) and (65) define a system of equations that solves for $u_t(r), L_t(r), w_t(r)$ and $\mathcal{Q}_t(r)$. Assuming trade costs are symmetric, we use equations (61) and (65) and introduce the function $f_1(\cdot)$, which is the ratio of the left-hand sides of (65) and (61).

$$f_1(r) = \frac{\bar{a}_t(r)^{-1}w_t(r)^{1+\theta}L_t(r)^{1-\alpha+(1-\mu-\gamma_1/\xi)\theta}\mathcal{Q}_t(r)^{(1-\chi)\mu\theta}\varphi_t(r)^{-(1+(1-\mu-\gamma_1/\xi)\theta)}H(r)}{\left(\frac{\bar{b}_t(r)}{u_t(r)}\right)^{-\theta}L_t(r)^{\lambda\theta}w_t(r)^{-\theta}\varphi_t(r)^{\theta}}$$

$$= \bar{a}_t(r)^{-1}w_t(r)^{1+2\theta}L_t(r)^{1-\alpha-\theta(\lambda+\gamma_1/\xi-(1-\mu))}$$

$$\times \varphi_t(r)^{-(1+\theta(2-\mu-\gamma_1/\xi))}\mathcal{Q}_t(r)^{(1-\chi)\mu\theta}H(r)\left(\frac{\bar{b}_t(r)}{u_t(r)}\right)^{\theta} \tag{66}$$

Obviously, $f_1(r)$ equals the right-hand sides.

$$f_1(r) = \frac{\int_S \left(\frac{\bar{b}_t(v)}{u_t(v)}\right)^{\theta}L_t(v)^{1-\lambda\theta}\varphi_t(v)^{-(1+\theta)}w_t(v)^{1+\theta}H(v)\varsigma(r,v)^{-\theta}dv}{\int_S \bar{a}_t(v)L_t(v)^{\alpha-(1-\mu-\gamma_1/\xi)\theta}\varphi_t(v)^{(1-\mu-\gamma_1/\xi)\theta}\mathcal{Q}_t(v)^{-(1-\chi)\mu\theta}w_t(v)^{-\theta}\varsigma(r,v)^{-\theta}dv}$$

Under the assumption that $\varsigma(r,v) = \varsigma(v,r)$, we can express $f_1(\cdot)$ as shown below.

$$f_1(r) = \frac{\int_S f_1(v)^{-\lambda} f_2(v,r) dv}{\int_S f_1(v)^{-(1+\lambda)} f_2(v,r) dv}$$

$$f_2(v,r) = \left(\frac{\bar{b}_t(v)}{u_t(v)}\right)^{\theta(1+\lambda)} \bar{a}_t(v)^{-\lambda} L_t(v)^{1-\lambda\theta-\lambda[\alpha-1+\theta(\lambda+\gamma_1/\xi-(1-\mu))]} Q_t(v)^{(1-\chi)\mu\theta\lambda}$$

$$\times \varphi_t(v)^{-(1+\lambda)(1+\theta)+\lambda\theta(\gamma_1/\xi-(1-\mu))} w_t(v)^{(1+\lambda)(1+\theta)+\theta} H(v)^{1+\lambda} \varsigma(v,r)^{-\theta}$$

We follow the procedure of Desmet et al., 2018 and Theorem 2.1 in Zabreyko et al., 1975 to argue that $f_1(r) = f_1$. Then, we solve for $w_t(r)/\varphi_t(r)$ using equation (66).

$$\left(\frac{w_t(r)}{\varphi_t(r)}\right) = f_1^{\frac{1}{1+2\theta}} \bar{a}_t(r)^{\frac{1}{1+2\theta}} L_t(r)^{-\frac{1-\alpha-\theta(\lambda+\gamma_1/\xi-(1-\mu))}{1+2\theta}}$$

$$\times \varphi_t(r)^{-\frac{\mu+\gamma_1/\xi}{1+2\theta}} Q_t(r)^{-\frac{(1-\chi)\mu\theta}{1+2\theta}} H(r)^{-\frac{1}{1+2\theta}} \left(\frac{\bar{b}_t(r)}{u_t(r)}\right)^{-\frac{\theta}{1+2\theta}}$$

We insert the expression for $w_t(r)/\varphi_t(r)$ in equation (61) and manipulate terms to obtain equation (67).

$$\left(\frac{\bar{b}_t(r)}{u_t(r)}\right)^{-\frac{\theta(1+\theta)}{1+2\theta}} \bar{a}_t(r)^{-\frac{\theta}{1+2\theta}} L_t(r)^{\flat_L}$$

$$\times Q_t(r)^{\frac{(1-\chi)\mu\theta^2}{1+2\theta}} H(r)^{\frac{\theta}{1+2\theta}} \varphi_t(r)^{-\frac{(\mu+\gamma_1/\xi)\theta^2}{1+2\theta}}$$

$$= \kappa_1 \int_S \left(\frac{\bar{b}_t(v)}{u_t(v)}\right)^{\frac{\theta^2}{1+2\theta}} \bar{a}_t(v)^{\frac{1+\theta}{1+2\theta}} L_t(v)^{\flat_R} Q_t(v)^{-(1-\chi)\mu\frac{\theta(1+\theta)}{1+2\theta}}$$

$$\times H(v)^{\frac{\theta}{1+2\theta}} \varphi_t(v)^{\frac{(\mu+\gamma_1/\xi)\theta(1+\theta)}{1+2\theta}} \varsigma(r,v)^{-\theta} dv \tag{67}$$

Where the terms $\flat_L$ and $\flat_R$ are defined as follow.

$$\flat_L = \lambda\theta - \frac{\theta}{1+2\theta}[\alpha-1+\theta(\lambda+\gamma_1/\xi-(1-\mu))]$$

$$\flat_R = 1 - \lambda\theta + \frac{1+\theta}{1+2\theta}[\alpha-1+\theta(\lambda+\gamma_1/\xi-(1-\mu))]$$

We utilize the expression for migration shares, given by equation (3), and solve for $L_t(r)$.

$$L_t(r) = H(r)^{-1} u_t(r)^{1/\Omega} m_2(r)^{-1/\Omega} \left(\frac{L_t}{\int_S u_t(v)^{1/\Omega} m_2(v)^{-1/\Omega} dv}\right) \tag{68}$$

We employ this expression and insert it in equation (67).

$$\bar{b}_t(r)^{-\frac{\theta(1+\theta)}{1+2\theta}}\bar{a}_t(r)^{-\frac{\theta}{1+2\theta}}\mathcal{Q}_t(r)^{\frac{(1-\chi)\mu\theta^2}{1+2\theta}}H(r)^{\frac{\theta}{1+2\theta}-\flat_L}$$

$$\times \varphi_t(r)^{-\frac{(\mu+\gamma_1/\xi)\theta^2}{1+2\theta}}m_2(r)^{-\frac{\flat_L}{\Omega}}u_t(r)^{\frac{\flat_L}{\Omega}+\frac{\theta(1+\theta)}{1+2\theta}}$$

$$= \kappa_1\left(\frac{L_t}{\int_S u_t(v)^{1/\Omega}m_2(v)^{-1/\Omega}dv}\right)^{\flat_R-\flat_L}$$

$$\times \int_S \bar{b}_t(v)^{\frac{\theta^2}{1+2\theta}}\bar{a}_t(v)^{\frac{1+\theta}{1+2\theta}}\mathcal{Q}_t(v)^{-(1-\chi)\mu\frac{\theta(1+\theta)}{1+2\theta}}$$

$$\times H(v)^{\frac{\theta}{1+2\theta}-\flat_R}\varphi_t(v)^{\frac{(\mu+\gamma_1/\xi)\theta(1+\theta)}{1+2\theta}}m_2(v)^{-\frac{\flat_R}{\Omega}}u_t(v)^{\frac{\flat_R}{\Omega}-\frac{\theta^2}{1+2\theta}}\varsigma(r,v)^{-\theta}dv \qquad (69)$$

We combine equations (8), (10) and (44) to find an expression for the price of energy.

$$\mathcal{Q}_t(r) = \left(\kappa^\epsilon(1+\tau_t(r))^{1-\epsilon}\mathcal{Q}_t^f(r)^{1-\epsilon}+(1-\kappa)^\epsilon(1-s_t(r))^{1-\epsilon}\mathcal{Q}_t^c(r)^{1-\epsilon}\right)^{\frac{1}{1-\epsilon}}$$

$$= \left(\kappa^\epsilon(1+\tau_t(r))^{1-\epsilon}\left(\frac{f(CumCO2_t)}{\zeta_t^f(r)}\right)^{1-\epsilon}+(1-\kappa)^\epsilon(1-s_t(r))^{1-\epsilon}\left(\frac{1}{\zeta_t^c(r)}\right)^{1-\epsilon}\right)^{\frac{1}{1-\epsilon}}$$

$$= \left(\kappa^\epsilon(1+\tau_t(r))^{1-\epsilon}\left(\frac{f(CumCO2_t)}{(y_t^w/y_{t-1}^w)^{v^j}}\right)^{1-\epsilon}+(1-\kappa)^\epsilon(1-s_t(r))^{1-\epsilon}\left(\frac{1}{(y_t^w/y_{t-1}^w)^{v^j}}\right)^{1-\epsilon}\right)^{\frac{1}{1-\epsilon}} \qquad (70)$$

We rewrite global average real GDP, y_t^w, making use of equations (3) and (4).

$$y_t^w = \int_S\left(\frac{L_t(v)H(v)}{L_t}\right)y_t(v)dv$$

$$= \left(\frac{L_t}{\int_S u_t(v)^{1/\Omega}m_2(v)^{-1/\Omega}dv}\right)^{1+\lambda}\int_S L_t^{-1}H(v)^{-\lambda}u_t(v)^{1+\frac{1}{\Omega}[1+\lambda]}m_2(v)^{-\frac{1}{\Omega}[1+\lambda]}\bar{b}_t(v)^{-1}dv \qquad (71)$$

Therefore, equations (69), (70) and (71) define a system of equations that solves for $u_t(r)$ and $\mathcal{Q}_t(r)$. In order to guarantee existence and uniqueness of the solution, we can consider (i) $\epsilon = 1$ or (ii) $v^f = v^c = v$.

In the first case, the energy price $\mathcal{Q}_t(r)$ collapses to:

$$\mathcal{Q}_t(r) = \left(\frac{y_t^w}{y_{t-1}^w}\right)^{-(\kappa v^f+(1-\kappa)v^c)}\left(\frac{(1+\tau_t(r))f(CumCO2_t)}{\kappa}\right)^\kappa\left(\frac{(1-s_t(r))}{(1-\kappa)}\right)^{1-\kappa}$$

In the second case, the energy price $\mathcal{Q}_t(r)$ collapses to:

$$\mathcal{Q}_t(r) = \left(\frac{y_t^w}{y_{t-1}^w}\right)^{-v}\left(\kappa^\epsilon(1+\tau_t(r))^{1-\epsilon}f(CumCO2_t)^{1-\epsilon}+(1-\kappa)^\epsilon(1-s_t(r))^{1-\epsilon}\right)^{\frac{1}{1-\epsilon}}$$

Consequently, in both cases, we can represent $\mathcal{Q}_t(r)$ as the product a location-invariant term and an exogenous term $\hat{\mathcal{Q}}_t(r)$.

$$\mathcal{Q}_t(r) = \left(\frac{y_t^w}{y_{t-1}^w}\right)^{-\hat{v}}\hat{\mathcal{Q}}_t(r) \qquad (72)$$

We insert equation (72) in equation (69).

$$F_{L,t}(r)\hat{u}_t(r)^{\frac{\flat_L}{\Omega} + \frac{\theta(1+\theta)}{1+2\theta}} = \kappa_1 \int_S F_{R,t}(v)\hat{u}_t(v)^{\frac{\flat_R}{\Omega} - \frac{\theta^2}{1+2\theta}} \varsigma(r,v)^{-\theta} dv \qquad (73)$$

$$F_{L,t}(r) = \bar{b}_t(r)^{-\frac{\theta(1+\theta)}{1+2\theta}} \bar{a}_t(r)^{-\frac{\theta}{1+2\theta}} \hat{Q}_t(r)^{\frac{(1-\chi)\mu\theta^2}{1+2\theta}}$$

$$\times H(r)^{\frac{\theta}{1+2\theta} - \flat_L} \varphi_t(r)^{-\frac{(\mu+\gamma_1/\xi)\theta^2}{1+2\theta}} m_2(r)^{-\frac{\flat_L}{\Omega}}$$

$$F_{R,t}(v) = \bar{b}_t(v)^{\frac{\theta^2}{1+2\theta}} \bar{a}_t(v)^{\frac{1+\theta}{1+2\theta}} \hat{Q}_t(v)^{-(1-\chi)\mu\frac{\theta(1+\theta)}{1+2\theta}}$$

$$\times H(v)^{\frac{\theta}{1+2\theta} - \flat_R} \varphi_t(v)^{\frac{(\mu+\gamma_1/\xi)\theta(1+\theta)}{1+2\theta}} m_2(v)^{-\frac{\flat_R}{\Omega}}$$

Where $F_{L,t}(\cdot)$ and $F_{R,t}(\cdot)$ are exogenous functions and $\hat{u}_t(r) = u_t(r) \cdot U_t$, with U_t given by:

$$U_t = \left(y_{t-1}^w\right)^{-\hat{v}(1-\chi)\mu\theta} \left(\frac{L_t}{\int_S u_t(v)^{1/\Omega} m_2(v)^{-1/\Omega} dv}\right)^{\flat_R - \flat_L + \hat{v}(1-\chi)\mu\theta(1+\lambda)}$$

$$\times \left(\int_S L_t^{-1} H(v)^{-\lambda} u_t(v)^{1+\frac{1}{\Omega}[1+\lambda]} m_2(v)^{-\frac{1}{\Omega}[1+\lambda]} \bar{b}_t(v)^{-1} dv\right)^{\hat{v}(1-\chi)\mu\theta}$$

It follows from Theorem 2.19 in Zabreyko et al., 1975 that the solution to equation (73) exists and is unique if:

$$\frac{\flat_R}{\Omega} - \frac{\theta^2}{1+2\theta} \leq \frac{\flat_L}{\Omega} + \frac{\theta(1+\theta)}{1+2\theta}$$

$$\frac{\alpha}{\theta} + \frac{\gamma_1}{\xi} \leq \lambda + \Omega + (1-\mu) \qquad (74)$$

To obtain $u_t(\cdot)$ from $\hat{u}_t(\cdot)$, substitute $u_t(r) = \hat{u}_t(r)/U_t$ in the expression for U_t.

$$U_t = \left(y_{t-1}^w\right)^{-\frac{\hat{v}(1-\chi)\mu\theta}{\hat{v}(1-\chi)\mu\theta-\theta}} \left(\frac{L_t}{\int_S \hat{u}_t(v)^{1/\Omega} m_2(v)^{-1/\Omega} dv}\right)^{\frac{\flat_R - \flat_L + \hat{v}(1-\chi)\mu\theta(1+\lambda)}{\hat{v}(1-\chi)\mu\theta-\theta}}$$

$$\times \left(\int_S L_t^{-1} H(v)^{-\lambda} \hat{u}_t(v)^{1+\frac{1}{\Omega}[1+\lambda]} m_2(v)^{-\frac{1}{\Omega}[1+\lambda]} \bar{b}_t(v)^{-1} dv\right)^{\frac{\hat{v}(1-\chi)\mu\theta}{\hat{v}(1-\chi)\mu\theta-\theta}}$$

When departing from $\epsilon = 1$ or $v^f = v^c = v$, we solve the model for every period t as follows: (i) guess y_t^w and E_t^f; (ii) compute $CumCO2_t$ and $Q_t(\cdot)$ with equations (9) and (70); (iii) rewrite equation (69)

as shown below and solve for $\hat{u}_t(\cdot)$

$$F_{L,t}(r)\hat{u}_t(r)^{\frac{\flat_L}{\Omega}+\frac{\theta(1+\theta)}{1+2\theta}} = \kappa_1 \int_S F_{R,t}(v)\hat{u}_t(v)^{\frac{\flat_R}{\Omega}-\frac{\theta 2}{1+2\theta}}\varsigma(r,v)^{-\theta}dv \tag{75}$$

$$F_{L,t}(r) = \bar{b}_t(r)^{-\frac{\theta(1+\theta)}{1+2\theta}}\bar{a}_t(r)^{-\frac{\theta}{1+2\theta}}\mathcal{Q}_t(r)^{\frac{(1-\chi)\mu\theta 2}{1+2\theta}}$$

$$\times H(r)^{\frac{\theta}{1+2\theta}-\flat_L}\varphi_t(r)^{-\frac{(\mu+\gamma_1/\xi)\theta 2}{1+2\theta}}m_2(r)^{-\frac{\flat_L}{\Omega}}$$

$$F_{R,t}(v) = \bar{b}_t(v)^{\frac{\theta 2}{1+2\theta}}\bar{a}_t(v)^{\frac{1+\theta}{1+2\theta}}\mathcal{Q}_t(v)^{-(1-\chi)\mu\frac{\theta(1+\theta)}{1+2\theta}}$$

$$\times H(v)^{\frac{\theta}{1+2\theta}-\flat_R}\varphi_t(v)^{\frac{(\mu+\gamma_1/\xi)\theta(1+\theta)}{1+2\theta}}m_2(v)^{-\frac{\flat_R}{\Omega}}$$

$$\hat{u}_t(r) = u_t(r)U_t$$

$$U_t = \left(\frac{L_t}{\int_S u_t(v)^{1/\Omega}m_2(v)^{-1/\Omega}dv}\right)^{\frac{1}{\frac{1}{\Omega}-\frac{\theta}{\flat_R-\flat_L}}} = \left(\frac{L_t}{\int_S \hat{u}_t(v)^{1/\Omega}m_2(v)^{-1/\Omega}dv}\right)^{-\frac{\flat_R-\flat_L}{\theta}} \tag{76}$$

Then, (iv) retrieve $u_t(\cdot), L_t(\cdot), y_t(\cdot)$ and $e_t^f(\cdot)$; (v) compute $y_t'^w$ and $E_t'^f$ with the results of the previous period, if those values are close enough to the guesses, the procedure for period t ends, otherwise update $y_t^w = y_t'^w$ and $E_t^f = E_t'^f$ and return to step (i).

The arguments above prove the following proposition:

Lemma 1. *For any t and for all $r \in S$, given $CumCO2_{t-1}, L_t, T_t(\cdot), \bar{b}_t(\cdot), \bar{a}_t(\cdot), \varsigma(\cdot,\cdot), m(\cdot,\cdot)$ and $H(\cdot)$, the equilibrium energy price $\mathcal{Q}_t(\cdot)$, wage $w_t(\cdot)$, population density $L_t(\cdot)$ and utility $u_t(\cdot)$ schedules satisfy equations (3), (4), (8), (10), (44) as well as the system of equations*

$$w_t(r) = \bar{w}\bar{a}_t(r)^{\frac{1}{1+2\theta}}L_t(r)^{\frac{\alpha-1+\theta(\lambda+\gamma_1/\xi-(1-\mu))}{1+2\theta}}\mathcal{Q}_t(r)^{-\frac{(1-\chi)\mu}{1+2\theta}}H(r)^{-\frac{1}{1+2\theta}}\left(\frac{\bar{b}_t(r)}{u_t(r)}\right)^{-\frac{\theta}{1+2\theta}},$$

$$\left(\frac{\bar{b}_t(r)}{u_t(r)}\right)^{-\theta}L_t(r)^{-\lambda\theta}w_t(r)^{-\theta} = \kappa_1\left(\int_S \bar{a}_t(v)L_t(v)^{\alpha-(1-\mu-\gamma_1/\xi)\theta}\mathcal{Q}_t(r)^{-(1-\chi)\mu\theta}w_t(r)^{-\theta}\varsigma(r,v)^{-\theta}dv\right),$$

where κ_1 is a time-invariant constant and the climatic variables $E_t^f, CumCO2_t, S_{t+1}, F_{t+1}, T_{t+1}, T_{t+1}(\cdot)$ are computed from equations (9), (14), (15), (16) and (17).

F.2 Fundamental Amenities and Productivities

To solve for the fundamental $\bar{b}_t(r)/u_t(r)$, we insert equation (66) in equation (61) and impose $\varphi_t(r) = 1$.

$$\left(\frac{\bar{b}_t(r)}{u_t(r)}\right)^{-\theta}L_t(r)^{\lambda\theta}w_t(r)^{-\theta} = \kappa_1 f_1^{-1}\left(\int_S H(v)\left(\frac{\bar{b}_t(v)}{u_t(v)}\right)^{\theta}L_t(v)^{1-\lambda\theta}w_t(v)^{1+\theta}\varsigma(r,v)^{-\theta}dv\right) \tag{77}$$

And retrieve $\bar{a}_t(r)$ from equation (78).

$$\bar{a}_t(r) = f_1^{-1}w_t(r)^{1+2\theta}L_t(r)^{1-\alpha-\theta(\lambda+\gamma_1/\xi-(1-\mu))}\mathcal{Q}_t(r)^{(1-\chi)\mu\theta}H(r)\left(\frac{\bar{b}_t(r)}{u_t(r)}\right)^{\theta} \tag{78}$$

We approximate equation (77), by substituting the exponent θ of $\bar{b}_t(r)/u_t(r)$ in the right-hand side with

$\theta - \epsilon_0$, where $\epsilon_0 > 0$ is a constant. For any positive ϵ_0, Zabreyko et al., 1975 guarantees that the approximation to equation (77) can be solved by an iterative procedure. Guess some initial distribution of $\bar{b}_t(r)/u_t(r)$, plug it into the right-hand side of equation (77) and use the left-hand side to compute an updated distribution of $\bar{b}_t(r)/u_t(r)$.

Having the solution of approximation to equation (77), one needs to check whether how accurate is the approximation. To do so, we solve for $\bar{a}_t(r)$ using equation and use $\bar{b}_t(r)/u_t(r)$ and $\bar{a}_t(r)$ to solve for $L_t(r)$ using equation (67). If the induced population levels from the solution of the fundamentals is close enough to the data on population levels, the procedure ends. Otherwise, we reduce the value and ϵ_0 and repeat the algorithm until deviations in population are small enough.

F.3 Balanced Growth Path

To prove the existence and uniqueness of a Balanced Growth Path, recall the evolution of amenities and technology, given by:

$$\bar{b}_t(r) = \left(1 + \delta^b(T_t(r)) \cdot \Delta T_t(r)\right) \bar{b}_{t-1}(r)$$

$$\bar{a}_t(r) = \left(1 + \delta^a(T_t(r)) \cdot \Delta T_t(r)\right) \left(\phi_{t-1}(r)^{\theta \gamma_1} \left[\int_S D(v, r)\bar{a}_{t-1}(v)dv\right]^{1-\gamma_2} \bar{a}_{t-1}(r)^{\gamma_2}\right)$$

For fundamental amenities to be constant over time, we require that local temperature reaches a Steady State for every cell. To show this behavior, remember that as the cost of extracting fossil fuels rises sharply, its use declines towards zero. Hence, in the long-run, carbon dioxide emissions converge to zero.

By assuming that emissions from deforestation also converge to zero in the long-run and the share of CO_2 emissions remaining in the atmosphere ℓ periods ahead, $(1 - \delta_\ell)$, converge to a constant value in the long-run, then the carbon stock in the atmosphere also converges to a constant value.

More specifically, employing the characterization of the carbon cycle outlined in equations (37)-(39), $S_{i,t+1}$ converges to zero, $i \in \{1, 2, 3\}$, and $S_{0,t+1}$ converges to $S^* = S_{0,2000} + a_0(maxCumCO2^{f,x})$, where $maxCumCO2^{f,x}$ represents the cumulative and finite flow of emissions from fuel combustion and deforestation.

By assuming that radiative forcing from non-CO_2 GHG converges to zero in the long-run, then radiative forcing, F_{t+1}, converges to a stable value given by $F^* = \varphi \log_2(S^*/S_{\text{pre-ind}})$, according to equation (15). Finally, under the assumption that the temperature response to an increase in radiative force ℓ periods ago, ζ_ℓ, converges to a constant value, global temperature reaches a Steady State. More precisely, employing equations (40) and (41), global temperature reaches a Steady State given by $T^* = \left(\frac{c_1/d_1}{1-e^{-1/d_1}} + \frac{c_2/d_2}{1-e^{-1/d_2}}\right) F^*$. Since global temperature achieves a stable level in the long-run, equation (17) implies the same conclusion for local temperature.

By the aforementioned arguments, fundamental amenities are constant in the Balanced Growth Path. When additionally imposing that total natality rates, $1 + n_t(r)$, converge to one as income grows, global

population achieves a stable value, L^*. Consequently, productivity growth rates follow:

$$\frac{\bar{a}_{t+1}(r)}{\bar{a}_t(r)} = \phi_t(r)^{\theta\gamma_1}\left[\int_S D\frac{\bar{a}_t(v)}{\bar{a}_t(r)}dv\right]^{1-\gamma_2} \tag{79}$$

In a BGP in which technology growth rates are constant, so $\bar{a}_{t+1}(r)/\bar{a}_t(r)$ is constant over time and space and $\bar{a}_t(s)/\bar{a}_t(r)$ is constant over time, the investment decision will also be constant over time but potentially different across locations. We divide equation (79) evaluated at region r with respect to that evaluated at region s to obtain:

$$\frac{\bar{a}_t(s)}{\bar{a}_t(r)} = \left(\frac{\phi(s)}{\phi(r)}\right)^{\frac{\theta\gamma_1}{1-\gamma_2}} = \left(\frac{L(s)/\varphi_t(s)}{L(r)/\varphi_t(r)}\right)^{\frac{\theta\gamma_1}{\xi(1-\gamma_2)}} \tag{80}$$

Where the last equality comes from equation (51). We arrange equation (80), integrate over s and solve for $\bar{a}_t(r)$.

$$L^* = \int_S L(s)H(s)ds = \int_S \left(\frac{\bar{a}_t(s)}{\bar{a}_t(r)}\right)^{\frac{\xi(1-\gamma_2)}{\theta\gamma_1}}\left(\frac{\varphi_t(s)}{\varphi_t(r)}\right)L(r)H(s)ds$$

$$\bar{a}_t(r) = \kappa_{2,t}\left(\frac{L(r)}{\varphi_t(r)}\right)^{\frac{\theta\gamma_1}{\xi(1-\gamma_2)}} \tag{81}$$

$$\kappa_{2,t} = \left(\int_S \bar{a}_t(s)^{\frac{\xi(1-\gamma_2)}{\theta\gamma_1}}\varphi_t(s)H(s)ds\right)^{\frac{\theta\gamma_1}{\xi(1-\gamma_2)}}(L^*)^{-\frac{\theta\gamma_1}{\xi(1-\gamma_2)}}$$

We insert equation (81) in equation (67) and define $\sharp_L$ and $\sharp_R$ as shown below.

$$\left(\frac{\bar{b}(r)}{u_t(r)}\right)^{-\frac{\theta(1+\theta)}{1+2\theta}}L(r)^{\sharp_L}\mathcal{Q}_t(r)^{\frac{(1-\chi)\mu\theta^2}{1+2\theta}}H(r)^{\frac{\theta}{1+2\theta}}\varphi_t(r)^{-\frac{\theta^2}{1+2\theta}\left(\mu+\frac{\gamma_1}{\xi}-\frac{\gamma_1}{\xi(1-\gamma_2)}\right)}$$

$$= \kappa_1\kappa_{2,t}\int_S\left(\frac{\bar{b}(v)}{u_t(v)}\right)^{\frac{\theta^2}{1+2\theta}}L(v)^{\sharp_R}\mathcal{Q}_t(v)^{-(1-\chi)\mu\frac{\theta(1+\theta)}{1+2\theta}}H(v)^{\frac{\theta}{1+2\theta}}\varphi_t(v)^{\frac{\theta(1+\theta)}{1+2\theta}\left(\mu+\frac{\gamma_1}{\xi}-\frac{\gamma_1}{\xi(1-\gamma_2)}\right)}\varsigma(r,v)^{-\theta}dv \quad (82)$$

$$\sharp_L = \lambda\theta - \frac{\theta}{1+2\theta}\left[\alpha-1+\theta\left(\lambda+\frac{\gamma_1}{\xi}+\frac{\gamma_1}{\xi(1-\gamma_2)}-(1-\mu)\right)\right]$$

$$\sharp_R = 1-\lambda\theta+\frac{1+\theta}{1+2\theta}\left[\alpha-1+\theta\left(\lambda+\frac{\gamma_1}{\xi}+\frac{\gamma_1}{\xi(1-\gamma_2)}-(1-\mu)\right)\right]$$

We substitute the migration shares, given by equation (68), in equation (82) and arrange terms.

$$\bar{b}(r)^{-\frac{\theta(1+\theta)}{1+2\theta}}\mathcal{Q}_t(r)^{\frac{(1-\chi)\mu\theta^2}{1+2\theta}}H(r)^{\frac{\theta}{1+2\theta}-\sharp_L}$$

$$\times \varphi_t(r)^{-\frac{\theta^2}{1+2\theta}\left(\mu+\frac{\gamma_1}{\xi}-\frac{\gamma_1}{\xi(1-\gamma_2)}\right)}m_2(r)^{-\frac{\sharp_L}{\Omega}}u_t(r)^{\frac{\sharp_L}{\Omega}+\frac{\theta(1+\theta)}{1+2\theta}}$$

$$= \kappa_1\kappa_{2,t}\left(\frac{L^*}{\int_S u_t(v)^{1/\Omega}m_2(v)^{-1/\Omega}dv}\right)^{\sharp_R-\sharp_L}$$

$$\times \int_S \bar{b}(v)^{\frac{\theta^2}{1+2\theta}}\mathcal{Q}_t(v)^{-(1-\chi)\mu\frac{\theta(1+\theta)}{1+2\theta}}H(v)^{\frac{\theta}{1+2\theta}-\sharp_R}$$

$$\times \varphi_t(v)^{\frac{\theta(1+\theta)}{1+2\theta}\left(\mu+\frac{\gamma_1}{\xi}-\frac{\gamma_1}{\xi(1-\gamma_2)}\right)}m_2(v)^{-\frac{\sharp_R}{\Omega}}u_t(r)^{\frac{\sharp_R}{\Omega}-\frac{\theta^2}{1+2\theta}}\varsigma(r,v)^{-\theta}dv \tag{83}$$

11

For the price of energy to be the product of a location-invariant term and a location-specific time-invariant term, $\mathcal{Q}_t(r) = \left(\frac{y_t^w}{y_{t-1}^w}\right)^{-\hat{v}} \mathcal{Q}(r)$, we assume (i) $\epsilon = 1$ or (ii) $v^f = v^c = v$.

When considering $\epsilon = 1$, $\varphi_t(r)$ collapses to:

$$\varphi_t(r) = \frac{\mu\chi + \gamma_1/\xi + \mu(1-\chi)\tilde{\kappa}(r)}{\mu + \gamma_1/\xi}$$

$$\lim_{\epsilon \to 1}\left(\frac{\tilde{\mathcal{Q}}_t(r)}{\mathcal{Q}_t(r)}\right)^{1-\epsilon} = \lim_{\epsilon \to 1}\left(\frac{\kappa^\epsilon(1+\tau(r))^{-\epsilon}\mathcal{Q}_t^f(r)^{1-\epsilon} + (1-\kappa)^\epsilon(1-s(r))^{-\epsilon}\mathcal{Q}_t^c(r)^{1-\epsilon}}{\kappa^\epsilon(1+\tau(r))^{1-\epsilon}\mathcal{Q}_t^f(r)^{1-\epsilon} + (1-\kappa)^\epsilon(1-s(r))^{1-\epsilon}\mathcal{Q}_t^c(r)^{1-\epsilon}}\right)$$

$$= \left(\frac{\kappa}{1+\tau(r)} + \frac{1-\kappa}{1-s(r)}\right) = \tilde{\kappa}(r)$$

And when considering $v^f = v^c = v$, $\varphi_t(r)$ collapses to:

$$\varphi_t(r) = \frac{\mu\chi + \gamma_1/\xi + \mu(1-\chi)\breve{\kappa}(r)}{\mu + \gamma_1/\xi}$$

$$\left(\frac{\tilde{\mathcal{Q}}_t(r)}{\mathcal{Q}_t(r)}\right)^{1-\epsilon} = \left(\frac{\kappa^\epsilon(1+\tau(r))^{-\epsilon}(\tilde{f})^{1-\epsilon}(y_t^w/y_{t-1}^w)^{-v(1-\epsilon)} + (1-\kappa)^\epsilon(1-s(r))^{-\epsilon}(y_t^w/y_{t-1}^w)^{-v(1-\epsilon)}}{\kappa^\epsilon(1+\tau(r))^{1-\epsilon}(\tilde{f})^{1-\epsilon}(y_t^w/y_{t-1}^w)^{-v(1-\epsilon)} + (1-\kappa)^\epsilon(1-s(r))^{1-\epsilon}(y_t^w/y_{t-1}^w)^{-v(1-\epsilon)}}\right)$$

$$= \left(\frac{\kappa^\epsilon(1+\tau(r))^{-\epsilon}(\tilde{f})^{1-\epsilon} + (1-\kappa)^\epsilon(1-s(r))^{-\epsilon}}{\kappa^\epsilon(1+\tau(r))^{1-\epsilon}(\tilde{f})^{1-\epsilon} + (1-\kappa)^\epsilon(1-s(r))^{1-\epsilon}}\right) = \breve{\kappa}(r)$$

Consequently, $\varphi_t(r)$ might vary across locations, but is constant over time. Now, we combine equation (83) and the definition of the energy price and manipulate terms.

$$F_L(r)\hat{u}_t(r)^{\frac{\sharp_L}{\Omega} + \frac{\theta(1+\theta)}{1+2\theta}} = \kappa_1\kappa_{2,t}\int_S F_R(v)\hat{u}_t(v)^{\frac{\sharp_R}{\Omega} - \frac{\theta^2}{1+2\theta}}\varsigma(r,v)^{-\theta}dv \tag{84}$$

$$F_L(r) = \bar{b}(r)^{-\frac{\theta(1+\theta)}{1+2\theta}}\mathcal{Q}(r)^{\frac{(1-\chi)\mu\theta^2}{1+2\theta}}H(r)^{\frac{\theta}{1+2\theta} - \sharp_L}\varphi(r)^{-\frac{\theta^2}{1+2\theta}\left(\mu + \frac{\gamma_1}{\xi} - \frac{\gamma_1}{\xi(1-\gamma_2)}\right)}m_2(r)^{-\frac{\sharp_L}{\Omega}}$$

$$F_R(r) = \bar{b}(r)^{\frac{\theta^2}{1+2\theta}}\mathcal{Q}(r)^{-\frac{(1-\chi)\mu\theta(1+\theta)}{1+2\theta}}H(r)^{\frac{\theta}{1+2\theta} - \sharp_R}\varphi(r)^{\frac{\theta(1+\theta)}{1+2\theta}\left(\mu + \frac{\gamma_1}{\xi} - \frac{\gamma_1}{\xi(1-\gamma_2)}\right)}m_2(r)^{-\frac{\sharp_R}{\Omega}}$$

Where $F_L(\cdot)$ and $F_R(\cdot)$ are exogenous functions and $\hat{u}_t(r) = u_t(r) \cdot U_t$, with U_t given by:

$$U_t = \left(y_{t-1}^w\right)^{-\hat{v}(1-\chi)\mu\theta}\left(\frac{L^*}{\int_S u_t(v)^{1/\Omega}m_2(v)^{-1/\Omega}dv}\right)^{\sharp_R - \sharp_L + \hat{v}(1-\chi)\mu\theta(1+\lambda)}$$

$$\times \left(\int_S L^{*-1}H(v)^{-\lambda}u_t(v)^{1+\frac{1}{\Omega}[1+\lambda]}m_2(v)^{-\frac{1}{\Omega}[1+\lambda]}\bar{b}(v)^{-1}dv\right)^{\hat{v}(1-\chi)\mu\theta}$$

It follows from Theorem 2.19 in Zabreyko et al., 1975 that the solution to equation (84) exists and is unique if:

$$\frac{\sharp_R}{\Omega} - \frac{\theta^2}{1+2\theta} \leq \frac{\sharp_L}{\Omega} + \frac{\theta(1+\theta)}{1+2\theta}$$

$$\frac{\alpha}{\theta} + \frac{\gamma_1}{\xi} + \frac{\gamma_1}{\xi(1-\gamma_2)} \leq \lambda + \Omega + (1-\mu) \tag{85}$$

12

To obtain $u_t(\cdot)$ from $\hat{u}_t(\cdot)$, substitute $u_t(r) = \hat{u}_t(r)/U_t$ in the expression for U_t.

$$U_t = \left(y_{t-1}^w\right)^{-\frac{\hat{v}(1-\chi)\mu\theta}{\hat{v}(1-\chi)\mu\theta-\theta}} \left(\frac{L^*}{\int_S \hat{u}_t(v)^{1/\Omega}m_2(v)^{-1/\Omega}dv}\right)^{\frac{\sharp_R-\sharp_L+\hat{v}(1-\chi)\mu\theta(1+\lambda)}{\hat{v}(1-\chi)\mu\theta-\theta}}$$

$$\times \left(\int_S L^{*-1}H(v)^{-\lambda}\hat{u}_t(v)^{1+\frac{1}{\Omega}[1+\lambda]}m_2(v)^{-\frac{1}{\Omega}[1+\lambda]}\bar{b}(v)^{-1}dv\right)^{\frac{\hat{v}(1-\chi)\mu\theta}{\hat{v}(1-\chi)\mu\theta-\theta}}$$

F.4 Backward Solution

Rewrite equations (2) and (6) as shown below and define the terms $\natural_L$, $\natural_R$ and κ_2.

$$\bar{b}_t(r) = \frac{\bar{b}_{t+1}(r)}{\Lambda_{t+1}^b(r)}$$

$$\bar{a}_t(r) = \left(\frac{\mu+\gamma_1/\xi}{\gamma_1/\xi}\nu\right)^{\frac{\theta\gamma_1}{\xi\gamma_2}}\left(\int_S D(r,v)\bar{a}_t(v)\right)^{\frac{\gamma_2-1}{\gamma_2}}\left(\frac{\bar{a}_{t+1}(r)}{\Lambda_{t+1}^a(r)}\right)^{\frac{1}{\gamma_2}}L_t(r)^{-\frac{\theta\gamma_1}{\xi\gamma_2}}$$

$$\Lambda_{t+1}^x(r) = \Lambda^x(T_{t+1}(r),\Delta T_t(r)),\quad x\in\{a,b\}$$

$$\natural_L = \lambda\theta - \frac{\theta}{1+2\theta}[\alpha-1+\theta(\lambda+\gamma_1/\xi-\gamma_1/(\xi\gamma_2)-(1-\mu))]$$

$$\natural_R = 1-\lambda\theta + \frac{1+\theta}{1+2\theta}[\alpha-1+\theta(\lambda+\gamma_1/\xi-\gamma_1/(\xi\gamma_2)-(1-\mu))]$$

$$\kappa_2 = \kappa_1\left(\frac{\mu+\gamma_1/\xi}{\gamma_1/\xi}\nu\right)^{\frac{\theta\gamma_1}{\xi\gamma_2}}$$

Then, insert them in equation (67).

$$\left(\frac{\bar{b}_{t+1}(r)}{\Lambda_{t+1}^b(r)}\right)^{-\frac{\theta(1+\theta)}{1+2\theta}}\left(\left(\int_S D(r,s)\bar{a}_t(s)ds\right)^{\frac{\gamma_2-1}{\gamma_2}}\left(\frac{\bar{a}_{t+1}(r)}{\Lambda_{t+1}^a(r)}\right)^{\frac{1}{\gamma_2}}\right)^{-\frac{\theta}{1+2\theta}}$$

$$\times L_t(r)^{\natural_L}\mathcal{Q}_t(r)^{\frac{(1-\chi)\mu\theta^2}{1+2\theta}}H(r)^{\frac{\theta}{1+2\theta}}\varphi_t(r)^{\frac{-(\mu+\gamma_1/\xi)\theta^2}{1+2\theta}}u_t(r)^{\frac{\theta(1+\theta)}{1+2\theta}}$$

$$= \kappa_2\int_S\left(\frac{\bar{b}_{t+1}(v)}{\Lambda_{t+1}^b(v)}\right)^{\frac{\theta^2}{1+2\theta}}\left(\left(\int_S D(v,s)\bar{a}_t(s)ds\right)^{\frac{\gamma_2-1}{\gamma_2}}\left(\frac{\bar{a}_{t+1}(v)}{\Lambda_{t+1}^a(v)}\right)^{\frac{1}{\gamma_2}}\right)^{\frac{1+\theta}{1+2\theta}}$$

$$\times L_t(v)^{\natural_R}\mathcal{Q}_t(v)^{-(1-\chi)\mu\frac{\theta(1+\theta)}{1+2\theta}}H(v)^{\frac{\theta}{1+2\theta}}\varphi_t(v)^{(\mu+\gamma_1/\xi)\frac{\theta(1+\theta)}{1+2\theta}}u_t(v)^{-\frac{\theta^2}{1+2\theta}}\varsigma(r,v)^{-\theta}dv \tag{86}$$

And substitute the migration shares, given by equation (4), in equation (86).

$$
\left(\frac{\bar{b}_{t+1}(r)}{\Lambda_{t+1}^b(r)}\right)^{-\frac{\theta(1+\theta)}{1+2\theta}}\left(\frac{\bar{a}_{t+1}(r)}{\Lambda_{t+1}^a(r)}\right)^{-\frac{\theta}{1+2\theta}\frac{1}{\gamma_2}}
$$

$$
\times\, \mathcal{Q}_t(r)^{\frac{(1-\chi)\mu\theta^2}{1+2\theta}}H(r)^{-\natural_L+\frac{\theta}{1+2\theta}}\varphi_t(r)^{-\frac{(\mu+\gamma_1/\xi)\theta^2}{1+2\theta}}m_2(r)^{-\frac{\natural_L}{\Omega}}u_t(r)^{\frac{\natural_L}{\Omega}+\frac{\theta(1+\theta)}{1+2\theta}}
$$

$$
=\kappa_2\left(\int_S D(v,s)\bar{a}_t(s)ds\right)^{\frac{\gamma_2-1}{\gamma_2}}\left(\frac{L_t}{\int_S u_t(v)^{1/\Omega}m_2(v)^{-1/\Omega}dv}\right)^{\natural_R-\natural_L}
$$

$$
\int_S\left(\frac{\bar{b}_{t+1}(v)}{\Lambda_{t+1}^b(v)}\right)^{\frac{\theta^2}{1+2\theta}}\left(\frac{\bar{a}_{t+1}(v)}{\Lambda_{t+1}^a(v)}\right)^{\frac{1+\theta}{1+2\theta}\frac{1}{\gamma_2}}
$$

$$
\times\, \mathcal{Q}_t(v)^{-(1-\chi)\mu\frac{\theta(1+\theta)}{1+2\theta}}H(v)^{-\natural_R+\frac{\theta}{1+2\theta}}\varphi_t(v)^{\frac{(\mu+\gamma_1/\xi)\theta(1+\theta)}{1+2\theta}}m_2(v)^{-\frac{\natural_R}{\Omega}}u_t(v)^{\frac{\natural_R}{\Omega}-\frac{\theta^2}{1+2\theta}}\varsigma(r,v)^{-\theta}dv \tag{87}
$$

Rewrite equation (86) as follows:

$$
B_{L,t}(r)\hat{u}_t(r)^{\frac{\natural_L}{\Omega}+\frac{\theta(1+\theta)}{1+2\theta}}=\kappa_1\int_S B_{R,t}(v)\hat{u}_t(v)^{\frac{\natural_R}{\Omega}-\frac{\theta^2}{1+2\theta}}\varsigma(r,v)^{-\theta} \tag{88}
$$

$$
B_{L,t}(r)=\left(\frac{\bar{b}_{t+1}(r)}{\Lambda_{t+1}^b(r)}\right)^{-\frac{\theta(1+\theta)}{1+2\theta}}\left(\frac{\bar{a}_{t+1}(r)}{\Lambda_{t+1}^a(r)}\right)^{-\frac{\theta}{1+2\theta}\frac{1}{\gamma_2}}\mathcal{Q}_t(r)^{\frac{(1-\chi)\mu\theta^2}{1+2\theta}}
$$

$$
\times\, H(r)^{-\natural_L+\frac{\theta}{1+2\theta}}\varphi_t(r)^{-\frac{(\mu+\gamma_1/\xi)\theta^2}{1+2\theta}}m_2(r)^{-\frac{\natural_L}{\Omega}}
$$

$$
B_{R,t}(v)=\left(\frac{\bar{b}_{t+1}(v)}{\Lambda_{t+1}^b(v)}\right)^{\frac{\theta^2}{1+2\theta}}\left(\frac{\bar{a}_{t+1}(v)}{\Lambda_{t+1}^a(v)}\right)^{\frac{1+\theta}{1+2\theta}\frac{1}{\gamma_2}}\mathcal{Q}_t(v)^{-(1-\chi)\mu\frac{\theta(1+\theta)}{1+2\theta}}
$$

$$
\times\, H(v)^{-\natural_R+\frac{\theta}{1+2\theta}}\varphi_t(v)^{\frac{(\mu+\gamma_1/\xi)\theta(1+\theta)}{1+2\theta}}m_2(v)^{-\frac{\natural_R}{\Omega}}
$$

Where $B_{L,t}(\cdot)$ and $B_{R,t}(\cdot)$ are exogenous functions and $\hat{u}_t(r)=u_t(r)\cdot U_t$, with U_t given by:

$$
U_t=\left(\frac{\mu+\gamma_1/\xi}{\gamma_1/\xi}\nu\right)^{\frac{\theta\gamma_1}{\xi\gamma_2}\frac{\Omega}{\natural_R-\natural_L-\theta\Omega}}\left(\int_S D(v,s)\bar{a}_t(s)ds\right)^{\frac{\gamma_2-1}{\gamma_2}\frac{\Omega}{\natural_R-\natural_L-\theta\Omega}}\left(\frac{L_t}{\int_S u_t(v)^{1/\Omega}m_2(v)^{-1/\Omega}dv}\right)^{\frac{(\natural_R-\natural_L)\Omega}{\natural_R-\natural_L-\theta\Omega}} \tag{89}
$$

To obtain $u_t(\cdot)$ from $\hat{u}_t(\cdot)$, substitute $u_t(r)=\hat{u}_t(r)/U_t$ in the expression for U_t.

$$
U_t=\left(\frac{\mu+\gamma_1/\xi}{\gamma_1/\xi}\nu\right)^{-\frac{\gamma_1}{\xi\gamma_2}}\left(\int_S D(v,s)\bar{a}_t(s)ds\right)^{-\frac{\gamma_2-1}{\gamma_2\theta}}\left(\frac{L_t}{\int_S \hat{u}_t(v)^{1/\Omega}m_2(v)^{-1/\Omega}dv}\right)^{-\frac{\natural_R-\natural_L}{\theta}} \tag{90}
$$

Summarizing, we solve the model for every period t as follows: (i) guess L_t, y_t^w and E_t^f; (ii) compute $CumCO2_t$ and $\mathcal{Q}_t(\cdot)$ with equations (9) and (70); (iii) use equation (87) and solve for $\hat{u}_t(\cdot)$; (iv) retrieve $u_t(\cdot), L_t(\cdot), y_t(\cdot)$ and $e_t^f(\cdot)$; (v) compute $L_t', y_t'^w$ and $E_t'^f$ with the results of the previous step, if those values are close enough to the guesses, the procedure for period t ends, otherwise update $L_t=L_t'$, $y_t^w=y_t'^w$ and $E_t^f=E_t'^f$ and return to step (i).

14

F.5 Migration Costs

To solve for the migration costs, $m_2(r)$, recall the expression for migration shares.

$$u_t(r) = m_2(r)H(r)^\Omega L_t(r)^\Omega \left(\frac{L_t}{\int_S u_t(v)^{1/\Omega} m_2(v)^{-1/\Omega} dv} \right)^{-\Omega}$$

And substitute it in equation (67).

$$\bar{b}_t(r)^{-\frac{\theta(1+\theta)}{1+2\theta}} \bar{a}_t(r)^{-\frac{\theta}{1+2\theta}} L_t(r)^{\flat_L + \frac{\Omega\theta(1+\theta)}{1+2\theta}} \mathcal{Q}_t(r)^{\frac{(1-\chi)\mu\theta^2}{1+2\theta}}$$
$$\times H(r)^{\frac{\theta[1+\Omega(1+\theta)]}{1+2\theta}} m_2(r)^{\frac{\theta(1+\theta)}{1+2\theta}} \varphi_t(r)^{\frac{-(\mu+\gamma_1/\xi)\theta^2}{1+2\theta}}$$
$$= \kappa_1 \left(\frac{L_t}{\int_S u_t(s)^{1/\Omega} m_2(s)^{-1/\Omega}} \right)^{\frac{\Omega\theta}{1+2\theta}}$$
$$\times \int_S \bar{b}_t(v)^{\frac{\theta^2}{1+2\theta}} \bar{a}_t(v)^{\frac{1+\theta}{1+2\theta}} L_t(v)^{\flat_R - \frac{\Omega\theta^2}{1+2\theta}} \mathcal{Q}_t(v)^{-(1-\chi)\mu\frac{\theta(1+\theta)}{1+2\theta}}$$
$$\times H(v)^{\frac{\theta[1-\Omega\theta]}{1+2\theta}} m_2(v)^{-\frac{\theta^2}{1+2\theta}} \varphi_t(v)^{(\mu+\gamma_1/\xi)\frac{\theta(1+\theta)}{1+2\theta}} \varsigma(r,v)^{-\theta} dv \tag{91}$$

We impose the normalization $\min_s m_2(s) = 1$.

G   Sensitivity Results of the Baseline Scenario

In this section, we provide additional results for the baseline scenario and test the sensitivity of the numerical results to different discount factors, elasticities of energy substitution and size of fuel deposits.

G.1   Additional Results of the Baseline Scenario

Figure 37 shows the evolution of local temperature from the year 2000 to 2200 and Figure 38 the histogram of amenity and productivity losses attributed to global warming in the year 2200.
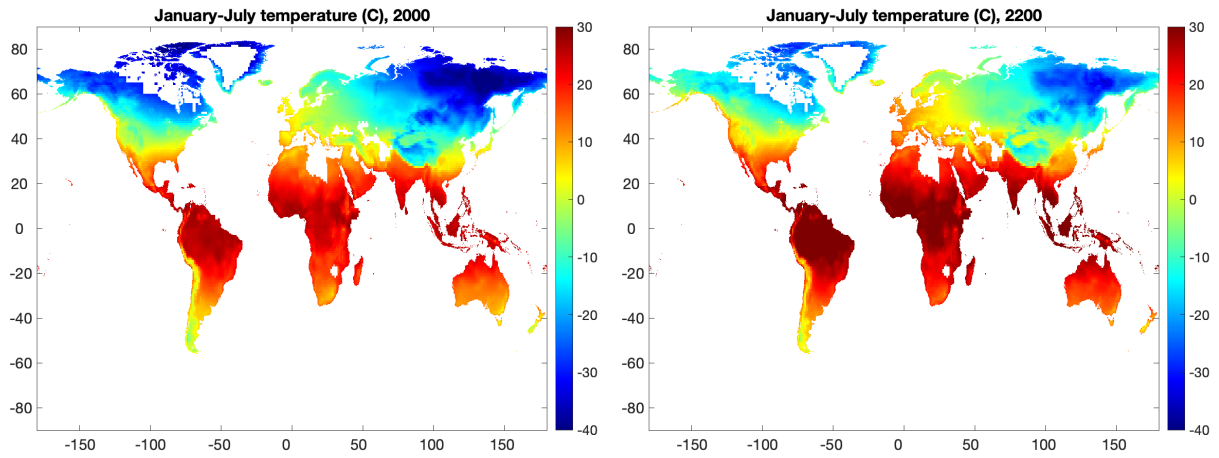
Figure 37: Local January-July temperature in 2000 and 2200.
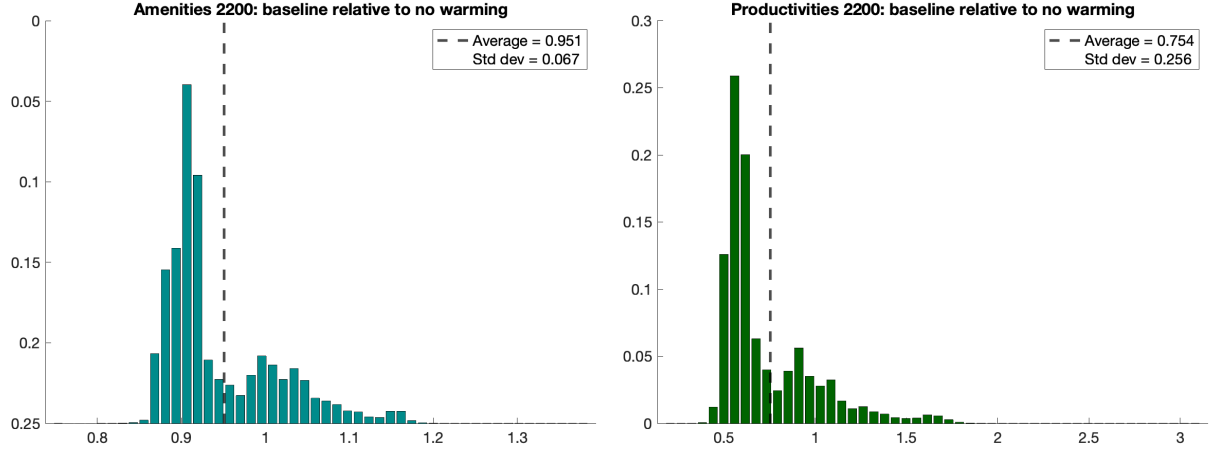
Figure 38: Histogram of losses in amenities and productivities from global warming in the year 2200.

G.2 Additional Results of the Environmental Policies

Figures 39 and 40 present the spatial distribution of real GDP gains from a 200% carbon tax and a 75% clean energy subsidy relative to the baseline scenario with no environmental policies, respectively. The spatial patterns are in line with those of welfare. However, North of Africa and Middle East tend to display larger distortions in real GDP, since those regions are more intensive in fossil fuels.
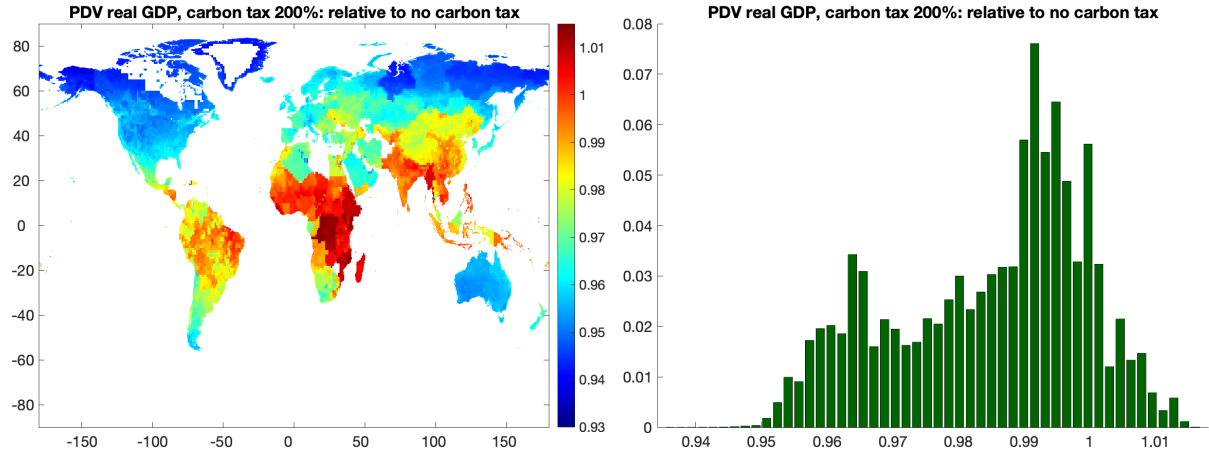
Figure 39: Local real GDP effects of a carbon tax of 200% with a discount factor of $\beta = 0.965$.

G.3 Baseline Results with a Discount Factor of $\beta = 0.969$

Figures 41 and 42 explore the spatial dimension of welfare and real GDP losses when considering a higher discount factor of $\beta = 0.969$, rather than $\beta = 0.965$ as in Section 4. The spatial patterns and the shape of the histograms resemble those of Figures 8 and 28. However, when considering this higher discount factor, losses in global average welfare and real GDP are roughly 3.2% and 0.3% larger, respectively.

Figure 43 displays the spatial distribution of real GDP and welfare for the baseline case, the worst- and

16
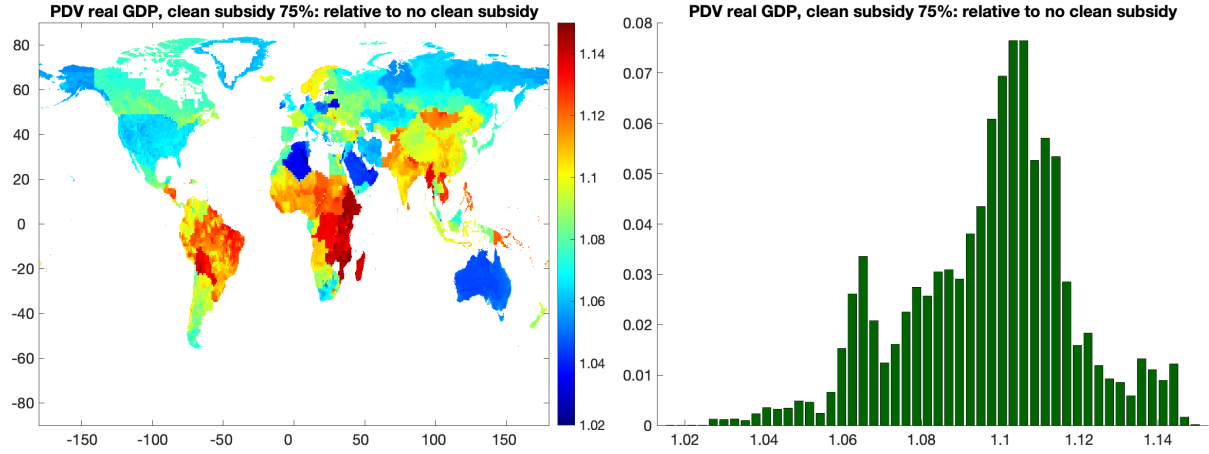
Figure 40: Local real GDP effects of a clean energy subsidy of 75% with a discount factor of $\beta = 0.965$.
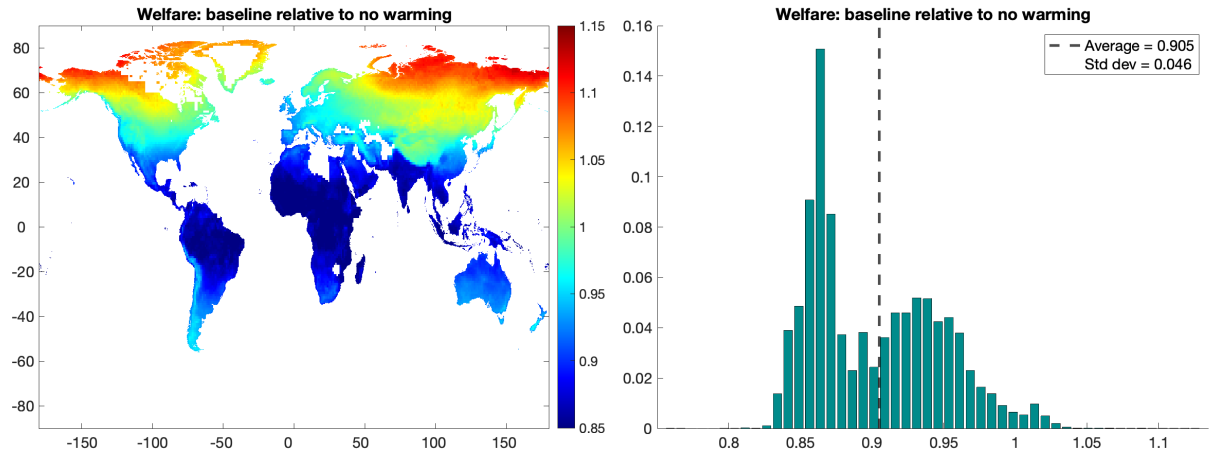
Figure 41: Welfare losses due to global warming with a discount factor of $\beta = 0.969$.
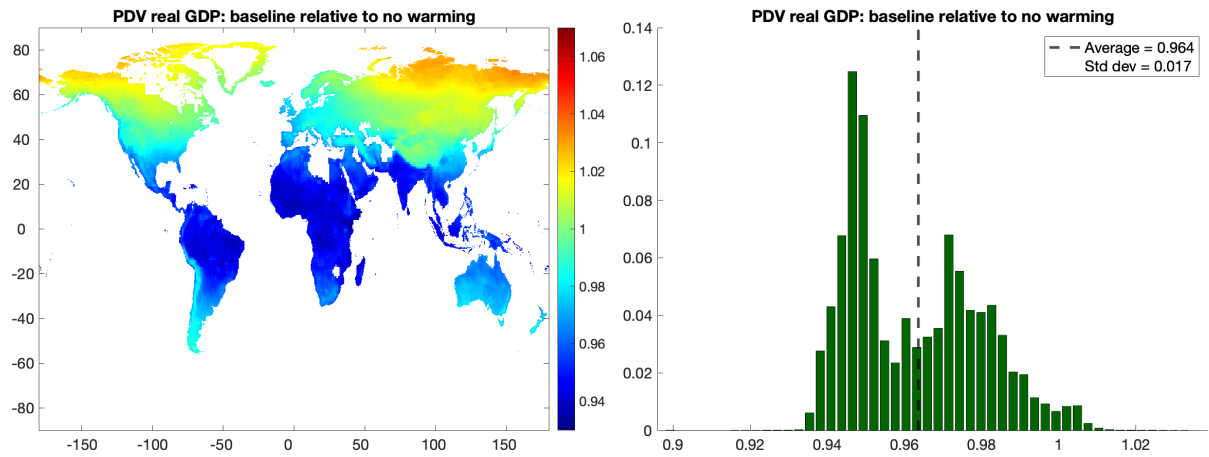
Figure 42: Real GDP losses due to global warming with a discount factor of $\beta = 0.969$.

best-scenario. The overall shape of the distributions is similar to that of Figures 10 and 29, but the greater discount factor rises the level of damages.
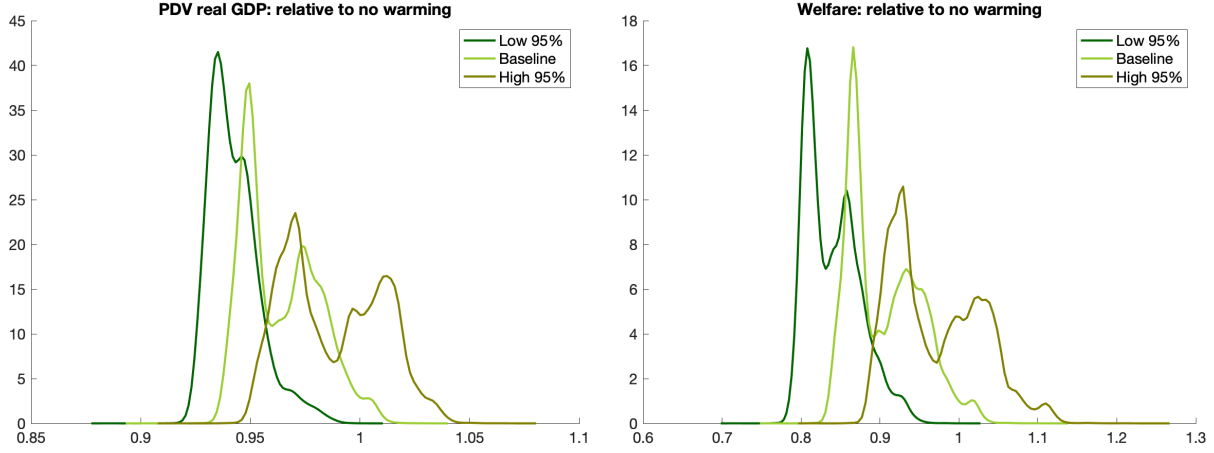
Figure 43: Real GDP and welfare distribution losses by uncertainty level with a discount factor of $\beta = 0.969$.

G.4 Sensitivity to Elasticity of Substitution between Energy Sources

In this subsection, we explore the robustness of the quantitative results when considering different degrees of substitution between fossil fuel and clean energy, $\epsilon \in \{0.5, 1.6, 3, 6\}$. Figure 44 displays the evolution of global carbon dioxide emissions and temperature, across different energy substitution levels, where $\epsilon = 1.6$ denotes the benchmark calibration.
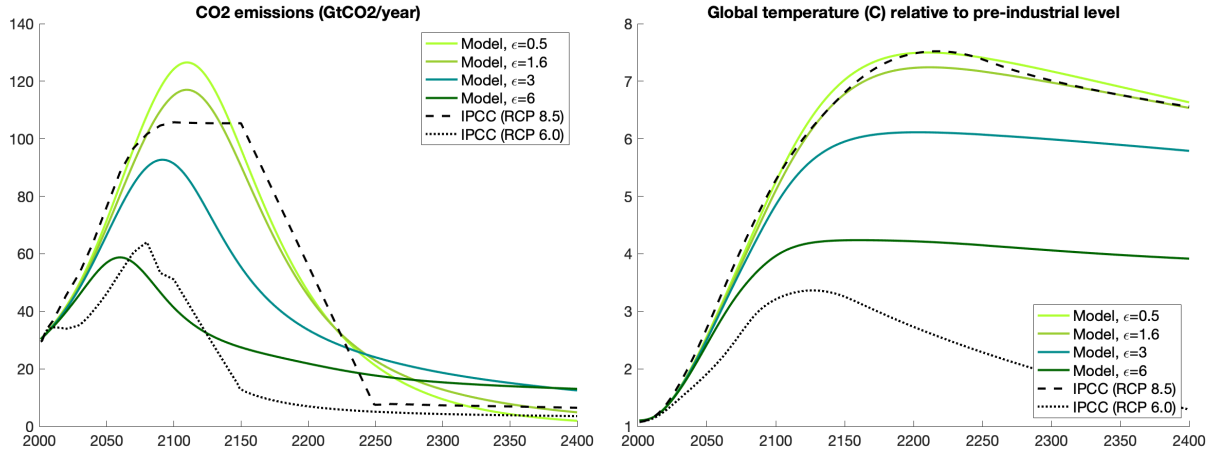
Figure 44: CO_2 emissions and global temperature across different elasticities of energy substitution.

Since the elasticity of energy productivity growth with respect to global real GDP growth is higher for clean than for dirty energy ($v^c = 1.22 > 1.16 = v^f$), then increases in worldwide income imply greater reductions in the price of clean energy compared to that of fossil fuels.[74] Thus, with higher energy substi-

---

[74]If the relationship between the elasticities of clean and dirty energy productivity growth to real income growth were such that

tution, the economy consumes more of the relatively cheap source of energy, and less of the expensive one, leading to a flatter evolution of the CO_2 flow.

Figure 45 presents the transition of losses in worldwide real GDP and welfare. As global temperature rises at a slower speed with higher energy substitution, the adverse consequences of global warming attenuate.[75] In this sense, policies aiming at increasing the substitutability between clean and dirty energy sources, like research to reduce the cost of clean energy storage, are projected to have a remarkable impact. Furthermore, the attenuation of warming damages is expected to be larger the higher (lower) the elasticity of clean (dirty) energy productivity growth to real income growth, ϑ^c (ϑ^f), or the steeper extraction cost functions, $f(\cdot)$, as they increase the relative price of dirty to clean energy.
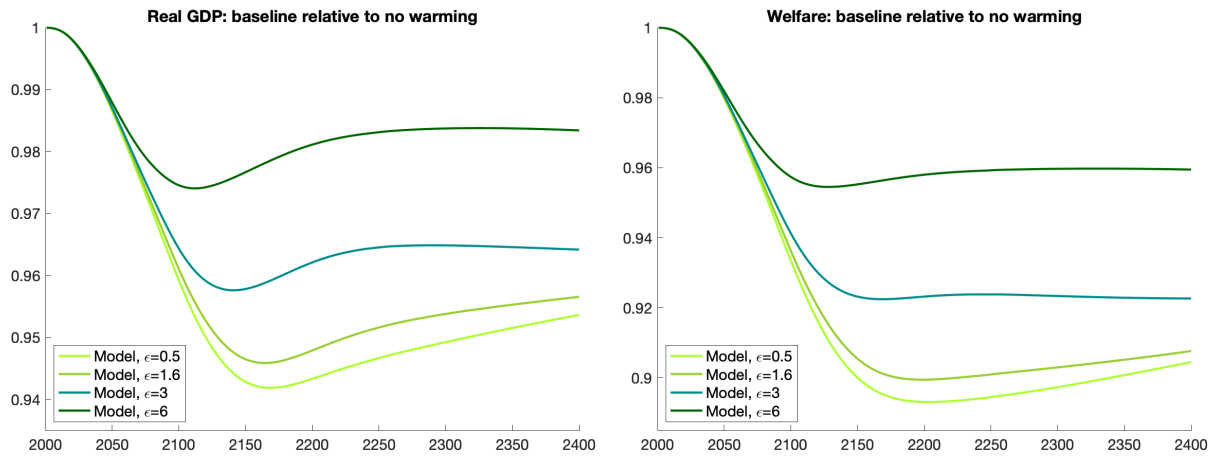
Figure 45: Real GDP and welfare losses over time across different elasticities of energy substitution.
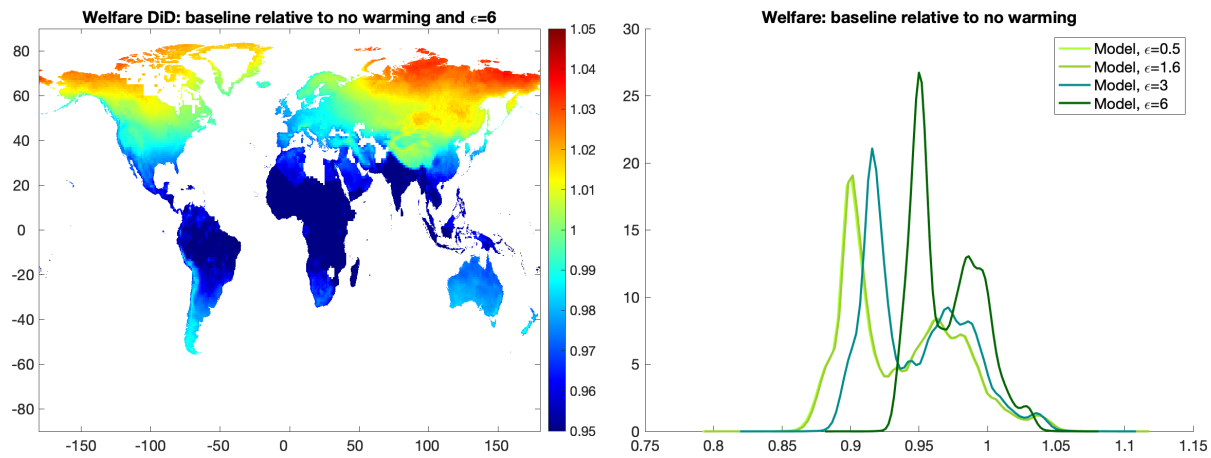
Figure 46: Welfare losses over space across different elasticities of energy substitution.

When exploring the cross-section of warming damages, the coldest regions are relatively better-off un-

---

$\upsilon^c < \upsilon^f$, then with more energy substitution, the evolution of the carbon dioxide flow would be steeper.

[75]To the extent that all the carbon available in the ground is depleted, the long-run global temperature is insensitive to the elasticity of substitution across energy sources.

der lower energy substitution, as in those cases, temperature reaches greater values, inducing amenity- and productivity-gains in such places. The converse occurs for tropical regions. Henceforth, greater energy substitution, diminishes both the gains in cold places and the losses in warm places, reducing the dispersion of warming damages on welfare. Figure 46 shows the ratio of welfare losses in the benchmark scenario ($\epsilon = 1.6$) with respect to that in high energy substitution case ($\epsilon = 6$) and the comparison of the spatial distribution of welfare losses under different values for ϵ.

Now, we evaluate the sensitivity of environmental policies to different degrees of energy substitution. First, we assess the effect of an spatial- and time-invariant carbon tax of 200%, keeping clean energy subsidies at 0%. Figure 47 displays in solid curves the evolution of global carbon dioxide emissions and temperature without abatement and in dashed curves those with the introduction of a free geoengineering technology in 2100.
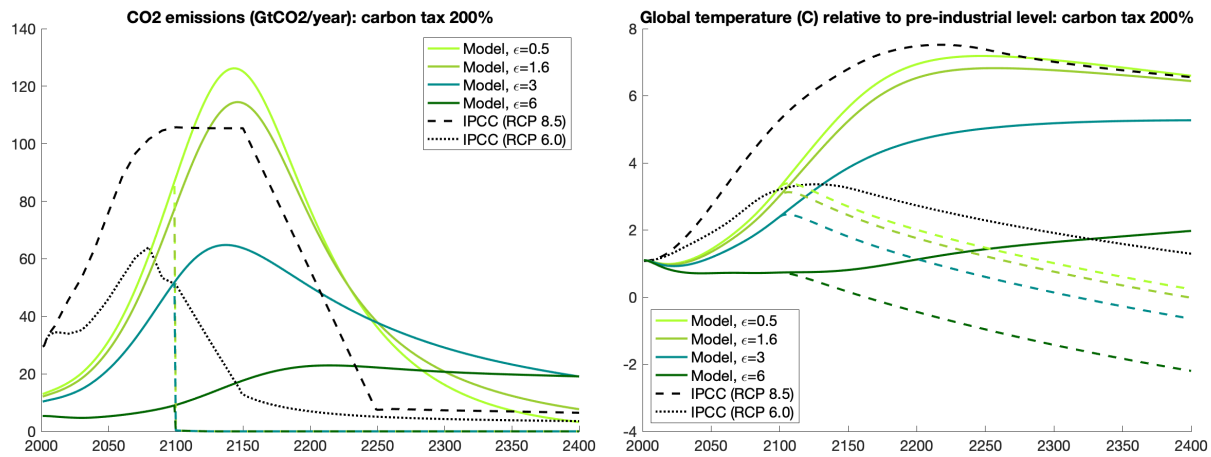
Figure 47: CO_2 emissions and global temperature with a carbon tax of 200% across different elasticities of energy substitution.

Conditional on the same proportional carbon tax, its implementation leads to a larger decline in the use of fossil fuels at impact with higher energy substitution, as firms can more easily substitute energy consumption towards clean sources. Over time, the evolution of carbon dioxide emissions is more protracted with greater values of ϵ.

Since the cumulative CO_2 flow released to the atmosphere monotonically declines as the energy substitution increases, the introduction of an abatement yields stronger differences in long-run temperature with respect to the absence of such technology.

When examining the global real GDP and welfare losses, Figure 48, we observe that the distortion in output in the first periods due to the implementation of a carbon tax is smaller when energy types are more substitutable. In the transition, even though, temperature is more sensitive to environmental policies with greater energy substitution, the evolution of economic benefits arising from the carbon tax is more modest. This effect is explained by the behavior of total population: the introduction of the CO_2 levy reduces income in the first periods, being this decline greater with lower energy substitution. Accordingly, the smaller ϵ,

the larger the increase in natality rates and global population. Summarizing, the larger rise in productivity from higher population levels outweighs the temperature differences when ϵ is low. So, in those cases, the economic benefits of a carbon tax augment for the next centuries.[76]
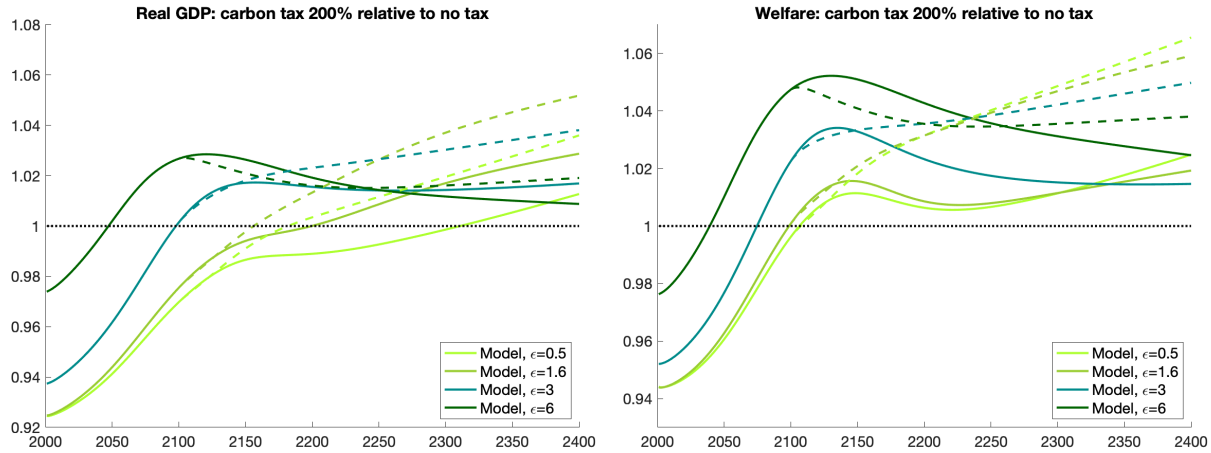

Figure 48: Real GDP and welfare with a carbon tax of 200% across different elasticities of energy substitution.

Tables 8 and 9 summarize the global real GDP and welfare gains for a carbon tax of 200% under different discount factors and elasticities of substitution between fossil fuel and clean energy. The former compares the scenario with carbon taxes and no abatement with respect to the benchmark case, whereas the latter compares the scenario with carbon taxes and the introduction of a costless geoengineering technology in 2100 with respect to the benchmark case.

For low discount factors, the initial production distortions have a greater weight, so economic benefits rise with energy substitution. For high discount factors, real GDP displays a concave shape in the energy elasticity of substitution.

	PDV of real GDP			Welfare		
	BGP gr	β=0.965	β=0.969	BGP gr	β=0.965	β=0.969
ϵ=0.5	2.919%	0.973	1.005	2.810%	0.992	1.015
ϵ=1.6	3.086%	0.986	1.063	2.979%	0.996	1.026
ϵ=3	3.080%	0.997	1.029	2.973%	1.005	1.019
ϵ=6	3.075%	1.008	1.002	2.975%	1.022	1.024

Table 8: PDV of real GDP and welfare gains with a carbon tax of 200%, with no abatement, under different elasticities of energy substitutions and discount factors.

---

[76]Note that relative real GDP and welfare can be slightly lower in the abatement case for a couple of decades after the invention of the abatement technology. The reason is that the difference in temperatures between the benchmark scenario with and without abatement can be larger than the difference in temperature with and without abatement in the scenario with a carbon tax, depending on the second derivative of the temperature function at the time the abatement technology arrives. After a few decades, this effect is always dominated by the faster increases in temperature in the case without abatement.

	PDV of real GDP			Welfare		
	BGP gr	β=0.965	β=0.969	BGP gr	β=0.965	β=0.969
ϵ=0.5	2.928%	0.981	1.022	2.836%	1.005	1.045
ϵ=1.6	3.097%	0.995	1.107	3.008%	1.011	1.080
ϵ=3	3.096%	1.004	1.077	3.007%	1.017	1.072
ϵ=6	3.092%	1.010	1.038	3.007%	1.023	1.058

Table 9: PDV of real GDP and welfare gains with a carbon tax of 200%, with the introduction of an abatement technology in 2100, under different elasticities of energy substitutions and discount factors.

As for the cross-section of welfare gains under a carbon tax of 200% with no abatement, higher levels of energy substitution shift to the right and increase the dispersion of the welfare distribution. In other words, tropical regions gain more from carbon taxes with higher energy substitution, due to the larger decline in temperature and the smaller production losses in the first periods, as the rise in the price of the energy composite is less pronounced.[77]
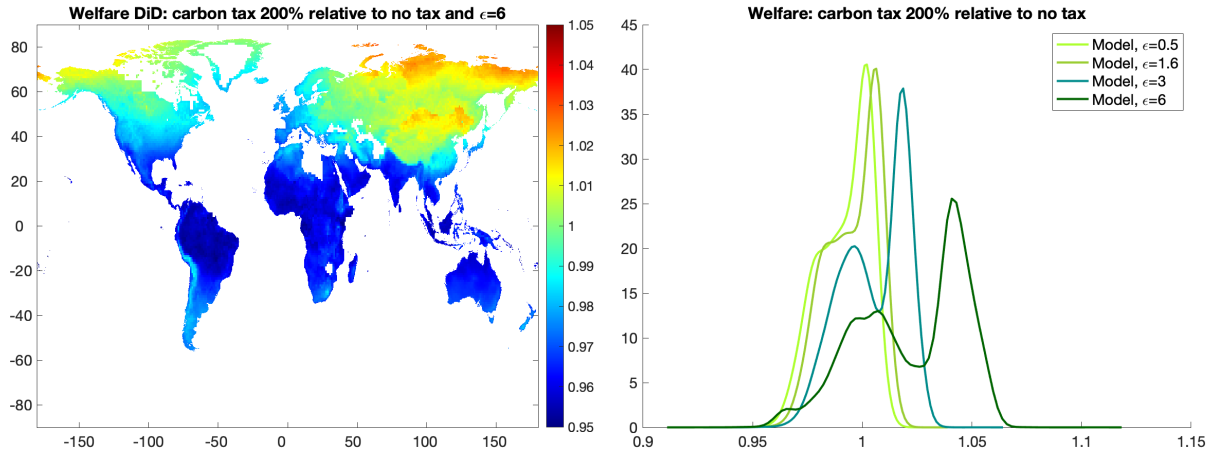
Figure 49: Welfare gains over space with a carbon tax of 200% across different elasticities of energy substitution.

Now, we examine the effect of a spatial- and time-invariant clean energy subsidy of 75%, keeping carbon taxes at 0%. As expected, higher energy substitution leads to greater declines in CO_2 emissions and a more prolonged path for global temperature, as illustrated in Figure 50.

At impact, the subsidy on clean energy leads to a reduction in the composite price of energy, so that the countries initially using more clean energy relatively to fossil fuels undergo greater declines in the composite price of energy. Those declines are larger, the higher the energy elasticity.

On average, developed countries tend to be more intensive in clean energy, attracting more households to those places. So, the relocation of persons towards the most productive places is stronger when energy

---

[77]Tropical regions tend to be more carbon intensive and a carbon tax generates larger production distortions.
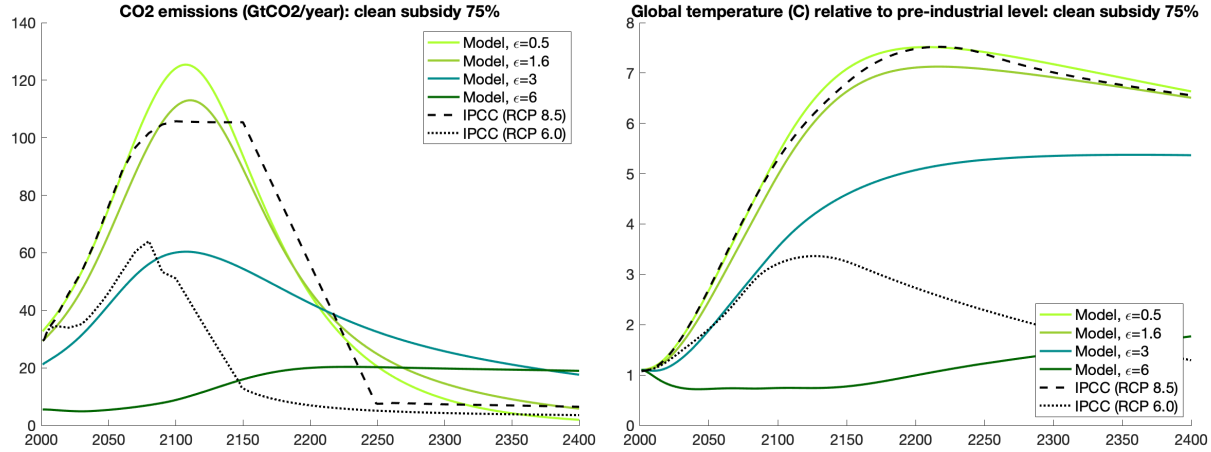
Figure 50: CO_2 emissions and global temperature with a clean energy subsidy of 75% across different elasticities of energy substitution.

sources are more substitutable, augmenting global real GDP and welfare, as shown in Figure 51.

The boost in innovation, due to the population allotment towards productive places, and the more protracted path for global temperature with high ϵ, rise the economic benefits of the environmental policy for the subsequent decades until they reach a peak. Afterwards, global real GDP and welfare benefits start to diminish, as the income increase reduces natality rates and so does global population. Table 10 summarizes the global real GDP and welfare gains of a clean energy subsidy of 75% under different degrees of energy substitution and discount factors.
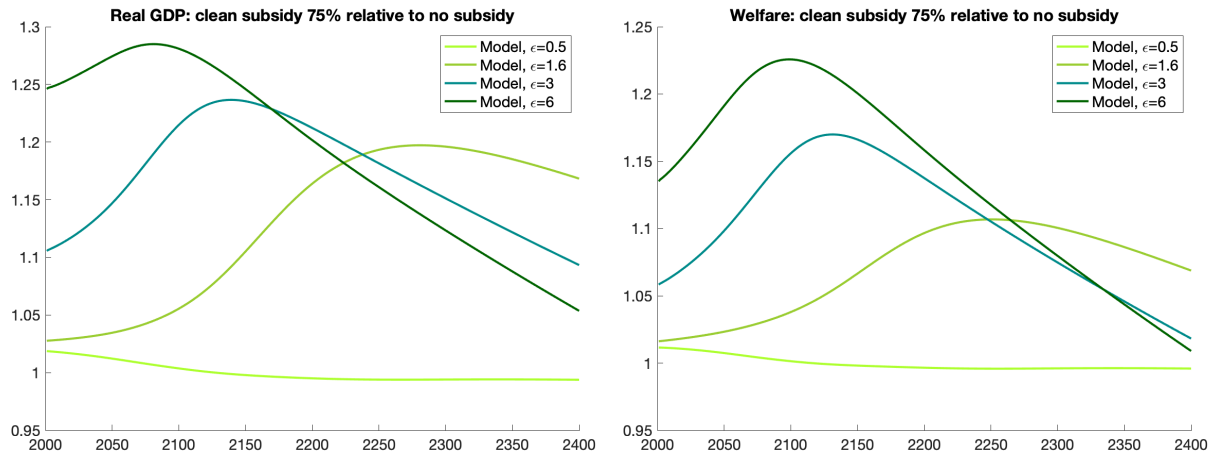
Figure 51: Real GDP and welfare with a clean energy subsidy of 75% across different elasticities of energy substitution.

23

	PDV of real GDP			Welfare		
	BGP gr	β=0.965	β=0.969	BGP gr	β=0.965	β=0.969
ϵ=0.5	2.903%	1.003	0.998	2.794%	1.001	0.998
ϵ=1.6	3.044%	1.098	1.007	2.935%	1.053	1.000
ϵ=3	3.024%	1.154	0.935	2.917%	1.091	0.970
ϵ=6	3.012%	1.183	0.896	2.913%	1.122	0.960

Table 10: PDV of real GDP and welfare gains with a clean energy subsidy of 75% under different elasticities of energy substitutions and discount factors.

G.5   Sensitivity to Carbon Deposit Size

In this subsection, we explore the robustness of the quantitative results when considering different sizes of carbon deposits. Schwerhoff and Stuermer, 2020 argue that over the past three centuries, extraction of non-renewable resources has increased, but their real prices do not display an increasing trend. They predict that the interaction of innovation and geological properties allows for a constant real resource price on the Balanced Growth Path.[78]

To incorporate this conclusion in our analysis, we consider that the extraction cost function is characterized by the same parameters $(f_1, \cdots, f_5)$, but modify the carbon deposit size according to $maxCumCO2 \in$ {9,700 GtCO$_2$,19,500 GtCO$_2$,45,300 GtCO$_2$}, where 19,500 GtCO$_2$ denotes the benchmark calibration; 9,700 GtCO$_2$ the CO$_2$ emissions for the next five centuries according to the RCP 6.0; and 45,300 GtCO$_2$ the stock of fossil fuels resources estimated in Table 4 of Gaedicke et al., 2020.

Figure 52 compares the extraction cost functions under different carbon deposit sizes, so that with larger carbon deposits we are able to reconcile the findings by Schwerhoff and Stuermer, 2020 in terms of constant extraction costs for a sufficiently long period of time.

Figure 53 illustrates that larger carbon deposits generate greater peaks in CO$_2$ emissions occurring progressively later in time, as the extraction cost function displays a larger flat part. Since the extraction cost functions rise sharply when the resource gets exhausted, carbon dioxide emissions eventually decline towards zero. Accordingly, the larger carbon deposits not only generates higher long-run temperatures, but also faster temperature increases in the short-run.

The monotonically increase in the temperature evolution with greater carbon stocks in the ground amplifies economic losses over time, as depicted in Figure 54. In this sense, greater deposits of fossil fuels widen the dispersion of welfare losses across regions, because warm (cold) regions face amenity and productivity deteriorations (improvements) with higher temperature levels, as shown in Figure 55.

Now, we evaluate the sensitivity of environmental policies to different sizes of carbon deposits. First, we assess the effect of an spatial- and time-invariant carbon tax of 200%, keeping clean energy subsidies at 0%. Figure 56 displays in solid curves the evolution of global carbon dioxide emissions and temperature

---

[78]Moreover, they also predict a constant growth rate of extraction, since innovation converts previously inaccessible lower grade deposits into economic recoverable reserves and since greater resource quantities are found in progressively lower grade deposits (Fundamental Law of Geochemistry).
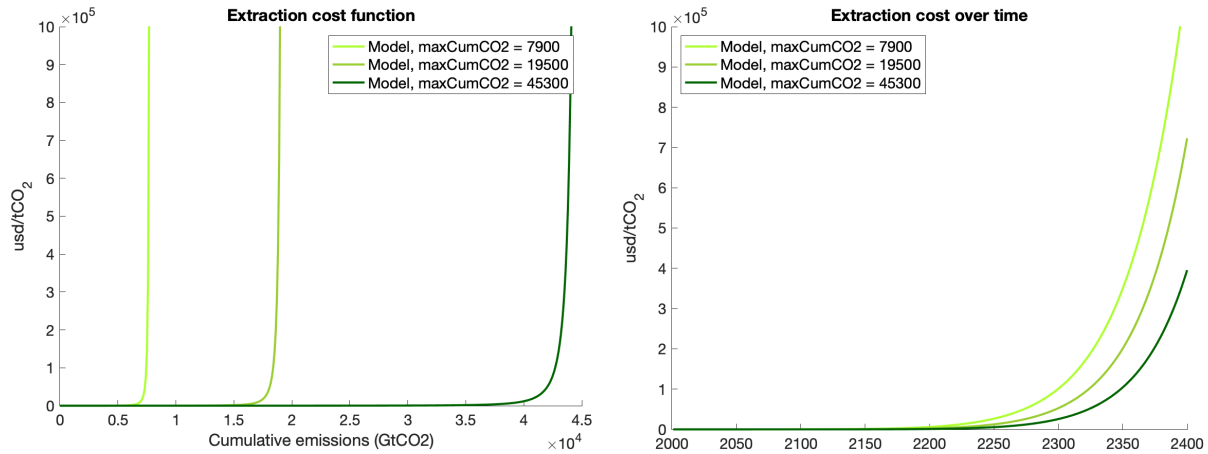
Figure 52: Extraction cost function across different sizes of carbon deposits.
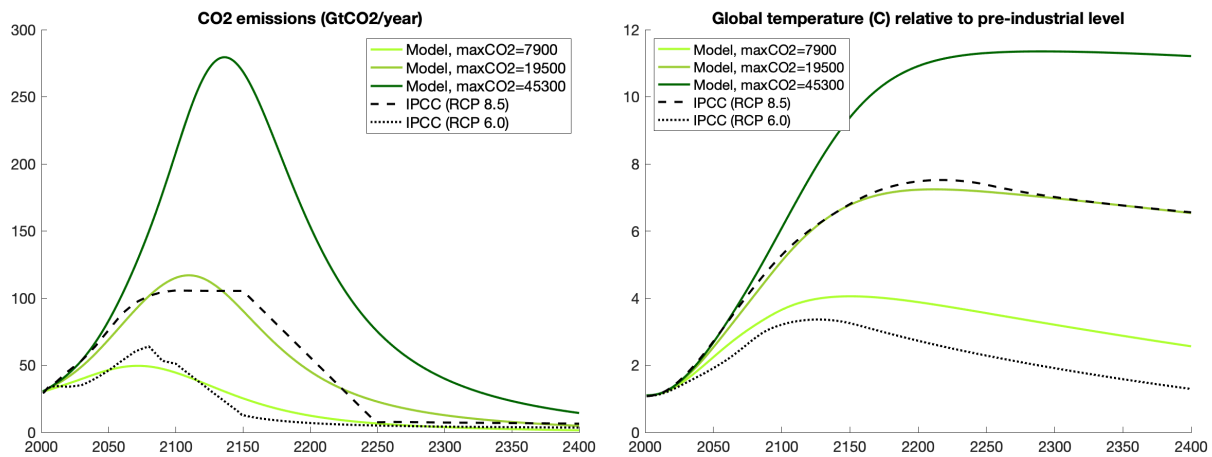

Figure 53: CO$_2$ emissions and global temperature across different sizes of carbon deposits.
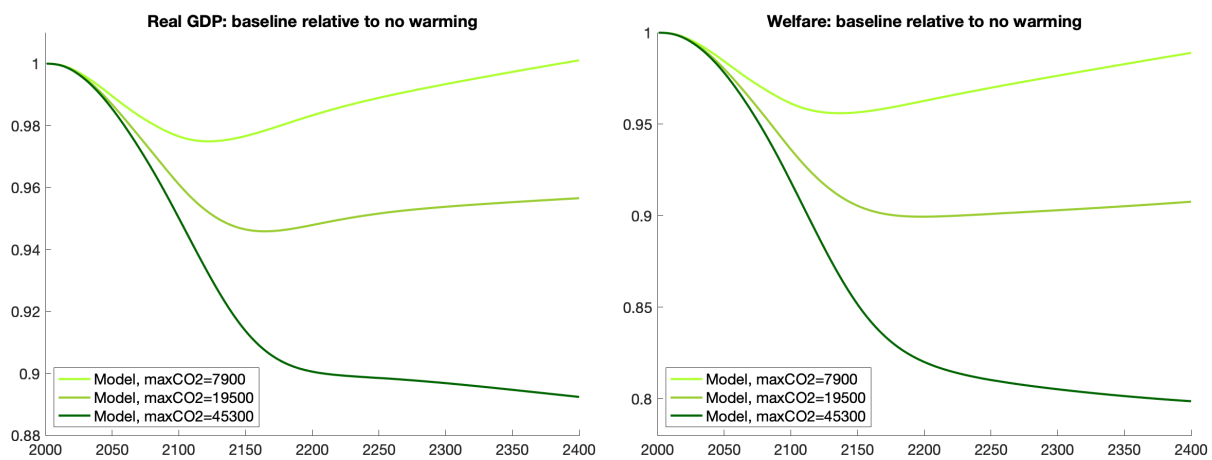

Figure 54: Real GDP and welfare losses over time across different sizes of carbon deposits.
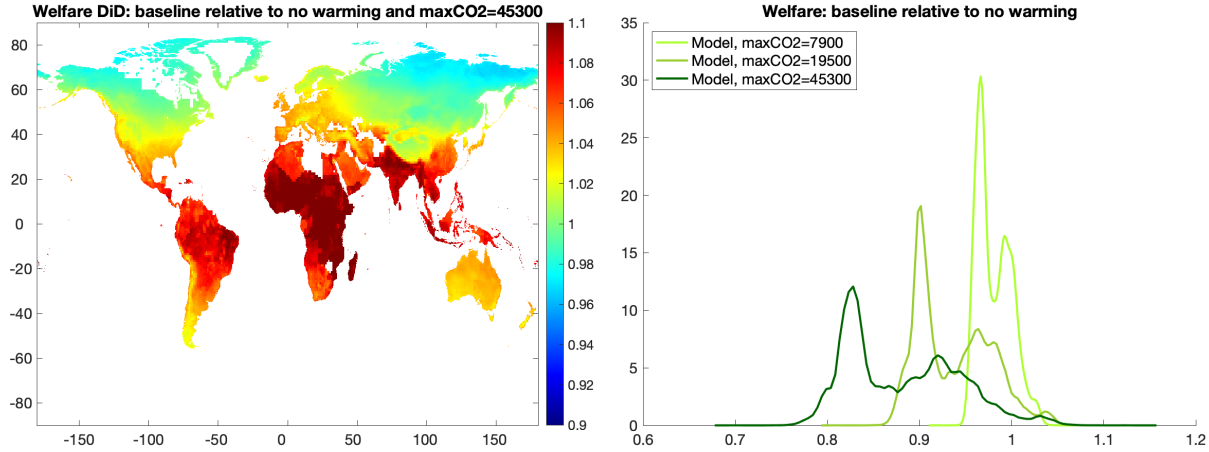
Figure 55: Welfare losses over space across different sizes of carbon deposits.

without abatement and in dashed curves those with the introduction of a free geoengineering technology in 2100. A carbon tax has the same effect on CO_2 emissions at impact, regardless of the deposit size, since the extraction cost curves have basically the same derivative when evaluated at zero.
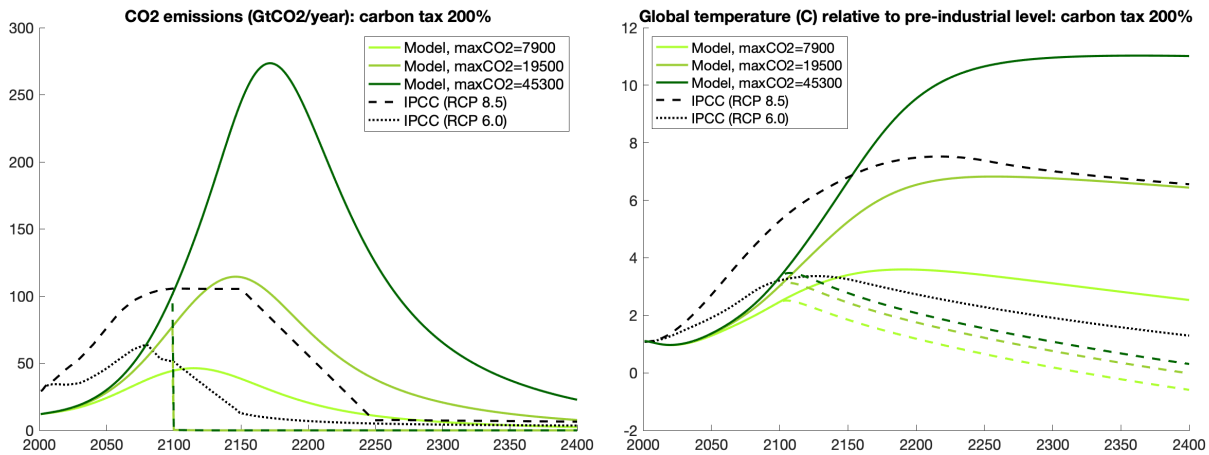
Figure 56: CO_2 emissions and global temperature with a carbon tax of 200% across different sizes of carbon deposits.

When analyzing the evolution of economic benefits of the carbon tax, the initial decline in production is identical across deposit sizes, leading to the same real GDP and welfare global losses at impact. However, over the next decades, welfare is higher the lower the carbon deposit, since the extraction cost curve displays a higher slope, amplifying the rise in fossil fuel price and thus the temperature decline. This situation reverts after one century, because for the scenario with large carbon deposits, the level of cumulative extraction induces a sharp increase in the price of fossil fuels. In the long-run, the welfare benefits of the carbon tax across carbon deposits converge to the same trend.

When considering the introduction of a costless geoengineering technology in 2100, the welfare im-

26

provements due to the environmental policy in the long-run are greater with larger carbon deposits, because the difference in long-run temperature with and without the abatement is higher.[79] Tables 11 and 12 summarize the global real GDP and welfare gains for a carbon tax of 200%, and a carbon tax of 200% with an abatement technology under different discount factors and sizes of carbon deposits.
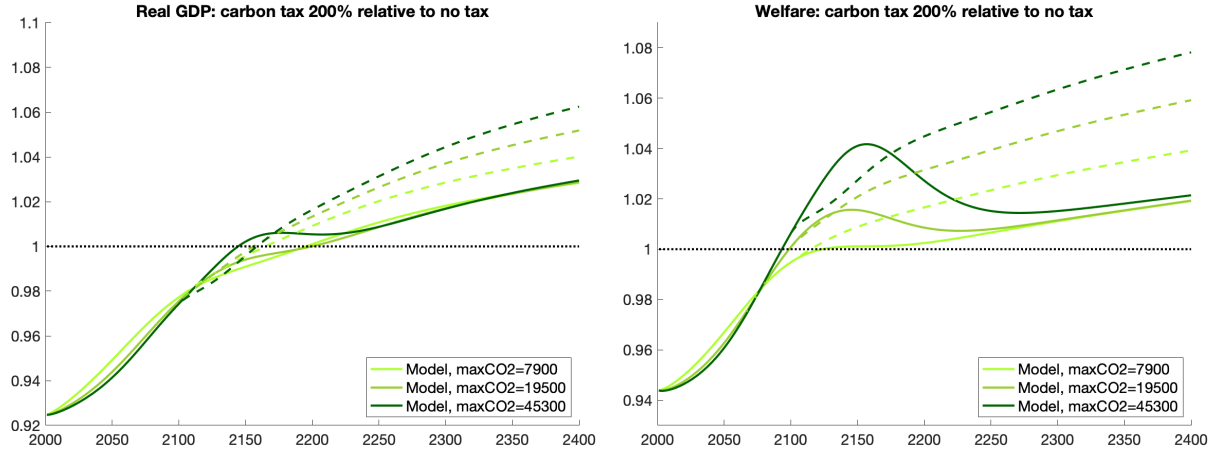

Figure 57: Real GDP and welfare with a carbon tax of 200% across different sizes of carbon deposits.

	PDV of real GDP			Welfare		
	BGP gr	β=0.965	β=0.969	BGP gr	β=0.965	β=0.969
$maxCumCO2$=7900 GtCO$_2$	3.094%	0.988	1.065	2.997%	0.994	1.028
$maxCumCO2$=19500 GtCO$_2$	3.086%	0.986	1.063	2.979%	0.996	1.026
$maxCumCO2$=45300 GtCO$_2$	3.075%	0.986	1.057	2.957%	1.001	1.027

Table 11: Real GDP and welfare gains with a carbon tax of 200%, with no abatement, under different sizes of carbon deposits and discount factors.

	PDV of real GDP			Welfare		
	BGP gr	β=0.965	β=0.969	BGP gr	β=0.965	β=0.969
$maxCumCO2$=7900 GtCO$_2$	3.098%	0.993	1.086	3.011%	1.003	1.056
$maxCumCO2$=19500 GtCO$_2$	3.097%	0.995	1.107	3.008%	1.011	1.080
$maxCumCO2$=45300 GtCO$_2$	3.096%	0.996	1.126	3.007%	1.018	1.101

Table 12: PDV of real GDP and welfare gains with a carbon tax of 200%, with abatement, under different sizes of carbon deposits and discount factors.

Now, we examine the effect of a spatial- and time-invariant clean energy subsidy of 75%, keeping car-

---

[79]Note that relative real GDP and welfare can be slightly lower in the abatement case for a couple of decades after the invention of the abatement technology. The reason is that the difference in temperatures between the benchmark scenario with and without abatement can be larger than the difference in temperature with and without abatement in the scenario with a carbon tax, depending on the second derivative of the temperature function at the time the abatement technology arrives. After a few decades, this effect is always dominated by the faster increases in temperature in the case without abatement.

bon taxes at 0%. Figure 58 shows that the clean subsidy yields minuscule reductions in the flow of CO_2 emissions and the path for global temperature, regardless of the size of fossil fuel deposits.
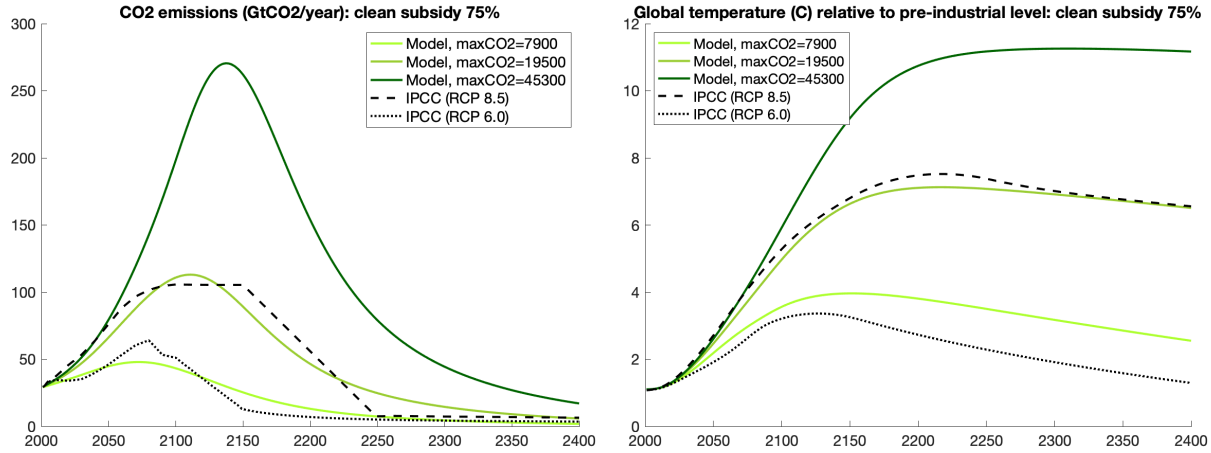

Figure 58: CO_2 emissions and global temperature with a clean energy subsidy of 75% across different sizes of carbon deposits.

The implementation of a green subsidy generates larger short-run benefits in terms of global real GDP and welfare the smaller the carbon deposit, as illustrated in Figure 59. Since extraction costs are higher the smaller the carbon deposit, a clean subsidy has a larger effect on the relative price of fossil fuels to clean energy. Consequently, more households migrate towards the clean-intensive places, which tend to be high-productive places, rising global production and welfare.
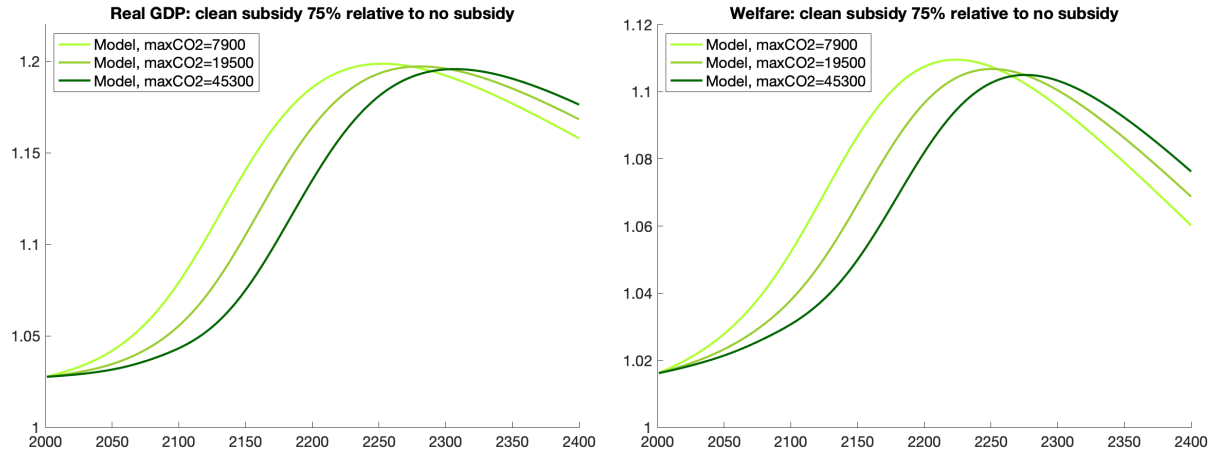

Figure 59: Real GDP and welfare with a clean energy subsidy of 75% across different sizes of carbon deposits.

Table 13 summarizes the global real GDP and welfare gains of a clean energy subsidy of 75% under different discount factors and sizes of carbon deposits. For low (high) discount factors, real GDP and welfare rise with smaller (greater) carbon deposits.

28

The Balanced Growth Path growth rate of real GDP and welfare, for both carbon taxes and clean subsidies, rise with lower carbon deposits, as the short-run high price of fossil fuels reduces income, increasing natality rates and consequently global population.

	PDV of real GDP			Welfare		
	BGP gr	β=0.965	β=0.969	BGP gr	β=0.965	β=0.969
$maxCumCO2$=7900 GtCO$_2$	3.050%	1.109	0.982	2.952%	1.058	0.986
$maxCumCO2$=19500 GtCO$_2$	3.044%	1.098	1.007	2.935%	1.053	1.000
$maxCumCO2$=45300 GtCO$_2$	3.036%	1.088	1.031	2.915%	1.048	1.012

Table 13: PDV of real GDP and welfare gains with a clean energy subsidy of 75% under different sizes of carbon deposits and discount factors.

H   Global Warming in the Worst-Scenario

This section shows the effects of global warming when considering that the damage functions $\Lambda^a(\cdot), \Lambda^b(\cdot)$ are described by the lower 95% confidence interval. Additionally, we quantify the role of environmental policies in improving real GDP and welfare in the most pessimistic scenario.

H.1   The Welfare Cost of Global Warming in the Worst-Scenario

Figure 60 displays the spatial configuration of fundamental amenities and productivities in the year 2200 in the worst-scenario relative to the counterfactual scenario with no warming damages. The most affected places face amenity and productivity losses of 27% and 86%, respectively. As a comparison, in the benchmark scenario, the most affected places experienced losses of 25% and 80%, respectively.[80]

On average, the economy experiences welfare losses of 13% and real GDP losses of 8%, which are larger than those projected in the benchmark case: 6% and 3%, respectively. The most damaged zones in the planet face welfare losses of 26%, whereas a minuscule 0.003% fraction of population, located in arctic zones, experience welfare gains. Figures 61 and 62 present the spatial distribution of welfare and real GDP losses.

H.2   Environmental Policies in the Worst-Scenario

As shown in Figure 63, the implementation of a carbon tax has the same real GDP and welfare changes at impact, as in the benchmark scenario. However, as time evolves the slopes of both variables are higher than those of the baseline case, as CO_2 levies have a higher potential to improve real GDP and welfare. As a comparison, in the worst-scenario, for a tax of 200%, welfare losses become zero by the year 2063; whereas in the baseline case that event occurs 36 years later.

---

[80]Lower amenities and productivities in the worst-scenario translate into lower income, with respect to the benchmark case. Hence, natality rates augment, yielding higher levels of global population in the most pessimistic scenario.
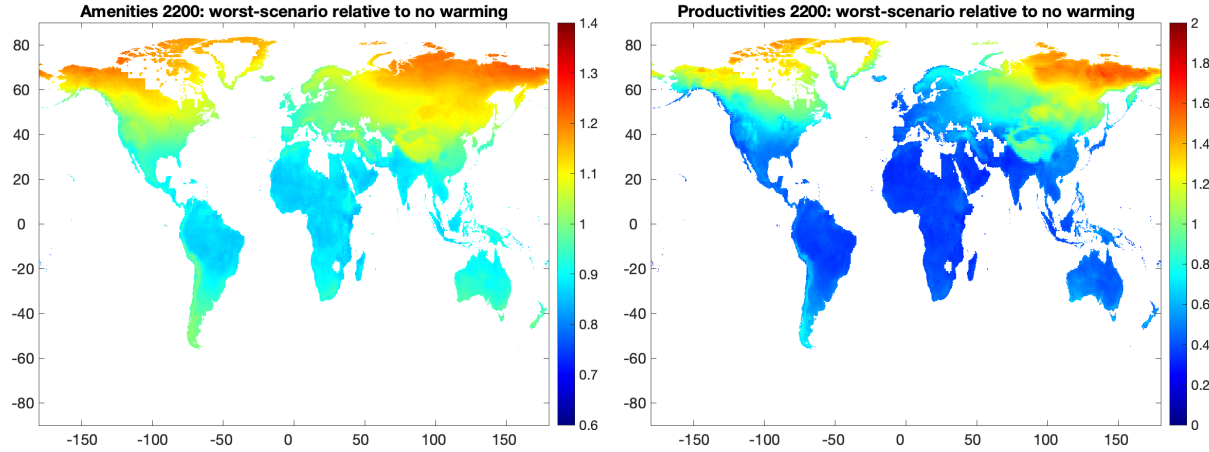
Figure 60: Losses in amenities and productivities from global warming in the year 2200 in the worst-scenario.
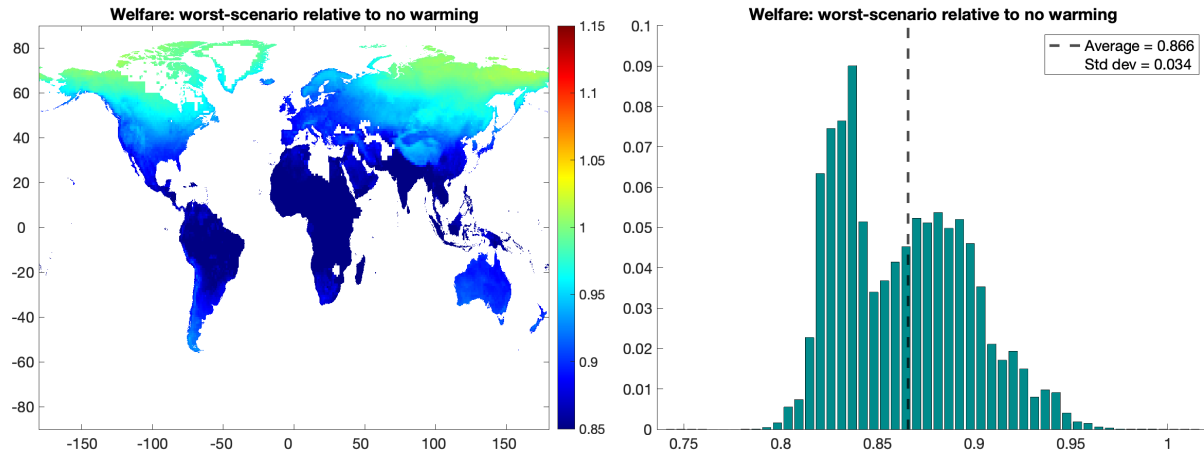

Figure 61: Welfare losses due to global warming in the worst-scenario.

After those points in time, real GDP and welfare keep rising above the levels of the baseline case. When considering a tax of 200% and a discount factor of $\beta = 0.969$, welfare rises by 3.3% in the worst-scenario and by 2.6% in the benchmark scenario.

Under the introduction of an abatement technology, the benefits for the economy are much higher, as illustrated by the dashed curves in Figure 63. By the year 2400, global average welfare (real GDP) gains with the geoengineering technology in the most pessimistic scenario reach a value of 10.1% (7.0%); whereas in the benchmark scenario, they are 5.9% (5.2%).

Table 14 quantifies the gains in global average real GDP and welfare from the implementation of taxes of 50%, 100% and 200% on the use of fossil fuels with respect to a scenario with no CO_2 levies, when no geoengineering technology is introduced. Table 15 performs a similar comparison, but taking into account the presence of a free abatement technology in 2100.

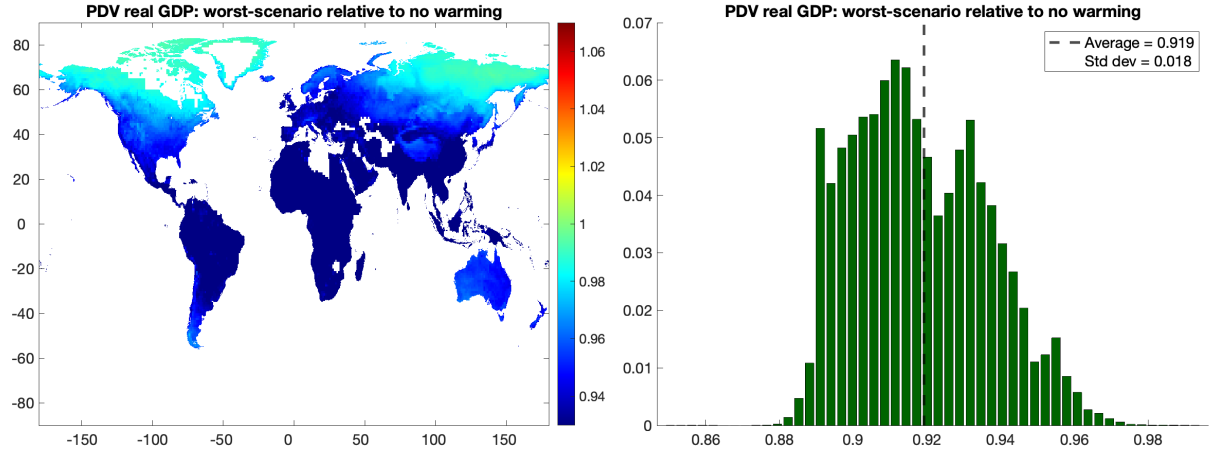As clean energy subsidies barely affect the temperature path, their effects on the economy are very

30

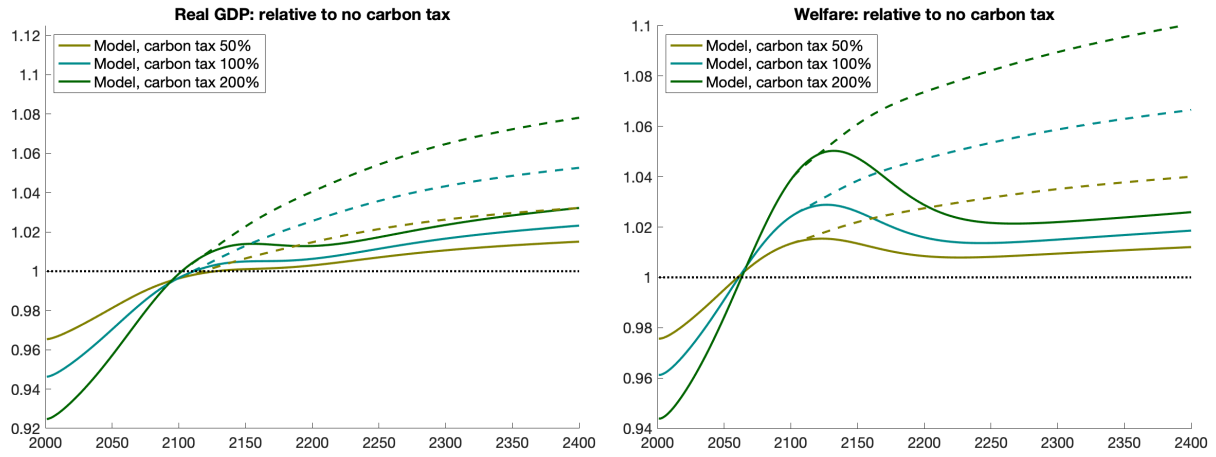Figure 62: Real GDP losses due to global warming in the worst-scenario.

Figure 63: Real GDP and welfare gains under different carbon taxes in the worst-scenario with an abatement technology introduced in 2100.

	PDV of real GDP			Welfare		
	BGP gr	β=0.965	β=0.969	BGP gr	β=0.965	β=0.969
τ=0%	3.085%	1	1	2.982%	1	1
τ=50%	3.089%	0.997	1.027	2.985%	1.005	1.015
τ=100%	3.090%	0.997	1.042	2.986%	1.009	1.023
τ=200%	3.092%	0.997	1.059	2.987%	1.014	1.033

Table 14: PDV of real GDP and welfare gains for different carbon taxes and discount factors in the worst-scenario.

similar with respect to those of the benchmark case. Table 16 shows the values of global average real GDP and welfare gains when enforcing subsidies on the use of clean energy of 25%, 50% and 75%.

31

	PDV of real GDP			Welfare		
	BGP gr	β=0.965	β=0.969	BGP gr	β=0.965	β=0.969
τ=0%	3.085%	1	1	2.982%	1	1
τ=50%	3.089%	1.005	1.053	2.985%	1.017	1.045
τ=100%	3.090%	1.010	1.088	2.986%	1.030	1.075
τ=200%	3.092%	1.016	1.132	2.987%	1.046	1.115

Table 15: PDV of real GDP and welfare gains for different carbon taxes and discount factors in the worst-scenario with an abatement technology introduced in 2100.

	PDV of real GDP			Welfare		
	BGP gr	β=0.965	β=0.969	BGP gr	β=0.965	β=0.969
s=0%	3.085%	1	1	2.982%	1	1
s=25%	3.082%	1.011	1.003	2.978%	1.007	1.003
s=50%	3.075%	1.033	1.004	2.970%	1.021	1.004
s=75%	3.053%	1.097	0.995	2.946%	1.053	0.996

Table 16: PDV of real GDP and welfare gains for different clean energy subsidies and discount factors in the worst-scenario.

I Adaptation

This section deepens on the relevance of adaptation channels in shaping the economic consequences of global warming. More specifically, we compare the temporal and spatial dimension of warming losses in real GDP when considering economies with higher migration, commercial and innovation frictions. Those patterns display large similarities with those of welfare discussed in Section 5.
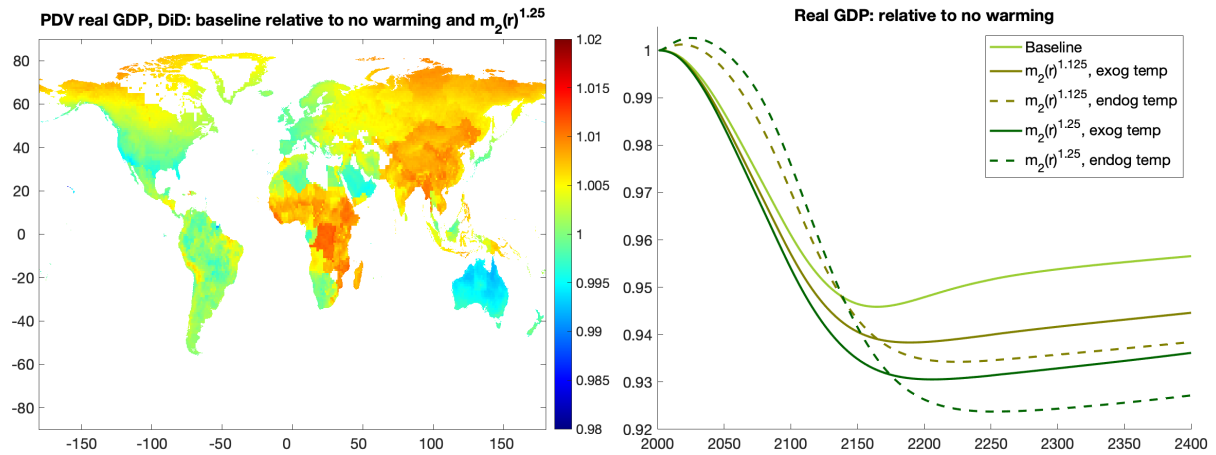

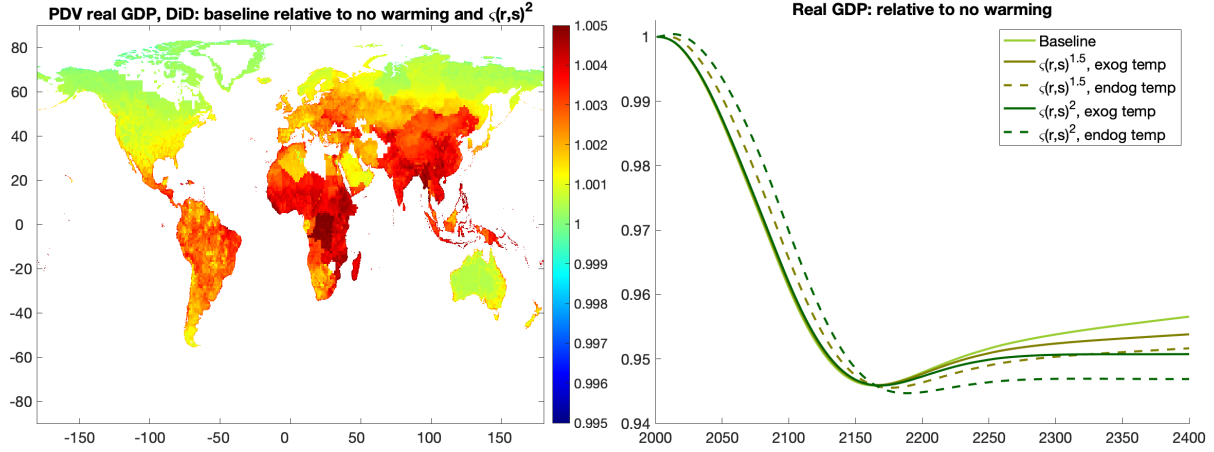Figure 64: Real GDP across different migration costs.

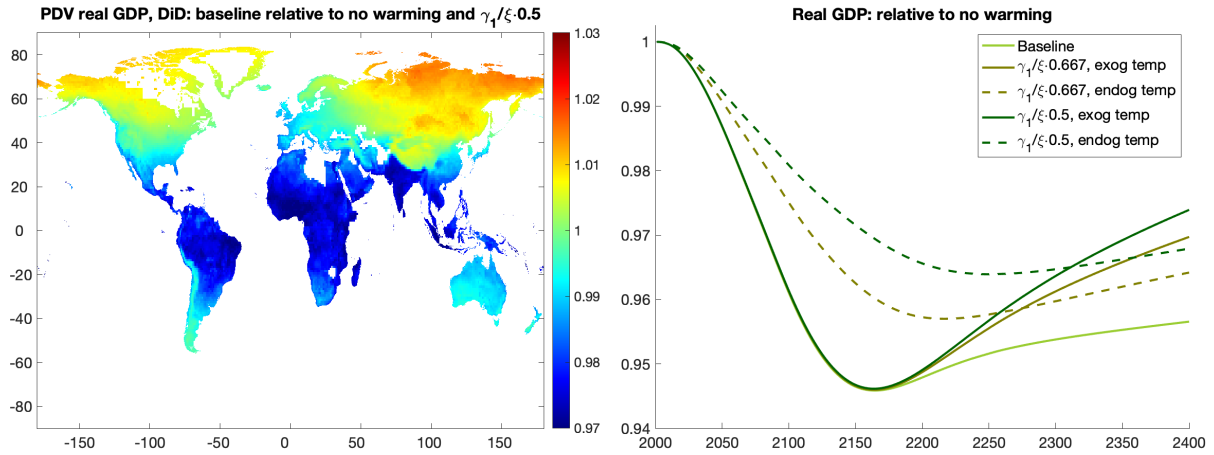Figure 65: Real GDP across different iceberg trade costs.

Figure 66: Real GDP across different innovation costs.

J Additional Results Regarding Environmental Policies

In this section we delve into the economic response over time and space of the implementation of carbon taxes, assess the welfare benefits of joint carbon taxes and clean energy subsidies, provide additional results regarding the introduction of an abatement technology in 2100 and contrast the results when the geoengineering innovation becomes available one century later.

J.1 Temporal and Spatial Evolution of Carbon Taxes

At impact, the implementation of a carbon tax of 200% rises the price of energy faced by firms in every cell of the world. However, these increases are heterogeneous: places in which fossil fuels are relatively expensive, like Canada and Europe, face smaller increases in the total energy price, as shown in Figure 67.

Even though at impact all regions are damaged from the implementation of a CO_2 levy, the places with lower increases in the total price of energy suffer less, as they attract more households, rising current
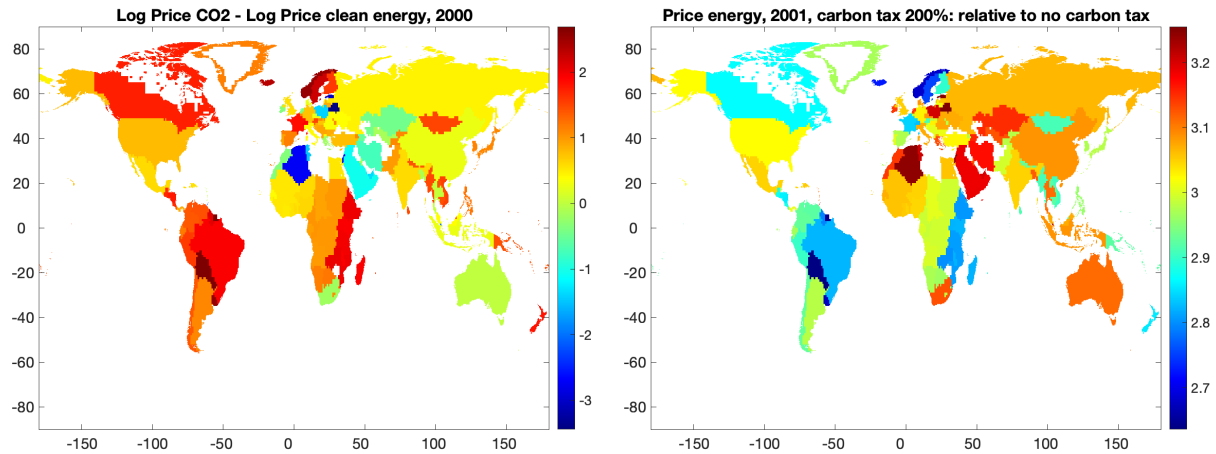
Figure 67: Relative price in fossil fuels and clean energy in the year 2000, and energy price increase with a carbon tax of 200% in the year 2001.

productivity through agglomeration externalities. Figure 68 compares real GDP and welfare in the year 2001 under the implementation of a CO_2 tax of 200% with respect to a scenario with no environmental policy.
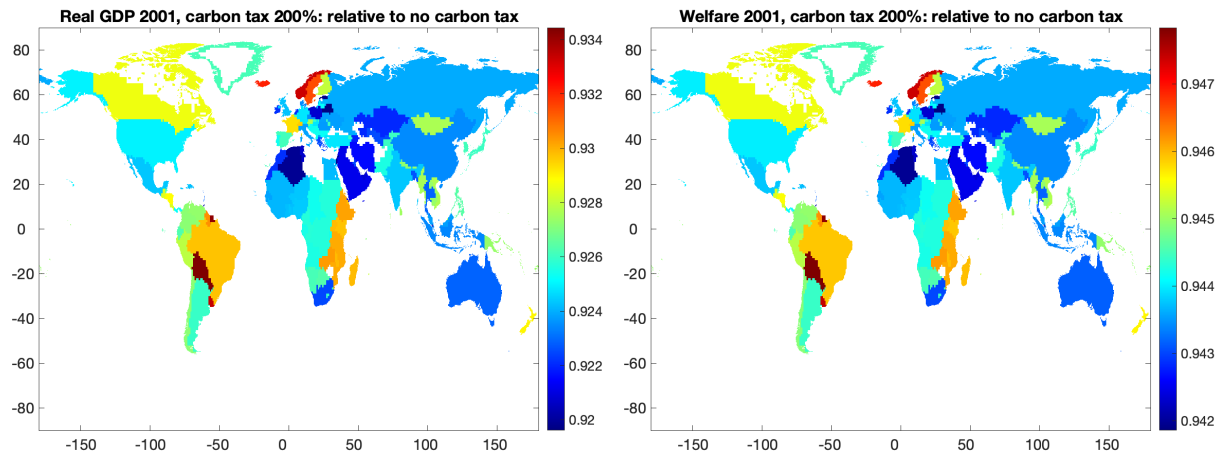

Figure 68: Local real GDP and welfare effects of a carbon tax of 200% in the year 2001.

As time evolves, and as a consequence of the carbon tax, warm regions avoid higher temperatures, whereas cold places are not able to achieve more suitable temperatures for residing and producing. Figure 69 shows the evolution of real GDP and welfare after one century. These maps suggest that the effect of temperature outweighs that of the initial distribution of relative prices.

After another century, the welfare effects preserve the same spatial pattern. However, real GDP has a different spatial configuration, as displayed in Figure 70. The places that have the highest use of fossil fuels with respect to clean energy are projected to undergo losses in real GDP by the year 2200. This is attributed to the large tax burden originated from the high use of fossil fuels.
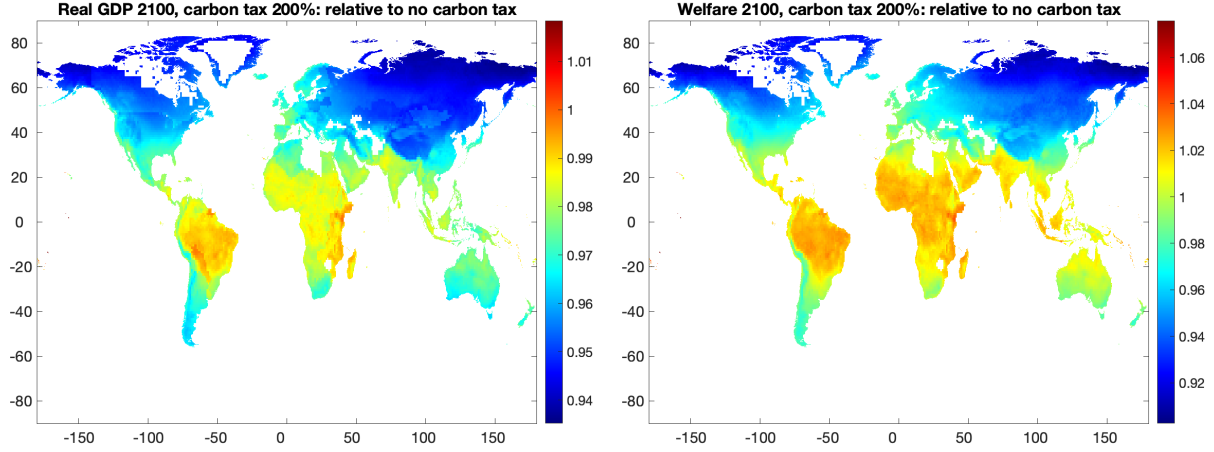
34

Figure 69: Local real GDP and welfare effects of a carbon tax of 200% in the year 2100.
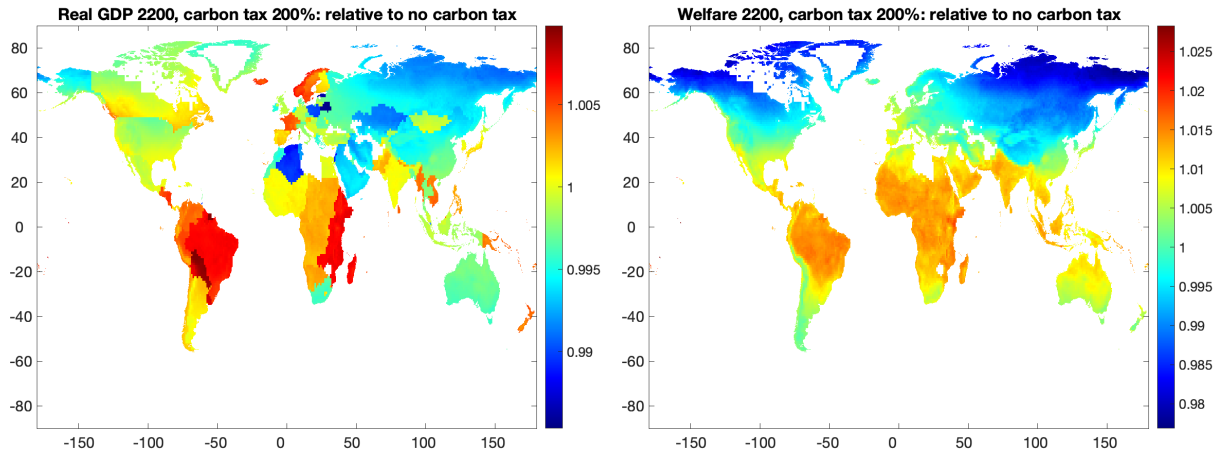

Figure 70: Local real GDP and welfare effects of a carbon tax of 200% in the year 2200.

J.2   Carbon Taxes and Clean Energy Subsidies

Tables 17 and 18 present the global average real GDP and welfare gains arising from the interactions between carbon taxes and clean energy subsidies, respectively, considering discount factors of $\beta = 0.965$ and $\beta = 0.969$. Additionally, Table 19 shows their growth rates in the Balanced Growth Path.

	PDV of real GDP, $\beta = 0.965$				PDV of real GDP, $\beta = 0.969$			
	s=0%	s=25%	s=50%	s=75%	s=0%	s=25%	s=50%	s=75%
τ=0%	1	1.012	1.034	1.098	1	1.005	1.008	1.007
τ=50%	0.993	1.005	1.028	1.093	1.028	1.031	1.031	1.022
τ=100%	0.990	1.002	1.024	1.090	1.044	1.046	1.044	1.029
τ=200%	0.986	0.998	1.021	1.087	1.063	1.063	1.058	1.035

Table 17: PDV of real GDP gains under different carbon taxes, clean energy subsidies and discount rates.

Welfare, $\beta = 0.965$				Welfare, $\beta = 0.969$			
	s=0%	s=25%	s=50%	s=75%	s=0%	s=25%	s=50%	s=75%
τ=0%	1	1.007	1.021	1.053	1	1.003	1.006	1.000
τ=50%	0.998	1.006	1.019	1.052	1.012	1.015	1.016	1.007
τ=100%	0.997	1.005	1.018	1.051	1.019	1.021	1.022	1.011
τ=200%	0.996	1.004	1.017	1.051	1.026	1.028	1.027	1.013

Table 18: Welfare gains under different carbon taxes, clean energy subsidies and discount rates.

Real GDP, BGP gr				Welfare, BGP gr			
	s=0%	s=25%	s=50%	s=75%	s=0%	s=25%	s=50%	s=75%
τ=0%	3.076%	3.073%	3.066%	3.044%	2.971%	2.967%	2.959%	2.935
τ=50%	3.081%	3.077%	3.070%	3.048%	2.974%	2.970%	2.962%	2.938
τ=100%	3.083%	3.080%	3.073%	3.049%	2.977%	2.972%	2.964%	2.939
τ=200%	3.086%	3.082%	3.075%	3.051%	2.979%	2.975%	2.966%	2.940

Table 19: Balanced-Growth-Path growth rate of real GDP and welfare for different carbon taxes and clean energy subsidies.

J.3 Carbon Taxes and Abatement in 2100

Figure 71 presents, in solid curves, the global average real GDP and welfare gains from the enforcement of different levels of carbon taxes, when no geoengineering technology arises, as in Figures 14 and 35. The dotted curves evaluate the benefits of carbon taxes under the introduction of a costless abatement technology in 2100 with respect to the benchmark scenario that considers no environmental policy and no abatement technology.[81] Table 20 summarizes the global real GDP and welfare gains of the implementation of different carbon taxes and the introduction of the abatement technology, with respect to the absence of both policies. The economic benefits overcome those of Table 2.

PDV of real GDP				Welfare			
	BGP gr	β=0.965	β=0.969	BGP gr	β=0.965	β=0.969
τ=0%	3.076%	1	1	2.971%	1	1
τ=50%	3.081%	0.997	1.044	2.974%	1.004	1.032
τ=100%	3.083%	0.996	1.072	2.977%	1.008	1.053
τ=200%	3.086%	0.995	1.107	2.979%	1.011	1.080

Table 20: PDV of real GDP and welfare for different carbon taxes and discount factors with an abatement technology introduced in 2100.

---

[81]The dashed curves of Figure 35 are calculated as the ratio of welfare (or real GDP) with carbon taxes and abatement with respect to zero carbon taxes and abatement. The dotted curves of Figure 71 are calculated as the ratio of welfare (or real GDP) with carbon taxes and abatement with respect to zero carbon taxes and no abatement.
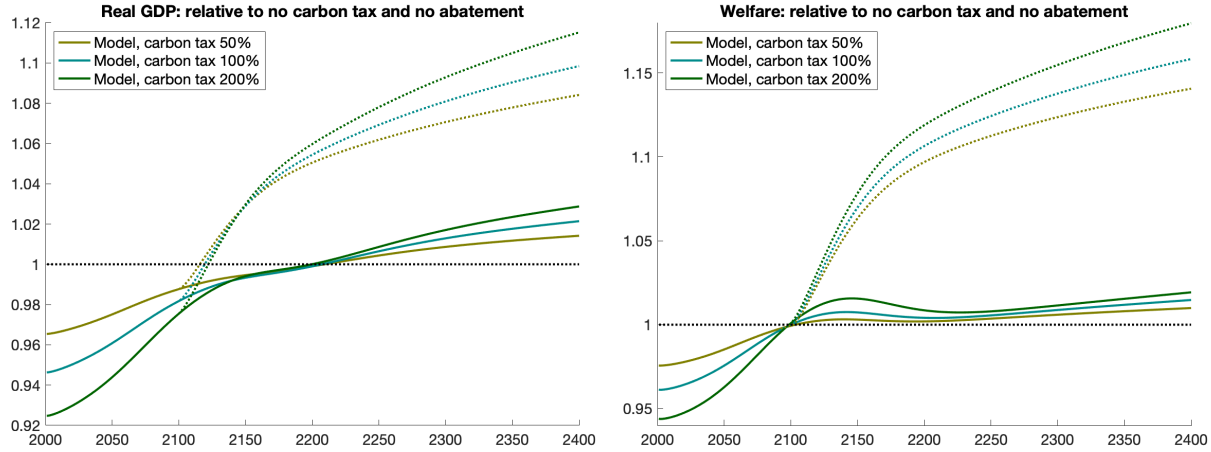
Figure 71: Real GDP and welfare for different carbon taxes with an abatement technology introduced in 2100.

J.4 Carbon Taxes and Abatement in 2200

We extend the analysis of the introduction of an abatement technology and assess its benefits in terms of real GDP and welfare when this innovation arises in the year 2200, rather than in the year 2100, as in Section 6.2. A century of delay in geoengineering advances provides more modest beneficial effects for the economy, as a higher share of the total stock of CO_2 has already been released to the atmosphere and, therefore, the reduction in long-run temperature is lower, as shown in Figure 72. Furthermore, the delay of this technology reduces the differences in the steady state temperature across carbon taxes, attenuating the benefits of stronger environmental policies.
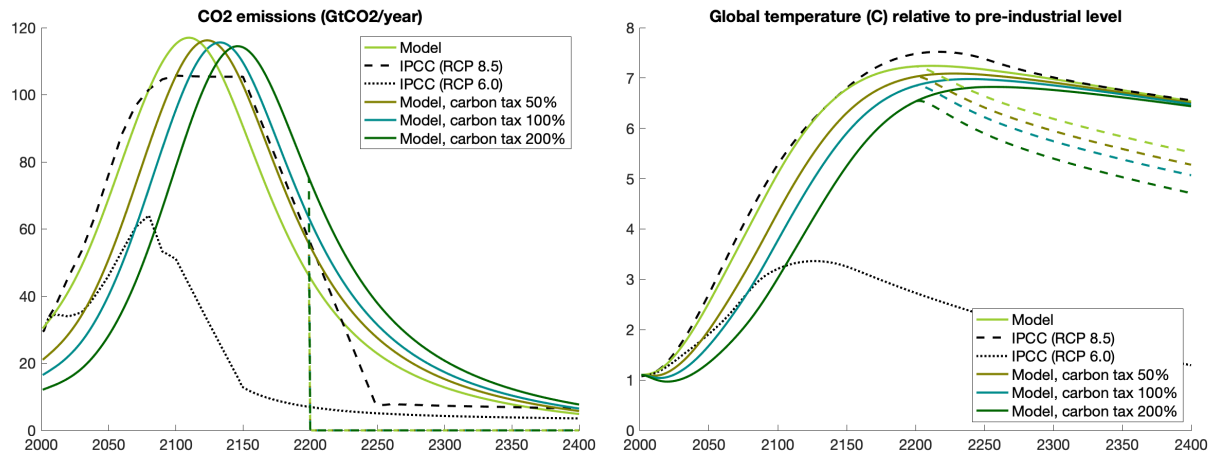

Figure 72: CO_2 emissions and global temperature for different carbon taxes with an abatement technology introduced in 2200.

Figure 73 and Table 21 perform a similar analysis to Figure 35 and Table 2. A century of delay in geoengineering advances reduces welfare and real GDP gains in 3.1% and 2.0% for a tax of 200% and a
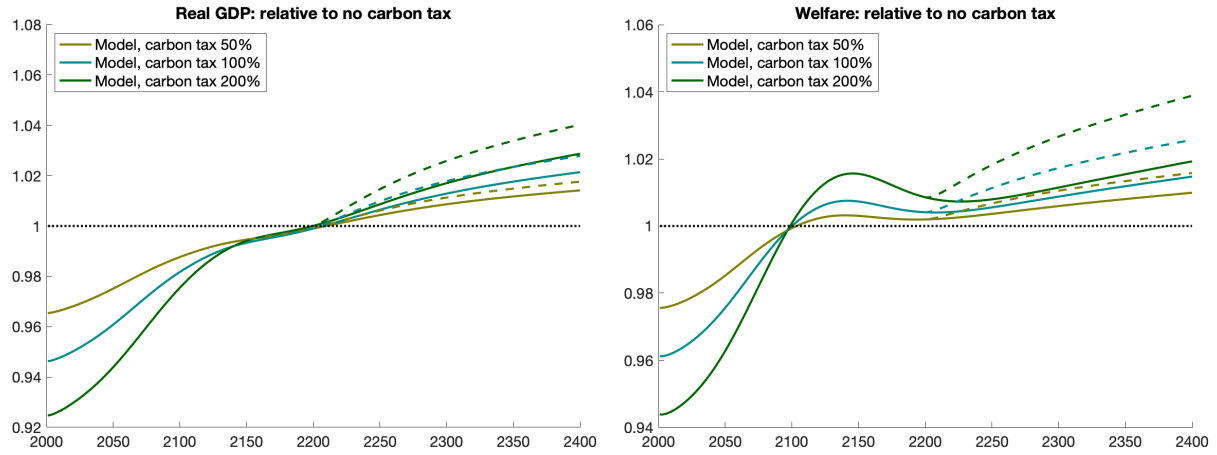
discount factor of $\beta = 0.969$.

Figure 73: Real GDP and welfare for different carbon taxes with an abatement technology introduced in 2200.

	PDV of real GDP			Welfare		
	BGP gr	β=0.965	β=0.969	BGP gr	β=0.965	β=0.969
τ=0%	3.076%	1	1	2.971%	1	1
τ=50%	3.081%	0.994	1.035	2.974%	1.000	1.019
τ=100%	3.083%	0.992	1.058	2.977%	1.000	1.032
τ=200%	3.086%	0.989	1.087	2.979%	1.002	1.049

Table 21: PDV of real GDP and welfare for different carbon taxes and discount factors with an abatement technology introduced in 2200.